UNIVERSITÉ DU QUÉBEC À MONTRÉAL

SPACE-TIME INTERACTIONS IN FOREST METACOMMUNITIES

THESIS

PRESENTED

AS PARTIAL REQUIREMENT

TO THE PH.D IN BIOLOGY

BY

HEDVIG NENZÉN

OCTOBER 2016

UNIVERSITÉ DU QUÉBEC À MONTRÉAL

INTERACTIONS SPATIO-TEMPORELLES DANS LES MÉTACOMMUNAUTÉS FORESTIÈRES

THÈSE
PRÉSENTÉE
COMME EXIGENCE PARTIELLE
DU DOCTORAT EN BIOLOGIE

PAR
HEDVIG NENZÉN

OCTOBRE 2016

ACKNOWLEDGMENTS

When we try to pick out anything by itself,
we find it hitched to everything else in the Universe.
-John Muir

I would like to thank my supervisors, Dominique Gravel and Pedro Peres-Neto, for suggesting such an interesting topic which is both theoretical and practical. They gave me the independence to explore, yet a topic coherent enough that I found my way back, but not without their guidance. Their timing was perfect because not every thesis unfolds at the same time as its topic.

I would like to thank the Forest Complexity Modelling programme, Christian Messier and Virginie -Arielle Angers, for funding and the chance to participate in summer workshops. I'm grateful to Veronique Martel and Lukas Seehausen for introducing me to the minute world of spruce budworm parasitoids. I'm also grateful to the spruce budworm group in Montreal and Patrick James, for helpful interactions. Elise Filotas has always encouraged me.

Thanks to Yan Boulanger for the dendrochronological data, and Emily Tissier and Alyssa Butler for reading the thesis.

Many thanks to the laboratory in Rimouski / Sherbrooke, in order of seniority: Claire, Isabelle, Steve, Renaud, Philippe, Tim, Idaline, Kevin, Isabelle, Camille, Matthew and Amaël. Also to my roommates for enduring my bad french and flat bread; Marion and Mathilde.

Many thanks to the laboratory in Montreal, in order of seniority: Bailey, Renato, Fred, Andrew, Wagner, Pedro and Emily. Marie-Helene and Rudolf for making my time in Montreal enjoyable.

Finally, to my parents who demonstrated the value of hard work and academic freedom.

CONTENTS

LIST OF TABLES

LIST OF FIGURES

RÉSUMÉ

Déterminer les causes de la répartition et des fluctuations des espèces est un important défi en écologie. Un exemple spectaculaire de fluctuations d'espèces est les épidémies d'insectes ravageurs, caractérisées par des densités élevées de population à travers un paysage. Malgré de nombreuses études empiriques et théoriques des fluctuations des espèces, les causes des épidémies sont loin d'être bien comprises et une meilleure compréhension de celles-ci pourrait en améliorer la gestion. Cette thèse porte sur les trois principales hypothèses proposées pour expliquer la synchronie des épidémies à large échelle spatiale - le climat, la dispersion, et les ennemis naturels. J'ai couplé des modèles statistiques et mécanistiques pour tester les trois hypothèses dans le contexte d'un insecte ravageur bien étudié ; la tordeuse des bourgeons de l'épinette (*Choristoneura fumiferana*). Le modèle a été paramétré avec des cartes spatiotemporelles de défoliation comme un proxy pour les densités de population. Les simulations indiquent que la dispersion non linéaire, comme prévu par l'effet Allee, était important pour produire des épidémies cycliques et synchrones. L'analyse statistique des cartes spatiotemporelles d'épidémie a montré que la dispersion se produit plus souvent entre les cellules voisines, mais que la dispersion à longue distance a également lieu occasionnellement. Des mécanismes abiotiques tels que le climat peuvent également synchroniser les épidémies à grande échelle (effet Moran). Des modèles statistiques ont montré que la dispersion avec toutes les variables climatiques reproduisent bien les épidémies de tordeuse observées. Ces estimations ont été utilisées en tant que paramètres dans des simulations pluriannuelles. L'autocorrélation temporelle, sous forme de plusieurs années avec un climat favorable a augmenté l'effet Moran et encouragée les épidémies. Cependant, même avec l'autocorrélation spatiotemporelle observée et la dispersion, le modèle a été incapable de reproduire la distribution spatiales en grappe des épidémies. Enfin, les meécanismes biotiques, sous la forme de divers ennemis naturels, peuvent affecter la dynamique des insectes, et les parasitoïdes en particulier peuvent les déstabiliser. Pour étudier le rôle des parasitoïdes, j'ai construit un modèle de métacommunauté dans lequel la dynamique de la tordeuse est déterminée par des interactions avec les parasitoïdes. Le modèle indique que hyperparasitoïdes de niveau supérieur peuvent interrompre le contrôle parasitoïde et générer des épidémies. Dans cette thèse, je réinterprète les épidémies d'insectes ravageurs comme un processus de métapopulation, et comme les modèles de métapopulation sont analogues à des modèles épidémiologiques, mon modèle peut être utile pour élaborer des stratégies de gestion. Le

comportement de dispersion de la tordeuse estimé peut être utilisé pour planifier la récolte des arbres tout en minimisant la dispersion et donc les épidémies. La surveillance des hyperparasitoïdes pourrait indiquer si une épidémie se produira bientôt. En conclusion, j'ai démontré que l'autocorrélation climatique temporelle pourrait amplifier les fluctuations des populations d'insectes dans le temps, et que la dispersion et les ennemis naturels interagissent pour regrouper spatialement les épidémies.

Mots-clé: métacommunauté, métapopulation, épidémies d'insectes ravageurs, défoliation

ABSTRACT

Determining the causes of species distributions and fluctuations is an important ecological challenge. One striking type of ecological dynamics are outbreaks of insect pests, defined as high population densities synchronously throughout a landscape. Despite many empirical and theoretical studies of species fluctuations, what drives outbreaks is far from well understood but could improve management. This thesis focused on the three main hypotheses proposed to synchronize outbreaks - climate, dispersal, and natural enemies. I coupled statistical and mechanistic models to test all three hypotheses for a well-studied insect pest, the spruce budworm (*Choristoneura fumiferana*). The resulting metapopulation model was parameterized with spatiotemporal defoliation maps as a proxy for population densities. Simulations indicated that nonlinear dispersal, as expected from the Allee effect, was important to produce synchronous, cyclic outbreaks. Statistical analysis of spatiotemporal outbreak maps showed that dispersal occurred most often between neighbouring stands, but that occasional long-distance dispersal also took place. Abiotic drivers such as climate may also synchronize large-scale outbreaks (Moran effect). Spatiotemporal climate and dispersal variables were tested to disentangle their relative importance. Statistical models showed that dispersal with all climate variables best fit observed budworm outbreaks. These estimates were employed as parameters in multi-year simulations to identify if climate autocorrelation synchronizes outbreaks. Temporal autocorrelation in the form of consecutive suitable years 'enhanced' the spatial Moran effect and encouraged outbreaks. However, even with observed spatiotemporal autocorrelation and dispersal, the model did not reproduce the spatial clusters of observed outbreaks. Finally, biotic drivers in the form of various natural enemies may affect outbreaks, and parasitoids in particular destabilize dynamics. To investigate the role of parasitoids I constructed a metacommunity model in which budworm dynamics were driven by parasitoid interactions. The model indicated that higher-level hyperparasitoids can interrupt parasitoid control and generate outbreaks. In this thesis, I reinterpreted insect pest outbreaks as a metapopulation process, and since metapopulation models are analogous to epidemiological models, my model can employ spatial epidemiological strategies to elaborate management strategies. The estimated budworm dispersal behaviour can be used to plan harvesting that minimizes dispersal and thus outbreaks. Monitoring hyperparasitoids could indicate if an outbreak will occur soon. In conclusion, I demonstrated that temporal

climate autocorrelation may amplify insect population fluctuations in time, and that dispersal and natural enemies interact to spatially cluster distributions.

Keywords: Metacommunity, dispersal, insect outbreaks, climate

INTRODUCTION

0.1 Overview

Determining the causes of species distributions and fluctuations is an important ecological challenge. What regulates whether a species is present at a particular time and place? One striking example of ecological dynamics are outbreaks, defined as synchronously high population densities throughout a landscape (Liebhold et al., 2004). Outbreaks are so striking because the tiny insects reach such high densities that they cause enormous impacts on their resource (Cooke et al., 2007). Large-scale spatiotemporal population fluctuations are also of interest because understanding why certain species fluctuate can help us to understand why other species have stable distributions. Ultimately, knowledge of ecological mechanisms can be employed to improve ecological management, whose goal is either to stabilize (prevent extinction) or desynchronize (prevent outbreaks) ecological dynamics. Here I developed a simple yet inclusive framework to model species outbreaks that focuses on the presence or absence of insect disturbance in the form of forest defoliation. The model is analogous to a metapopulation model (Levins, 1969), which was created to improve pest management but has rarely been applied to this goal. To make the metapopulation model more relevant, I extended it to represent and investigate the factors that drive outbreaks.

This thesis tested the three main hypotheses that are proposed to explain synchronous outbreaks - dispersal, climate, and natural enemies (Figure 0.1). The intrinsic hypothesis of outbreaks, dispersal, may synchronize outbreaks when individuals from a single population disperse throughout the landscape (Chapter

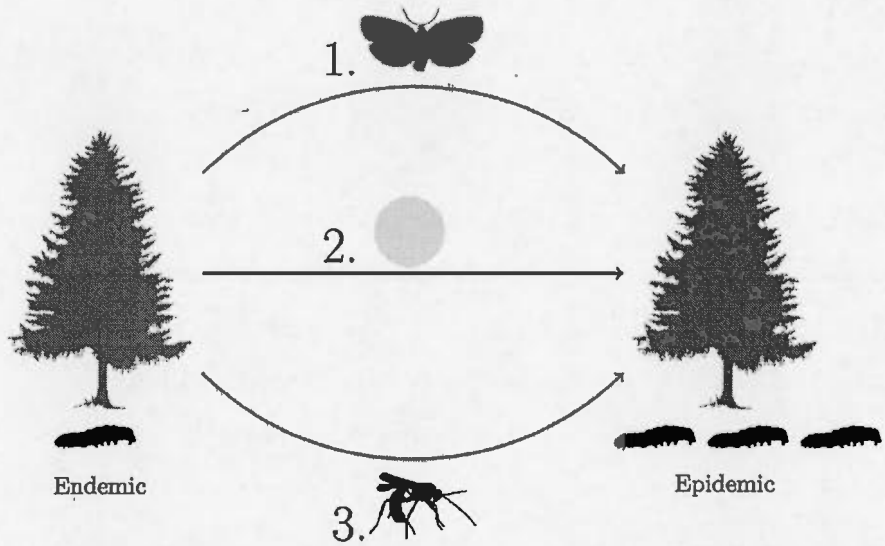

Figure 0.1 Three main hypotheses causing the transition from endemic densities and healthy (mature) forest, to epidemic densities in defoliated (infected) forest. Dispersal of adult moth individuals may synchronize outbreaks when immigrating individuals cause defoliation in another location (Chapter 1). Abiotic drivers such as temperature have also been proposed to cause large-scale outbreaks if they occur in many locations simultaneously (Chapter 2). Finally, biotic drivers in the form of natural enemies such as parasitoids, may synchronize outbreaks (Chapter 3).

1). Abiotic drivers such as spatially autocorrelated environmental variation has also been proposed to synchronize the dynamics of independent populations (the Moran effect, Chapter 2). Finally, biotic drivers in the form of natural enemies may affect outbreaks (Chapter 3).

I explored these synchronizing mechanisms in what is possibly the most throughly studied insect species: the spruce budworm (section 0.2). Quebec is in the middle of a large-scale outbreak in 2016; it is remarkable that yet again the outbreaks have returned every ~30 years. The budworm is an ideal study organism for such an in-depth investigation, because it displays rich dynamics in time and space. Theoretical, mathematical models are necessary to improve understanding of outbreaks, because merely description does not improve understanding of mechanisms driving them, and landscape-scale experiments are unfeasible. The objective of this thesis was to develop a framework flexible enough to test all three outbreak - causing mechanisms but realistic enough to reflect biological knowledge (section 0.4). To develop this framework I integrated other modelling approaches, namely metapopulation, multiple equilibria and epidemiological models. The resulting model was suitable to evaluate the intrinsic (Chapter 1), abiotic (Chapter 2) and biotic (Chapter 3) synchronizing mechanisms of landscape-wide, multi-year budworm outbreaks.

0.2 Spruce budworm as an example system

The Eastern spruce budworm (*Chorisoneura fumiferana* Lepidoptera: Tortricidae) is considered the most serious pest in the boreal and sub-boreal forests of North America (NRC, 2013). Given that budworm outbreaks cause large-scale defoliation and mortality of economically important trees, factors affecting its reproduction and survival are well-understood. The budworm completes its life cycle in a single year (Figure 0.2). The larvae emerge from diapause in spring

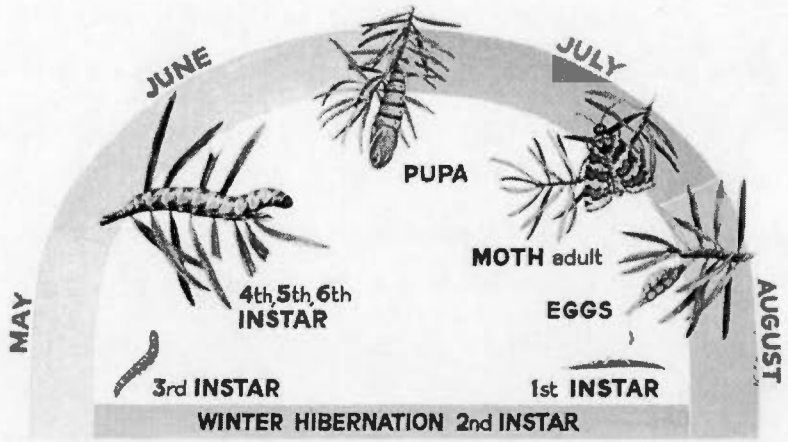

Figure 0.2 The spruce budworm lifecycle.

and feed on current-year buds (NRC, 2013). Precipitation during springtime larval emergence may lower survival rates (Lucuik, 1984). The larvae establish in a feeding site and develop through four instars, and summer temperatures strongly affect development rates and survival (Régnière, 1987). Summer temperatures modify fecundity and survival rates which influences tree defoliation levels (Blais, 1958; Gray, 2008). Pupation takes place in june, and adult moths emerge 10 days later. Adults find each other to mate with the help of pheromones, and the female lays around 200 eggs (Régnière et al., 2012). If densities are too low, mate-finding is more difficult, so the Allee effect has been observed in the budworm (Régnière et al., 2012). When eggs hatch the first instar larvae emerges and then spins a cocoon to hibernate in until the following spring (Nealis & Régnière, 2009). Extreme low and high winter temperatures may cause overwintering mortality (Régnière et al., 2012).

Budworm densities vary over orders of magnitude between endemic and epidemic periods, leading to tree defoliation (Royama, 1992; Sanders, 1996; Cappuccino et al., 1998). Régnière & Nealis (2007) document that budworm egg

densities per kilo of foliage fell from 2 233 to 11 during eight years. Higher defoliation rates in a stand influence budworm fecundity and survival rates (Régnière & Nealis, 2007). Especially young larvae experience higher mortality in heavily defoliated stands (Nealis & Régnière, 2004b; Fuentealba & Bauce, 2012). Defoliation destroys buds, causes abnormal growth of new twigs, and a reddish colour of dried needles. The budworm is a selective feeder, preferring mature balsam fir (*Abies balsamea*) and white spruce (*Picea glauca*) stands over other forest types (Royama et al., 2005; Nealis & Régnière, 2004b; Hennigar et al., 2008). High rates of defoliation decrease the photosynthetic capacity of the host tree (Baskerville & Kleinschmidt, 1980). One year of epidemic budworm densities weakens the tree, and if defoliation continues over several years tree mortality occurs (NRC, 2013). Bergeron et al. (1995) showed that average tree mortality within a stand was 50%, and occasionally reached 100%. Tree mortality increases with stand age but much variability remains unexplained, so it is likely that regional factors beyond stand age also determine tree mortality (Bergeron et al., 1995).

Budworm individuals can disperse large distances but it is unknown how much immigration is necessary to initiate defoliation elsewhere. Adult budworm moths can efficiently travel 48 km (Anderson & Sturtevant, 2011), and the maximum recorded distance is 450 km (Greenbank, 1956, 1980). Suitable meteorological and atmospheric conditions favour successful long distance dispersal (Sturtevant et al., 2013). The moths emigrate in larger numbers from defoliated stands with high budworm densities (Royama, 1984; Régnière & Nealis, 2007). Fecundities of adults is represented by the local egg to moth ratio (E/M ratio). A high E/M ratio compared to the apparent fecundity of moths can indicate that dispersal has occurred to a site (Royama, 1984; Nealis & Régnière, 2004b). Genetic studies show that gene flow between populations is high, indicating strong dispersal ability (James et al., 2015).

The budworm has many natural enemies, including predators, parasites and parasitoids (Régnière, 2001; Huber et al., 1996; Eveleigh et al., 2007). During budworm outbreaks, certain warbler species increase in population densities (Venier et al., 2009; Venier & Holmes, 2010). High-density budworm populations may experience parasitic mite infections (Houseweart, 1980). By far the best-studied natural enemy group are the parasitoids, with more than one hundred parasitoids and hyperparasitoids (Eveleigh et al., 2007; Smith et al., 2011). Parasitoids are often wasps with specific adaptations to attack their hosts (i.e. the budworm, Godfray & Shimada, 1999). During endemic periods the observed mortality rates from parasitoids are high (50-90% in Seehausen et al., 2014, 40-70% in Cappuccino et al., 1998, and all primary parasitoids, 62-75% in Dowden et al., 1950). Less is known of parasitoid mortality rates during epidemic periods, but the identity of the species present may change due to parasitoid life history. Parasitoids can either be univoltine and have one generation and one host per year, or bivoltine and have two generations and need two hosts to complete a life cycle; the budworm and an alternate host. Bivoltine parasitoids are limited by the density of the alternate host and can only partially increase in density to respond to high budworm densities (Régnière, 2001). The identity of alternate hosts is mostly unclear, but they may be present in deciduous forests (Cappuccino et al., 1998). Through their impact on natural enemies, surrounding forest composition can increase parasitoid densities, and ultimately also affect budworm densities (Cappuccino et al., 1998; Su et al., 1996).

Budworm outbreaks can be characterized through spatial, temporal and spatiotemporal data in increasing detail. Data on population-level density and survival time series are time- and labour-intensive to collect, so are only available for a few locations (e.g. Royama et al., 2005; Régnière & Nealis, 2007; Pureswaran et al., 2016). Chronicling older outbreaks is possible using dendrochronology

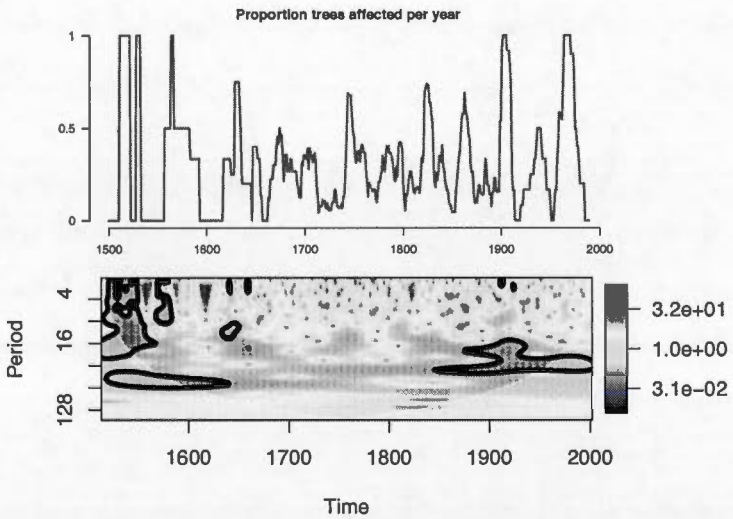

Figure 0.3 Top, Dendrochronological data from Boulanger et al. (2012) indicating the percentage of beams/trees showing growth reduction due to spruce budworm defoliation in one location in southern Quebec. Bottom, wavelet analysis of dendrochronological data, indicating the periodicity in each year. Defoliation has a significant periodicity of 35 years during 1850-2000 (significant periodicities are surrounded by black lines). 1650-1850 no dominant period was detected at this location.

because budworm defoliation reduces tree ring growth (Figure 0.3, Boulanger et al., 2012). The most comprehensive, multi-year and landscape-scale data is in the form of defoliation maps. Aerial defoliation surveys have been carried out 1968 - 2015 in Quebec and track the location of defoliated forest each year (Figure 2.1, section 2 for more details on data). Defoliation has been used as a proxy for population densities because insect densities have a large effect on forest ecosystems via tree defoliation and mortality (e.g. Williams & Liebhold, 2000; Bjørnstad et al., 2002).

Over time, the prevalence of budworm outbreaks are positively autocorrelated, and more specifically they appear to alternate between chaotic and cyclic dynamics. Outbreak dynamics may change over time; they may be non-stationary. A temporally explicit analysis indicates that outbreaks have occurred approximately every 35 years over the last 150 years and more irregularly earlier (Figure 0.3, wavelet analysis, Cazelles et al., 2008, see also Simard et al., 2006). Chaotic dynamics may be generated from nonlinear interactions between species life stages or between multiple species (Hastings et al., 1993; Benincà et al., 2008; Costantino et al., 1997). The complete dendrochronological time series is chaotic (maximal Lyapunov exponent $\lambda = 0.332$, data from 0.3, analyzed using Narzo & Narzo, 2010). However, the dynamics are not chaotic when analyzing only the last 150 years ($\lambda = -0.097$), during which the dynamics may be cyclic or random. Dendrochronology may generate time series with errors in older data and only represents dynamics in one one several location, therefore the results are not conclusive.

Describing budworm dynamics with combined spatiotemporal statistics is complicated because raw defoliation data is binary (presence or absence of defoliated trees) and many methods of analysis require continouos data (e.g. travelling waves, Bjørnstad et al., 1999). To describe spatiotemporal variation in local defoliation, one can assess what proportion of locations transition from defoliation

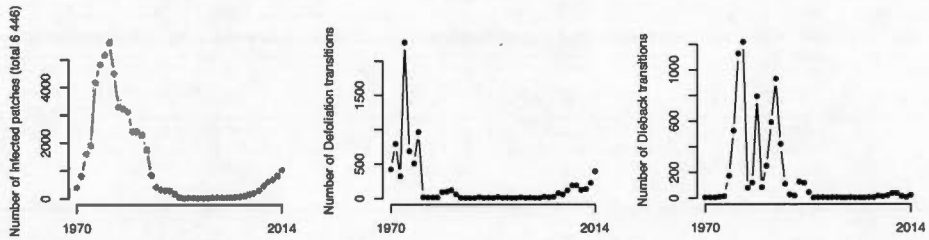

Figure 0.4 Episodic occurrences of defoliation and dieback events. Left, the total proportion of infected locations in spruce budworm defoliation data. Middle, the number of defoliation transitions (from non-defoliated to defoliated forest). Right, the number of dieback transitions (from defoliated to non-defoliated forest). The total number of locations was 6 446, and see section 2 for more details on data.

to non-defoliated, and vice versa, in each year. These transitions are episodic, i.e. multiple transitions interspersed among periods of range stasis, and they occur with greater variability than the resulting total defoliation (Figure 0.4, Johnson et al., 2006).

For several reasons, biological knowledge and statistical descriptions of the spruce budworm cannot explain why large-scale outbreaks occur. First, how local factors such as climate and natural enemies together translate to local population densities and stand defoliation is already complex and subject to many studies (Royama, 1992). Second, local defoliation may cycle due to local mechanisms, but other, regional mechanisms may cause this defoliation to take place simultaneously throughout the landscape (Peters et al., 2004a). Third, local and regional mechanisms may influence each other (Raffa et al., 2008). There is a gap between local knowledge and the large-scale mechanisms that may synchronize outbreaks. In other words, it is not the local destructiveness but the extent of the synchrony that should be studied to understand outbreaks (Cooke et al., 2007). I will now discuss the three main mechanisms that are thought to synchronize outbreaks on a landscape-scale.

0.3 Three mechanisms that synchronize outbreaks

Dispersal synchronizes local populations because individuals from a high-density population spread and increase population densities elsewhere. This is an intrinsic mechanism because it only depends on the species itself. Williams & Liebhold (2000) found that long-distance dispersal together with climatic spatial autocorrelation were the strongest determinants of budworm outbreaks. However, to build their simulation model they chose parameter values that produced outbreaks, so the parameter values may not be biologically realistic for the budworm. Dispersal must be strong to synchronize insect population cycles, however dispersal strength is difficult to estimate (Royama et al., 2005; Myers & Cory, 2013).

The Moran effect states that if two populations have similar population dynamics, the degree of correlation between them should be the same as the correlation in weather variables influencing their respective dynamics (Moran, 1953). The cross-correlation between two populations densities, r_p, should be identical to the cross-correlation between two environmental variables, r (Massie et al., 2015). Experiments can control the environmental drivers and quantify the strength of the Moran effect (Massie et al., 2015; Vasseur & Fox, 2009). Under natural conditions, the Moran effect has been identified in isolation from other mechanisms (without dispersal or natural enemies, Grenfell et al., 1998; Stenseth et al., 1999; Post & Forchhammer, 2002). In the field it is difficult to disentangle the effect of climate from other processes affecting population dynamics.

Synchronous fluctuations of interacting natural enemies may synchronize fluctuations of the fluctuating species (Bjørnstad et al., 2002; Cattadori et al., 2005; Allstadt et al., 2013). For example, predatory birds synchronize vole populations in multiple locations (Ims & Andreassen, 2000). In spatial theoretical

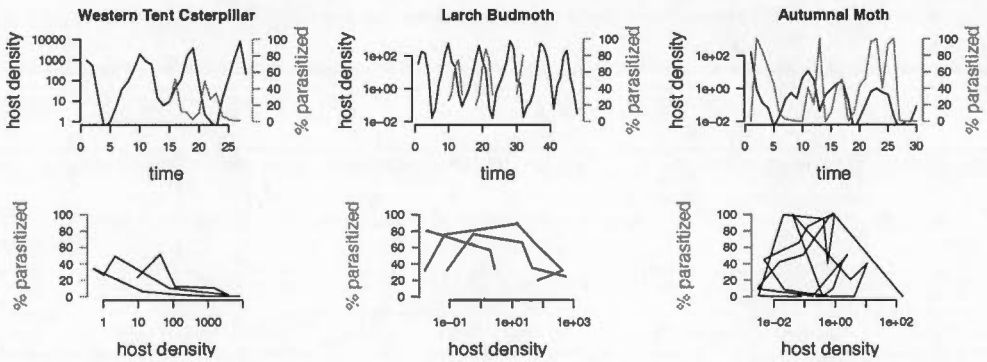

Figure 0.5 Top row, densities of host species (red line, note log scale) and percentage parasitized for (black line) three defoliator species over time. Bottom row, phase plots with host density plotted against percentage parasitized of the same species. Data from Myers & Cory (2013).

models with interacting resources and interacting prey and predators, suggest that biotic interactions can cause regional cycles by predator dispersal (Blasius et al., 1999). These results match lynx population fluctuations which are known to interact with prey such as hare (Blasius et al., 1999; Krebs et al., 2001). For forest insects, parasitoids are strong mortality agents, and parasitism rates oscillate together with host densities for several species (Figure 0.5, Myers & Cory, 2013). Due to particularities in species interactions, coexistence and dispersal dynamics of host-parasitoid systems are very different than predator-prey systems. However, the effect of parasitoids on insect dynamics is often unclear because classic population models cannot be directly validated (Hassell, 2000).

0.4 Modelling framework

I developed a quantitative framework to understand the three main mechanisms that synchronize outbreaks. The landscape-scale model was based on stand defoliation as a proxy for insect population densities. By modifying the transitions to represent different synchronizing mechanisms, the model was used to

investigate multiple hypotheses. I studied local forest transitions between healthy (endemic budworm densities, mature forest) and defoliated (epidemic budworm densities, infected forest) states. The landscape was made up of multiple forest stands (or cells, patches) and each stand could be in different states. The resulting dynamic model was analogous to a metapopulation model (Levins, 1969; Hanski, 1998) in which colonization and extinction probabilities were driven by biological processes. Metapopulation models are especially suitable to represent forest host densities that vary over order of magnitudes. I parameterized the model with spatiotemporal aerial surveys of one complete outbreak cycle and the start of the ongoing one. This simple, mechanistic and data-driven model (Cooke et al., 2007) was extended to explore intrinsic, abiotic and biotic drivers of outbreaks.

In landscape-scale studies experiments are impossible and instead models act as experiments. Usually, data and experiments are combined to investigate mechanisms of small-scale population processes that are amenable to experiments Turchin (1999). Testing the role of continental drivers is unfeasible, and unethical in the case of insect pests. Instead, to test mechanisms of what drives landscape processes, simulation models function as landscape-scale experiments. Outbreak patterns can be described statistically in space and time, but to provide inference into the processes that cause the patterns, simulation models are necessary (Cuddington et al., 2013). Assuming that each mechanism produces a distinct signature (Liebhold et al., 2004; Raffa et al., 2008; Bjørnstad et al., 1999), the model can be compared to data to validate if the model was able to reproduce these signatures. If the model reproduces the observed patterns, this possibly indicates that it is the right model. As solutions are non-unique and more than one model may produce the right fit, the model should be validated (Oreskes et al., 1994). Models should be elaborated from the observed data, and the resulting model should perform experiments to distinguish between hypotheses.

Current models cannot represent all mechanisms in the same framework, only providing a partial understanding of outbreaks. We can divide the currently-used models into two main classes; population models and landscape models (Sturtevant et al., 2015; Keane et al., 2015). Population models fit local density estimates to one- or two species population models, and in spatialized versions, dispersal links population densities in neighbouring populations (Royama, 1984; Williams & Liebhold, 2000). However, population-level data cannot be observed on a landscape-scale, so spatial population models cannot be correctly parameterized. On the other hand, landscape models are parametrized from observed defoliation patterns but they are developed in a top-down manner, in which patterns of outbreaks are imposed (Sturtevant et al., 2015). Therefore, the outbreak patterns do not emerge from underlying processes. Mechanistic landscape models do exist but often have so many parameters and interacting submodels that they become intractable (Keane et al., 2015). Models should reflect biological observations yet should be simple enough that we can understand them. If models are too complicated ecologists get lost in 'parameter space' (Cuddington et al., 2013). The framework presented in this thesis combines the mechanistic and mathematical rigour of population models, with the data and scale of disturbance models.

The modelling framework developed here is landscape (regional)-scale, i.e. the scale at which outbreaks take place. Instead of departing from population-level observations to formulate a population model, I depart from large-scale defoliation observations to formulate a landscape model. The drastic budworm fluctuations inspired the 'multiple equilibria' model, in which resource and predators drive changes between endemic and epidemic states (Ludwig et al., 1978, 1979). This model approaches a presence-absence model because budworm densities have two stable states; high and low, but it is still based on population densities. A coarser response (presence-absence instead of density) can lead to less error and stochas-

tic detail (Buckland & Elston, 1993). When estimating parameters of population processes, small parameter errors in for example growth rates propagate up to cause additional errors (Buckland & Elston, 1993). Fleming et al. (2002) showed that high and low-resolution models display different qualitative dynamics, and that populations with local cycles have stable dynamics when scaled up to a landscape scale. Modelling defoliation signifies a qualitative change in the population density, instead of a quantitative change in the case of population densities, and retains the emergent processes (Levins, 1966).

Using a landscape scale allows the model to be compared directly to defoliation observations from either remote sensing (Jepsen et al., 2009) or aerial survey data (Chapter 2). Using defoliation data to infer population densities is a valid simplification because insect density and defoliation are strongly correlated (Lysyk, 1990; Nealis & Régnière, 2004a; Zhang et al., 2014). Indeed, binary defoliation data is often transformed to continuous pseudo-density data and compared to population models (Williams & Liebhold, 2000; Bjørnstad et al., 2002; Johnson et al., 2006). However, this removes spatial detail and counts dispersal events as local population growth.

My modelling framework is mechanistic and dynamic because it models defoliation transitions, rather than the defoliation itself. Static (correlative, empirical) models test the relationship between the species distribution and explanatory variables, while dynamic models test the relationship between probabilities of transition between states and explanatory variables (Buckland & Elston, 1993). Studying transition probabilities is also advantageous because it allows a phase-dependent, temporally-explicit view of the outbreaks, in which defoliation and dieback probabilities depend on different drivers (Kausrud et al., 2011). Mechanistic models also avoid the assumption that the population is at equilibrium (García-Valdés et al., 2015), and fluctuating species are certainly not in equilib-

Table 0.1 Overview of the hypotheses of spruce budworm outbreaks, explored through various models.

Hypothesis	Model	Citation
Dispersal	Landscape	James et al., 2010
Dispersal	Population	Williams & Liebhold, 2000
Tritrophic	Population	Cooke et al., 2007
Temperature	Population	Régnière, 1987
Density-dependent	Demography	Royama, 1984
Host-plant interactions	Demography	Régnière & Nealis, 2007
Alternative Stable States	Multiple equilibria	Ludwig et al., 1978

rium with climate (Hastings, 2004). To identify what drives outbreaks, one should investigate the colonization and extinction events from which outbreak patterns emerge (Yackulic et al., 2015). Static models are based on statistical theory, while the assumptions of dynamic models are grounded in ecological theory (Cuddington et al., 2013).

Surprisingly, insect epidemics (outbreaks) have never been studied using epidemiological models even though the two are conceptually similar. The fields of epidemiology and metapopulation both study colonization and extinction of organisms among patches (Grenfell & Harwood, 1997; Earn et al., 1998, 2000). Epidemiology is concerned with how a disease affects its host, and less about the details of the disease within the body of the host (immunology and population ecology). Epidemiology constructs mechanistic models of the transmission of disease-causing agents among host organisms, and tries to disentangle extrinsic and intrinsic drivers of outbreaks (Koelle et al., 2005; Cash et al., 2013). The unit of study is the host which may be in one of three states: Susceptible, Infected or Recovered (SIR, Kermack & McKendrick, 1927). SIR models have shown that the type and strength of transmission determines disease dynamics (Keeling, 1999; Keeling & Eames, 2005; Riley, 2007; Rhodes et al., 1998). Epidemiology recognizes that models should be spatially-explicit because transmission probabilities

among populations are not constant (mass action). Rhodes & Anderson (1996) showed that adding spatially-heterogenous transmission can create periodic epidemics, by simulating a spatially-explicit SIR model. Comparing mechanistic epidemiological models to data has shown that 'inapparent' less detectable states, may change outbreak dynamics by increasing transmission (King et al., 2008). In this thesis I studied insect epidemics on a metapopulation scale, which allowed me to incorporate methods from epidemiology.

0.5 Thesis objectives

The objective was to study drivers of outbreaks with a metapopulation and landscape perspective, which allows direct parameterization and comparison between data and models and provides new insight into the processes underlying insect outbreaks. I carried out model simulations in which each stand in the landscape transitioned between endemic and epidemic insect densities, and observed the proportion of patches that were defoliated simultaneously (i.e, outbreaks). In nature, the Allee effect decreases local population growth rates at low densities due to mate-finding effects (Régnière et al., 2013), and was responsible for the episodic outbreaks of Gypsy Moth (Johnson et al., 2006). I determined if the Allee effect can alter dispersal and cause landscape outbreaks in a metapopulation model.

Abiotic drivers such as climate may also cause large-scale outbreaks, but have rarely been studied together with dispersal. In the second chapter, the metapopulation framework developed in chapter 1 was extended to represent both dispersal and climate drivers. It was then compared to observed spatiotemporal defoliation data in order to disentangle their relative importance. The local defoliation transitions were compared to multiple potential climate predictors as well as to the neighbourhood infection prevalence. These estimates were then employed

as parameters in multi-year simulations to identify if positive climate autocorrelation drive outbreaks. Temporal autocorrelation, in the form of successive years with suitable climate, has recently been observed to 'enhance' the spatial Moran effect, but has only been identified theoretically and experimentally (Massie et al., 2015; Gonzalez & Holt, 2002). To determine if spatial or temporal autocorrelation was more important, I carried out simulations with the original spatio-temporally and temporally autocorrelated climate variables.

To represent the role of natural enemies, I extended the landscape model to a metacommunity model with multiple interacting species (Leibold et al., 2004; Gravel et al., 2011b). I reinterpreted defoliation as the expression of biotic interactions between parasitoids and its host (the budworm). Parasitoid dynamics seem idiosyncratic (Tylianakis & Binzer, 2014), possibly because observations cannot be compared to expectations from a theoretical model. I developed a metacommunity model based on landscape-scale processes and data, to test if higher-order parasitoids are important in generating outbreaks.

CHAPTER I

EPIDEMIOLOGICAL LANDSCAPE MODELS REPRODUCE CYCLIC INSECT OUTBREAKS

Hedvig K Nenzén, Élise Filotas, Pedro Peres-Neto, Dominique Gravel

1.1 Abstract

Forest insect outbreaks can have large impacts on ecosystems and understanding the underlying ecological processes is critical for their management. Current process-based modeling approaches of insect outbreaks are often based on population processes operating at small spatial scales (i.e. within individual forest stands). As such, they are difficult to parameterize and offer limited applicability when modeling and predicting outbreaks at the landscape level where management actions take place. In this paper, we propose a new process-based landscape model of forest insect outbreaks that is based on stand defoliation, the Forest - Infected - Recovering - Forest (FIRF) model. We explore both spatially-implicit (mean field equations with global dispersal) and spatially-explicit (cellular automata with limited dispersal between neighboring stands) versions of this model to assess the role of dispersal in the landscape dynamics of outbreaks. We show that

density-dependent dispersal is necessary to generate cyclic outbreaks in the spatially-implicit version of the model. The spatially-explicit FIRF model with local and stochastic dispersal displays cyclic outbreaks at the landscape scale and patchy outbreaks in space, even without density-dependence. Our simple, process-based FIRF model reproduces spatiotemporally synchronous outbreaks and can provide an innovative approach to model and manage forest insect outbreaks at the landscape scale.

Keywords: insects, epidemics, landscape ecology, modeling

1.2 Introduction

Many species undergo massive outbreaks, fluctuations in population densities that occur synchronously in multiple locations, sometimes with surprising regularity in time (Elton, 1924; Liebhold et al., 2004). Forest insects in particular have large recurrent outbreaks, such as spruce budworm, larch budmoth, gypsy moth, autumnal/winter moth (Bjørnstad et al., 2002; Ims et al., 2004; Johnson et al., 2006; Williams & Liebhold, 2000; Tenow et al., 2012). Landscape-wide outbreaks of forest insects produce large-scale defoliation and mortality of host tree species, some extending over millions of hectares. Insect outbreaks modify forest succession and composition, and alter nutrient cycling, with profound consequences on ecosystem functions and services (Boyd et al., 2013; McCullough et al., 1998). These damages have led forest managers in affected territories to seek effective intervention strategies that dampen the consequences of insect outbreaks, and impede their propagation over large expanses.

To guide management, numerous hypotheses to explain outbreaks of forest insects have been explored and/or implemented in what can be broadly divided

into statistical and process-based models (Cuddington et al., 2013). Statistical (phenomenological, static, empirical) models describe and reproduce outbreaks from the characteristics of their distribution (e.g. outbreak location and duration, James et al., 2010). Because these models are derived from data sampled during past conditions, they may have limited ability to forecast the occurrence of outbreaks in changing management and weather conditions (Gustafson, 2013). On the other hand, process-based models (dynamic, mechanistic) are developed from ecological hypotheses about the plant-insect dynamics (Bjørnstad & Grenfell, 2001). Because they are based on ecological processes, these models are thought to be able to predict beyond sampled data (Cooke et al., 2007; Evans et al., 2012).

Most process-based models of insect outbreaks generally represent dynamics of population densities. The design, parameterization and validation of process-based models with local population-level dynamics presents two major difficulties: 1) it requires comprehensive knowledge of the many processes operating at the local population level, and 2) it requires estimates of insect densities. However, these requirements are difficult to meet because relationships between stand-scale processes and insect population dynamics at the landscape scale are mostly studied in single locations (e.g. Royama, 1984). Moreover, if a phenomena is studied at the wrong scale the resulting conclusions may be weak or unreliable (Meentemeyer et al., 2012; Peters et al., 2004b). To circumvent this lack of data and avoid scale-mismatch, we investigate a landscape-scale model that is independent of small-scale within-stand population processes. The model represents forest stands with three possible states: F, a forest stand at endemic insect densities, I, an infested / infected stand at epidemic insect densities, and R, a recovering stand in which forest regenerates following defoliation. The model exploits the fact that stand densities of forest insects show extreme fluctuations between endemic and epidemic periods, corresponding to the forest or infected states (Royama, 1984). We refer

to this model as a FIRF landscape model and explore its capacity to reproduce the macroscopic properties of insect outbreaks.

The FIRF dynamic model of forest insect outbreaks follows the frameworks of metapopulation and epidemiological models. In metapopulation models, local populations can be present or absent, and regional persistence depends on dispersal (Levins, 1969; Hanski, 1998). This wide class of models are also called disturbance-recovery, state-transition, occupancy and patch-dynamic models and have been applied to various ecological situations, such as fires (Malamud et al., 1998; Staver & Levin, 2012; Keane et al., 2015), mussel bed colonization (Guichard et al., 2003) and clustered patterns of desert vegetation (Kéfi et al., 2007). Similarly, epidemiological models consider hosts (analogous to local populations in the metapopulation models) as infected or not, and do not track the density of infectious agents within each host. Epidemiology provides a tractable theory to understand epidemics and applies vaccines against human, animal and plant diseases (Kermack & McKendrick, 1927; Riley, 2007; Keeling & Rohani, 2008). Epidemiological models in which one patch represents one host have been used to model dynamics of theoretical (Rhodes et al., 1998; Fuentes et al., 1999; Filipe & Maule, 2004; Neri et al., 2011b) and real epidemics (Kleczkowski et al., 1997; Eisinger & Thulke, 2008; Neri et al., 2011a; Filipe et al., 2012). Metapopulation and epidemiological models are related because both deal with the absence or presence of a species in multiple locations, not local densities (Earn et al., 1998; Grenfell & Harwood, 1997; Rhodes et al., 1998). However, to our knowledge, epidemiological and metapopulation landscape models have rarely been applied to study cyclic forest insect landscape epidemics (Keane et al., 2015).

The goal of this paper is to build a simple, macroscopic and process-based epidemiological model to explore the consequences of dispersal on insect outbreaks. Metapopulation and epidemiological models easily map onto the land-

scape dynamics of forest insects and present certain advantages over population models. Focusing on forests instead of insects matches the type of large-scale data surveyed regarding the effects of outbreaks (tree defoliation), not the density of insects (Gray, 2008; Bouchard & Auger, 2014). Simplifying the model by using a lower modeling resolution is computationally efficient and requires fewer parameters. Just like epidemiological models do not model virus densities within infected individuals, modeling the number of insects is too fine-scale to be informative at a landscape-level. The desired output for forest management is the proportion of forest stands that are affected, and for that reason we model forests instead of insects. Using metapopulation and epidemiology theory would allow forest managers to use insights from those fields, for example that the strength and type of disease transmission are essential determinants of distribution and epidemics (Hanski, 1998; Riley, 2007; Keeling et al., 2003).

We study two versions of our model: a spatially-explicit version in which insects disperse among forest stands arranged on a grid, and a spatially-implicit version with global dispersal (between all forest stands regardless of location). Comparing both versions reveals how limited dispersal distance of insects contributes to outbreak dynamics at the landscape scale. Our goal is to understand the conditions at which outbreaks occur, and to characterize the spatiotemporal signature of outbreaks emerging from between-stand insect dispersal. We first describe the rationale of the modeling approach, here inspired by the ecological dynamics of the spruce budworm, a major defoliator of North American forests. We then provide a detailed description of the spatially-implicit and spatially-explicit stochastic dispersal versions of the model. We explore the structural and parameter sensitivity of the model to understand the critical conditions required for outbreaks to occur. We specifically answer three questions; 1) Which dispersal parameters are required to produce outbreaks? 2) Which dispersal parameters

determine cyclic outbreaks? 3) Which dispersal parameters determine the spatial distribution of outbreaks?

1.3 Methods

We develop a general model of defoliating insect dynamics at the landscape scale, whose implementation is largely inspired by the extensive literature on the spruce budworm *Choristoneura fumiferana*. Spruce budworm outbreaks have occurred with intervals of around 30 years during the last 500 years (Morin et al., 2007; Boulanger et al., 2012), and have profoundly structured the dynamics of North American forests (Fleming, 2000). Budworm outbreaks damage around 15% of the surface of Canadian forests during each outbreak (NFS, 2013), representing large revenue losses.

1.3.1 FIRF model overview

The modeling unit is a forest stand and each stand can be in one of three possible states: F forest, I infected defoliated forest, and R recovering forest (Fig. 1.1). We adapt the epidemiological Susceptible-Infected-Recovering-Susceptible model ($SIRS$, Hethcote, 1976; Anderson & May, 1979) to insect outbreaks that have a dispersing consumer feeding on a stationary regenerating resource. Note that in our model each stand can only take one value, in contrast to population-based lattice models that simulate the fraction of states in each stand. The F forest and I infected states correspond to endemic and epidemic densities of spruce budworm that fluctuate over several order of magnitudes (Royama, 1984). During endemic periods the species is described as rare, while during epidemics there are hundreds of feeding larvae per kilogram of host foliage (Régnière et al., 2013). In our model, mature forest stands F have an endemic budworm density which does not cause stand-scale defoliation, thus the stand does not display symptoms

of infection. Infected stands I have an epidemic density of insects and display signs of defoliation. There is a recovering, immature forest state R because after defoliation forests die and regenerate, and young forests are rarely infected by budworm (Erdle & Maclean, 1999). Previous studies have shown that infection occurs more in mature forests ($>$ 60 years) compared to immature forests (85% vs. 42%, respectively, for the main host of spruce budworm (Balsam fir) from 1914-1979 outbreaks in Eastern North American temperate forests, Maclean & Olstaff, 1989). For simplicity we limit our investigation to only one type of host forest and have omitted unpalatable deciduous trees. The budworm completes its life cycle in one year, which we equate with one time step in the model.

A mature (susceptible) forest stand F can become infected I in two ways (Fig. 1.1). This is similar to epidemiological models where disease can be acquired by a primary, 'index' infection from an external source, or from a secondary transmission from an already infected host (Rhodes et al., 1998). First, a forest stand can be infected seemingly spontaneously when low densities transition to high densities even when no neighboring cells are infected, a so-called 'epicenter' (Hardy et al., 1983; Cooke et al., 2007). The probability of a spontaneous infection is set by the parameter β. The cause of a local infection is difficult to identify, and many studies have focused on linking their presence to factors such as weather, long-distance dispersal and natural enemy release (Blais, 1958; Royama et al., 2005). We explore the model both with and without spontaneous infection.

Second, a transition from forest F to infected I in one stand can occur due to insect dispersal from neighboring infested stands and successive establishment, with probability α. After an epicenter has occurred, dispersal is an important driver of spruce budworm dynamics (Williams & Liebhold, 2000; Cooke et al., 2007). Most dispersal occurs between neighboring stands. For example, during the 2003-2011 northern Quebec outbreak, dispersal events occurred 10-80 km from

an infected location (Bouchard & Auger, 2014). Although the budworm may be capable of occasional long-distance dispersal (Greenbank, 1980), this is difficult to quantify. We consider the side of a single stand to be 1-10 km, and we set the radius of dispersal to two stands. The dispersal range therefore covers the 24 stands closest to the stand of origin.

Dispersal dynamics of forest insect pests are often density-dependent, and more specifically driven by densities in the origin or arrival stand (Bowler & Benton, 2005). Mating success is lower at endemic population densities, due to an Allee effect (Régnière et al., 2013). We do not track insect densities explicitly and consequently indirectly model density-dependent dispersal through the proportion of infected stands in the neighborhood. Dispersal may be affected by insect densities around the stand where dispersal originates from, or by densities around the stand where dispersal arrives. Egg-laying females in infected high-density stands emigrate to uninfected stands to avoid food shortage (Royama, 1984; Nealis & Régnière, 2004a; Régnière et al., 2013). Alternatively, there is a lower probability of successful mating and immigration in arrival stands surrounded by uninfected stands. We explore landscape consequences of the Allee effect in the spatially-implicit model, and the consequences of emigration- and immigration-driven dispersal in the spatially-explicit model.

Emigration We consider that probability of emigration from the infected origin stand depends on the number of infected stands around the origin stand. As such, probability of dispersal from the origin stand depends on the number of infected stands in the neighborhood centered around the origin stand (the 24 closest stands).

Immigration Alternatively, we consider that the probability of a successful immigration is affected by the number of infected stands around the arrival stand. As such, the probability of dispersal to an arrival stand depends on the number of infected stands in the neighborhood centered around the arrival stand (the 24 closest stands).

Once a stand is infected, the infected forest has a probability γ_2 of dying and transitioning to a recovering forest stand. We assume that infection is lethal, meaning that once a forest stand has become infected, it cannot return to the mature forest state. We omit for simplicity trees that may be weakly defoliated and survive a spruce budworm outbreak episode (MacLean, 1980). We assume that budworm is the only source of forest stand mortality in the model and disregard senescence, especially because old-growth forests can also show budworm infection.

Recovering stands reach maturity with probability γ_1. The boreal forest has aerial seed dispersal and seedlings continuously establish underneath the forest canopy. Boreal coniferous species, at least Balsam fir, white and black spruce, have abundant natural regeneration (Bergeron et al., 1995) and therefore we omit spatially explicit dispersal constraints for trees. Therefore recovery to mature forest is a non-spatial process (well-mixed, Pascual & Guichard, 2005) that depends only on the total proportion of recovering forest in the landscape, $\gamma_1 R$.

Spatially-implicit model formulation

We now translate the biological description of the forest-insect dynamics given above to a spatially-implicit model with global dispersal. It is a mean-field approximation of the spatially-explicit model described later on and represents dynamics at the landscape scale, i.e. the variations in the amount of stands in each of the three states: forest F, infected I and recovering R. We therefore adapt

the compartmental Susceptible-Infected-Recovering-Susceptible model ($SIRS$) to insect outbreaks that have a dispersing consumer feeding on a regenerating resource. The landscape where infections take place contains a fixed number of forest stands, so the total proportions of stands in each state represent the landscape, $F + I + R = 1$ and $R = 1 - F - I$. The following system of two coupled differential equations describes the FIRF forest landscape dynamics (Fig. 1.1):

$$\frac{dF}{dt} = \gamma_1(1 - F - I) - \beta F - \alpha f(I)[1 - (1 - I)^{24}]F \tag{1.1a}$$

$$\frac{dI}{dt} = \beta F + \alpha f(I)[1 - (1 - I)^{24}]F - \gamma_2 I \tag{1.1b}$$

As described above, infection of a forest stand F occurs in two ways, either by a spontaneous infection, whose probability is set by β, or by insects dispersing to a mature forest stand from an already infected stand I, set by α. Transmission of infectious agents in epidemiological models is usually approximated by mass action where the transmission probability is proportional to the prevalence of both susceptible and infected states (i.e. αFI). In our model host trees are stationary and the transmission probability corresponds to insect dispersal. Each stand is potentially surrounded by multiple infected stands, but a single successful dispersal event is sufficient to cause infection. The neighborhood of each stand is the closest 24 stands, and the probability at which a no-dispersal event occurs from all 24 of them is thus $(1 - I)^{24}$. The probability of dispersal from *at least one* neighbor is $1 - (1 - I)^{24}$ (Fukś & Lawniczak, 2001; Guichard et al., 2003). This approximation allows us to implicitly include space, so a high proportion of infected forest stands means a high density of insects and population growth and indirectly a higher probability of infection.

The function $f(I)$ sets the density-dependent dispersal as follows (Fig. A.1, Hethcote & Levin, 1989):

$$f(I) = I^p I \tag{1.2}$$

Where p is a positive real number <= 1. An Allee effect is simulated as p gets closer to 1, indicating a lower infection probability when few stands are infected (Fig. A.1).

Spatially-explicit model formulation

We run a spatially-explicit model to investigate the effect of local dispersal on the infection dynamics. We consider a cellular automaton where each cell is a forest stand, and each stand is in *only* one of three potential states: mature forest, F, infected, I, or recovering, R. Therefore, the *total* proportion of each state is equivalent to the proportion modeled by the mean-field model. The transition rules between states are the following:

$$F \rightarrow I \text{ if } \beta \geq h \tag{1.3a}$$

$$F \rightarrow I \text{ if } \alpha f(I) \geq h \tag{1.3b}$$

$$I \rightarrow R \text{ if } \gamma_2 \geq h \tag{1.3c}$$

$$R \rightarrow F \text{ if } \gamma_1 \geq h \tag{1.3d}$$

where h is a uniformly distributed random number between 0 and 1. Dispersal depends on the proportion of infected stands in the immediate neighborhood, and one successful dispersal event is enough to cause an infection. Moreover, in the spatially-explicit version we differentiate between two types of dispersal process, immigration and emigration, which are characterized by different density-

dependent dispersal function.

Immigration Density-dependence in the arrival stand is represented by computing the number of infected stands surrounding the arrival stand (Fig. A.2). We determine $\overline{I}_F$, the proportion of infected stands in the neighborhood centered on arrival stand F. The dispersal function becomes:

$$f(I)_{Imm} = \overline{I}_F{}^p \tag{1.4}$$

Emigration Density-dependence from an infected origin stand is represented by computing the number of infected stands surrounding this origin stand (Fig. A.2). We determine $\overline{I}_I$, the proportion of infected stands in the neighborhood centered on origin stand I. The dispersal function becomes:

$$f(I)_{Emi} = \overline{I}_I{}^p \tag{1.5}$$

1.3.2 Model implementation and analysis

We compare the spatially-implicit and -explicit versions of the FIRF model with numerical simulations and specifically study the impact of dispersal α and density-dependence p parameters on occurrence, frequency and amplitude of outbreak cycles. We define outbreaks as cyclic oscillations in the proportion of stands that are infected (synchronized) and that the infected state covers more than 10% of the landscape at its maximum. To assess the presence of outbreaks we record the minimum and maximum proportion of infected stands I during each simulation. Furthermore, if outbreaks occur, we identify whether they are cyclic with regular return intervals, or episodic with irregular intervals. To determine the

outbreak interval in each simulation we calculate the spectral frequency with a Fast Fourier Transform and smooth the data with a window of 10 periodicities. The dominant period (the reciprocal of the frequency) that has the highest spectral power contributes most to the oscillations observed in the time series. We calculate the average dominant period of all repetitions above the threshold under the same parameters. All analyses were performed in the R environment (R Core Team, 2012).

We present the results from simulations without ($\beta = 0$) and with spontaneous infections ($0.00025 < \beta < 0.005$). Parameters α and p are varied $0 - 1$ in increments of 0.05 (Table S1), while β is varied $0 - 0.005$ by increments of 0.00025. The minimum time to reach mature forest in North American boreal forests range is 40 years (Burns & Honkala, 1990), and therefore we set γ_1 to 1/40. Tree mortality usually begins in the fifth year of infection, and full mortality occurs after around 10 years, when the tree is completely defoliated and unable to photosynthesize (MacLean, 1980). The infection duration at the stand scale varies regionally from 1-25 years (Gray, 2013). We therefore set γ_2 to 1/3, based on the number of years the infection lasts before killing a forest stand. Both spatially-implicit and -explicit simulations last 20 000 time steps and we discarded the first transient 1 000 steps. Each time step represents one year. The initial proportions are $F = 0.4$, $I = 0.1$ and $R = 0.5$.

Spatially-implicit model

Local stability analysis is performed to identify the critical conditions required for the occurrence of damped or sustained oscillations at different parameter values (Figure 1.2, Soetaert, 2009). Local stability analysis consists of evaluating the Jacobian matrix at the positive equilibrium points. Oscillations occur if the eigenvalues of the Jacobian are complex. Because the equations with

density-dependent dispersal in function $f(I)$ (Eqn 1.2) cannot be solved analytically, we use numerical local stability analysis instead of analytical. However, for comparison the analytical solutions for global mixing in dispersal, αFI, are presented in Supplementary materials section A.2. We numerically simulate the spatially-implicit model with a Runge-Kutta fourth-order integration with a time step of 0.1.

Spatially-explicit model

For the spatial simulations we use a square lattice of N^2 forest stands with periodic boundary conditions (torus, $N = 100$). As initial conditions we use the same proportions of states from the spatially-implicit model, distributed randomly in space. In each time step (year) we randomly select N^2 stands and update their states. A stand may therefore have no or multiple state changes per stand in a single time step. This method approximates continuous mean-field dynamics (asynchronous updating, Durrett & Levin, 1994). We run 20 stochastic simulations for each set of parameters.

We characterize the spatial structure of clustered infected stands, and measure if these clustered stands display a range of different sizes. The log-log slope of the size-frequency distributions can be fitted with a power-law relationship, and its exponent reflects how the size of infection patches is related to their frequency. The frequency distribution of many ecological phenomena display such scale-free behaviour (Pascual & Guichard, 2005). Human epidemics have been reported to exhibit power-law scaling (Rezende & Anderson, 1997). We define an infection patch as the spatially contiguous collection of infected stands that are connected by any of their 8 closest neighbors (Moore neighborhood). We determine the frequency of the different-sized infection patches by aggregating outbreaks from the 100 years with the highest outbreak proportion (indicated by n on Figure 1.4).

We then calculate the exponent of the relationship using a maximum likelihood estimator (Clauset et al., 2009).

1.4 Results

The FIRF models produce outbreaks in certain regions of parameter space and both with and without spontaneous infection ($\beta > 0$ or $\beta = 0$). In general, the conditions required to observe outbreaks differ between the spatially-implicit and -explicit models (Table 1.1, Fig. 1.3). The spatially-implicit model is deterministic while the spatially-explicit one is stochastic, which might explain the difference between them. We thus investigate if the stochastic models itself causes outbreaks and examine the cellular automaton with global dispersal between random stands. There are no outbreaks in a stochastic spatially-implicit model (i.e. global dispersal, results not shown), indicating that local dispersal between neighboring stands causes outbreaks, not stochastic dynamics.

Density-dependent dispersal promotes the occurrence of outbreaks in both local stability analysis (Supplementary materials sections A.1-A.2) and simulations in the spatially-implicit model (Eqns 1.1a - 1.1b). With density-independent dispersal ($p = 0$, Eqn 1.2), there are damped oscillations (complex eigenvalues with negative real parts, results not shown). With density-dependent dispersal ($p > 0$) there are both unstable and stable dynamics in different regions in parameter space (Fig. 1.2). On the bifurcation boundary between the positive and negative eigenvalues there should be eigenvalues with zero real parts which indicate cyclic outbreaks. In spatially-implicit numerical simulations up to half of the landscape can become infected simultaneously during outbreaks (Fig. 1.3 A, B for example simulations). With density-independent dispersal there are damped oscillations ($p = 0$, Fig. 1.3 A) and with density-dependent dispersal there are sustained cyclic outbreaks ($p > 0$, Fig. 1.3 B). Outbreaks are observed under certain

conditions of dispersal, namely when $0.4 < p < 0.5$ (Fig. 1.5A) and $0.1 < \alpha < 0.3$ (Fig. 1.5 D). Without spontaneous stand infection $\beta = 0$, there are no outbreaks in the spatially-implicit model (dotted lines in Fig. 1.5 A, D).

Outbreaks in the spatially-explicit model occur at the same parameters as in the spatially-implicit model, but also in larger regions of parameter space (Eqns 1.3a - 1.3d, Fig. 1.3 C, D for example simulations). With emigration-driven dispersal up to 30% of the area is infected at the same time (Fig. 1.5 C) and with immigration-driven dispersal outbreaks are smaller. Spatially-explicit simulations are less sensitive to the strength of density-dependent dispersal p (Fig. 1.5 B, C) and outbreaks occur when strength of dispersal $\alpha > 0.1$ (Fig. 1.5 E, F). In the absence of spontaneous infection sustained outbreaks occur in smaller regions of parameter space (Figs. A.3, 1.5 B, C, E, F).

Dispersal affects if outbreaks are cyclic (periodic) or irregular and the number of years between outbreaks (return interval). In both spatially-implicit and explicit models, outbreaks occur every 30-40 years at low values of density-dependence p (Fig. 1.6 A, B, C) and moderate dispersal α (Fig. 1.6 D, E, F). Spatially-explicit models produce longer cycles with stronger density-dependence p and stronger dispersal $\alpha < 0.6 - 0.8$ removes all cyclic outbreaks.

The spatially-explicit models generate clustered spatial structures (Fig. 1.4 A, B). The size of infection patches is larger when there are few spontaneous infections and moderate dispersal; when rare infections disperse through large areas of undisturbed susceptible forest (in terms of number of contiguous infection patches, Fig. 1.7 A, B). The outbreak size-frequencies indicate that the FIRF model has fewer large and more small infection patches, and the slope of the relationship is dependent on the parameters and model type. With low dispersal ($0.1 < \alpha < 0.2$), the slope is shallower, producing a larger proportion of large

and fewer smaller infection patches (Fig. 1.7 C, D). Emigration-driven dispersal produces more spatially clustered outbreaks for most parameter sets.

1.5 Discussion

We developed a process-based landscape model that simulates spatiotemporally synchronized insect outbreaks. Our model is inspired by Levins (1969) metapopulation model, but instead of presence and absence of species in habitat patches we simulate presence or absence of pest infections in forest stands, drawing inspiration from epidemiological models. Our framework, therefore, reflects observed endemic and epidemic periods as well as outbreak epicenters (Cooke et al., 2007). The process-based landscape FIRF model proposed here generates outbreak intervals comparable to real outbreaks, around 30 years (Boulanger et al., 2012). We find that dispersal alone in some regions of parameter space produces outbreaks, even without spontaneous infection. This implies that dispersal is sufficient to cause synchronous outbreaks, and that other processes may not be instrumental in explaining cyclic outbreaks. While damped oscillations are not sustained oscillations *per se*, they can result in quasi-periodic fluctuations when further amplified by environmental stochasticity (Peltonen et al., 2002; Ripa & Ranta, 2007). Our results highlight the necessity of explicitly modeling the spatial dimension when studying landscape-scale insect outbreaks, demonstrating the importance of dispersal in the emergence of insect outbreaks.

The model generates outbreaks with both spatially-implicit and -explicit dispersal, but through different processes. Density-dependent dispersal is necessary for the onset of outbreaks in the spatially-implicit model, but not in the spatially-explicit one. This means that outbreaks arise from the spatial implementation itself and does not require nonlinearity in dispersal. Even though dispersal is stochastic in each stand in the spatially-explicit model, on a landscape-scale

outbreaks recur with regular intervals. The spatially-explicit model formulation is more robust because the same results are obtained over a wider range of parameter values. Emigration-driven density-dependent dispersal produced larger outbreaks, suggesting that stand-specific resource-limitations can cause landscape outbreaks and should be further studied.

Our metapopulation-epidemiological FIRF model presents certain advantages over population-based models. The biggest advantage is that it does not require estimates of insect densities, which are difficult to obtain for entire landscapes, in particular for endemic densities. This means that the model could be parameterized using aerial observation data (as in Bouchard & Auger, 2014), and then used to validate dispersal assumptions. It is beyond the scope of this study to validate the model with observed outbreak data, and theoretical models can be useful without being parameterized from data (e.g. Blasius et al., 1999; Bjørnstad et al., 2002). Another advantage is that local population dynamics are represented only by their stand impact, so the FIRF model requires fewer adjustable parameters than a population model. Future studies could expand on the proposed theoretical framework to advance the understanding of forest insect landscape dynamics. For example, one could easily investigate the effect of landscape heterogeneity and connectivity on the dynamics of outbreaks. The effect of future environmental conditions on insect outbreak dynamics could also be evaluated by exploring different parameter values for forest mortality, γ_2, and recovery, γ_1. Although our model formulation was inspired by the spruce budworm, the parameter exploration suggests that our model is quite flexible and can be used to study various forest insect defoliators with different life histories and population characteristics. Not all insect defoliators display outbreaks (Liebhold & Kamata, 2000), just like some sets of parameters do not produce outbreaks.

We show that spatial models are preferable to study synchronized recurrent

outbreaks, which has practical implications for epidemiology because a correct model formulation is essential to implement effective vaccination programmes. For example, an individual-based model fit observed rabies occurrence data better than a classical mean-field formulation, and could offer more effective spatial vaccination strategies (Eisinger & Thulke, 2008). There are spatial epidemiological models with a variable transmission probability as implemented here, but they ignore recurrent infections and only follow the dynamics of one outbreak (but see Silva & Monteiro, 2014). Our model improves understanding of dispersal on recurrent landscape outbreaks, which is important for many epidemics, including forest insects.

1.6 Conclusion

Current forest management practices to control insect outbreaks are spatially-implicit, so the proposed spatially-explicit landscape model could improve management interventions. The model could be useful to elaborate outbreak management strategies for three reasons. First, it is a process-based model which is advantageous because it is driven by documented ecological processes and can be used under changing conditions (Cuddington et al., 2013). Second, the model is formulated at the scale at which landscape management occurs, i.e., forest stands, which is advantageous both theoretically and practically(Meentemeyer et al., 2012; Stevens et al., 2007). Third, due to its similarity to the highly applied discipline of epidemiology, our ecological metapopulation model opens new perspectives towards managing insect outbreaks. Here we show that lower dispersal probabilities produce smaller outbreaks, both in individual outbreak size and in total infected area. Management strategies could weaken outbreaks by minimizing insect dispersal through modifying the connectivity of susceptible mature forest stands, logging and/or establishment of non-host forest stands. Future versions of the model could be coupled with epidemiology-inspired management practices and

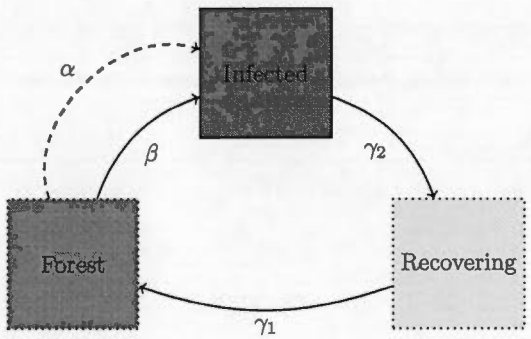

Figure 1.1 Schema of the transitions between the three different states of the Forest-Infected-Recovering-Forest model of forest insect outbreaks. β is the probability of spontaneous infections, α is the probability of infection spread, γ_2 is the probability of infection dieback, γ_1 is the probability of forest recovery to mature, susceptible forest (also see Table A.1).

explore their effects on outbreaks. Our process-based landscape FIRF framework suggests that interventions beyond the stand scale could lead to effective forest management by interfering with the spatial processes inherent in insect outbreaks.

1.7 Acknowledgements

Funding was provided by the Forest Complexity modeling program, Natural Sciences and Engineering Research Council of Canada - Collaborative Research and Training Experience and Discovery programmes, Canada Research Chairs, Université du Québec à Montréal and a Doctoral Research Fellowship from the Fonds de recherche du Québec - Nature et technologies. Thanks to Yan Boulanger, Lukas Seehausen and Veronique Martel for spruce budworm discussions, and to Christian Messier and Frédéric Guichard. Thanks to Amael Le Squin, Renato Silva, Alyssa Butler and numerous reviewers for comments on the manuscript.

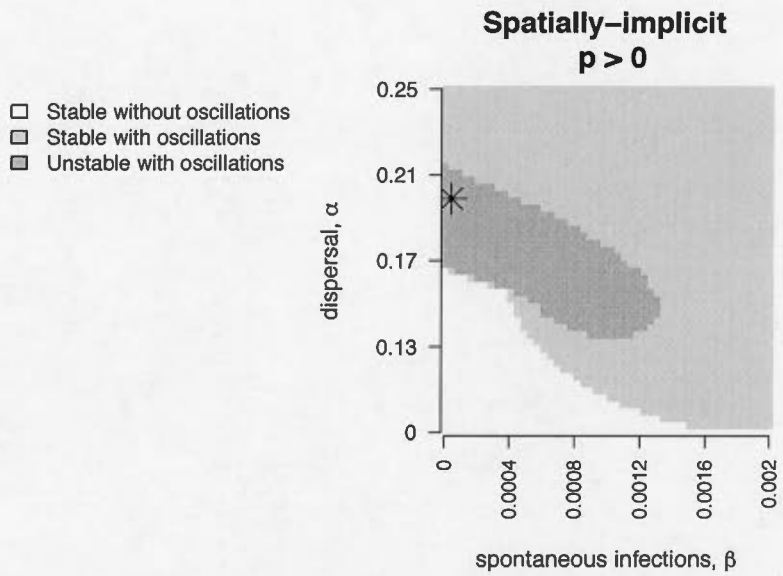

Figure 1.2 The presence of cyclic outbreaks of the density-dependent spatially-implicit model under different strengths of β and α probabilities. At low parameter values the dynamics are stable (negative eigenvalues, white). At higher dispersal α the dynamics become unstable with oscillations (complex eigenvalues with positive real parts, dark grey). At higher dispersal β and α the dynamics are stable with damped oscillations (complex eigenvalues with negative real parts, light grey). The parameters of Fig. 1.3 are indicated by the black star.

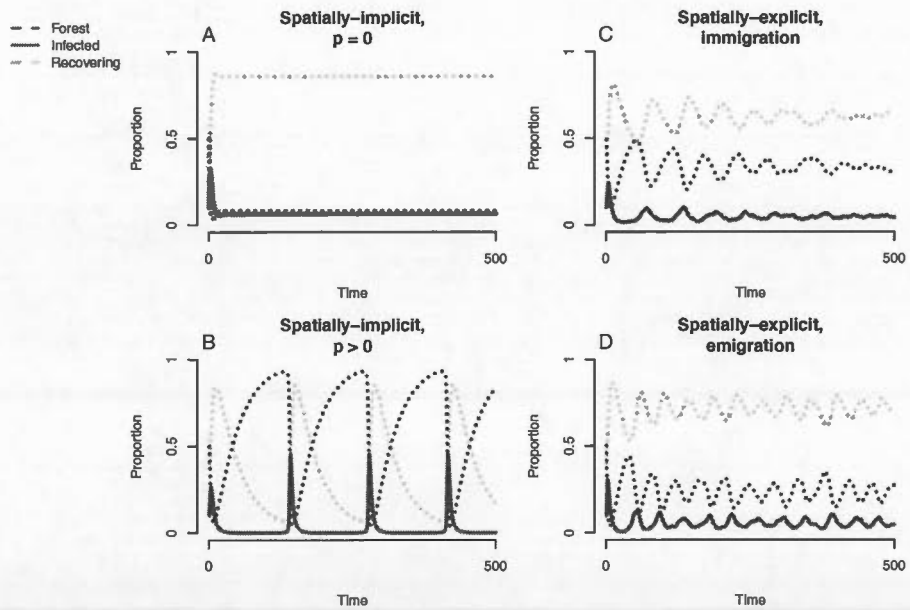

Figure 1.3 Examples of FIRF model simulations with the proportion of each forest state over time. A, Spatially-implicit model with density-independent dispersal ($p = 0$) and B density-dependent dispersal ($p > 0$). C, spatially-explicit immigration-driven density-dependent dispersal ($p > 0$). D, spatially-explicit emigration-driven dispersal model ($p > 0$). The parameters used are $\alpha = 0.2$, $\beta = 0.001$, $\gamma_1 = 1/40$, $\gamma_2 = 1/3$ and $p = 0.4$. We show the dynamics with $\beta = 0$ in Figure A.3.

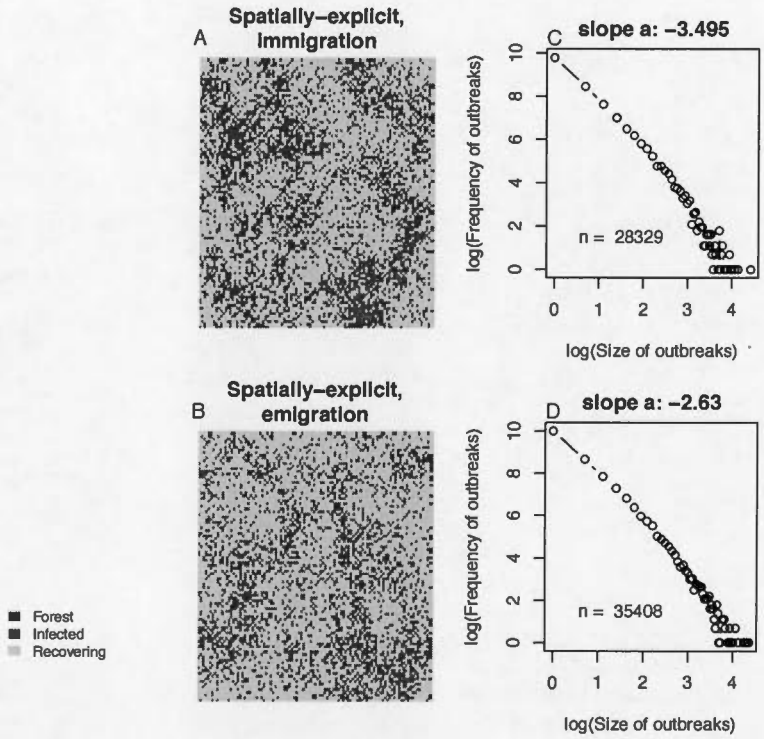

Figure 1.4 The spatial distribution of stands in one year during the simulation runs in Figure 1.3 (A, immigration-driven dispersal, B, emigration-driven dispersal) and the corresponding power-law slope (C, immigration-driven dispersal, D, emigration-driven dispersal). n indicates the number of infected patches that were used to calculate the power law, aggregated from the 100 years with highest infection prevalence in each simulation. Stands have the same colours as in 1.3 and the landscape scale is 100^2 stands.

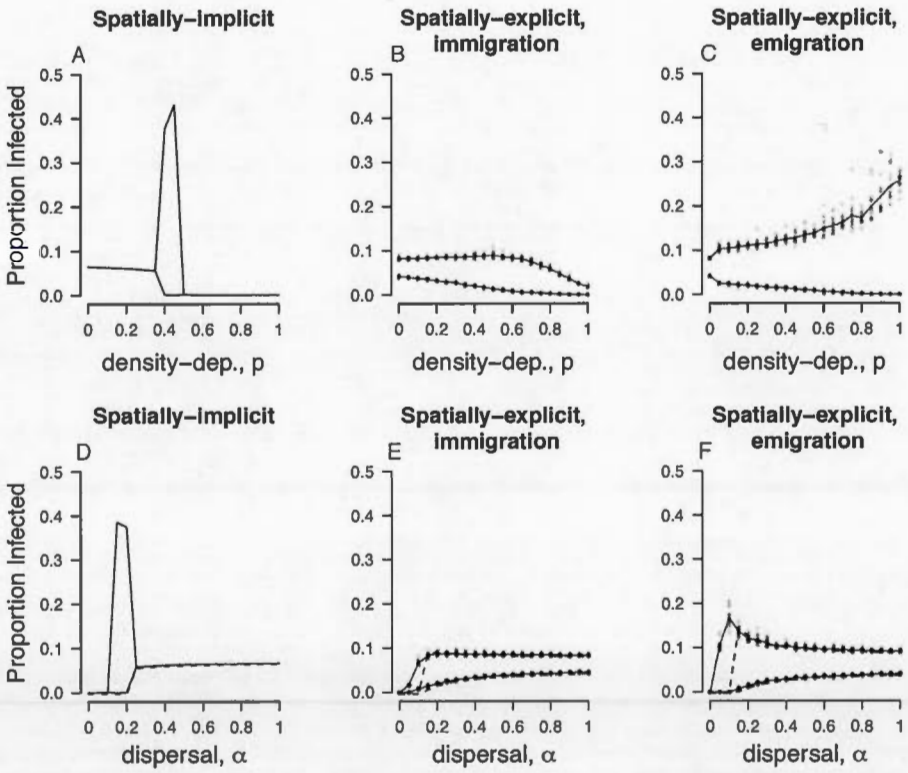

Figure 1.5 The minimum and maximum proportion of infected area per simulation as a function of density-dependence p (A-C) and dispersal α (D-F). Solid lines indicate averages from simulations with $\beta = 0.0001$ and points indicate values from each simulation. Dotted lines indicate $\beta = 0$. For clarity we do not show the values of each simulation when $\beta = 0$. A, D, Spatially-implicit model. B, E, Spatially-explicit immigration-driven dispersal, C, F, Spatially-explicit emigration-driven dispersal. Other parameters are the same as in Fig. 1.3. The proportion infected is calculated after the transient period of 1 000 years.

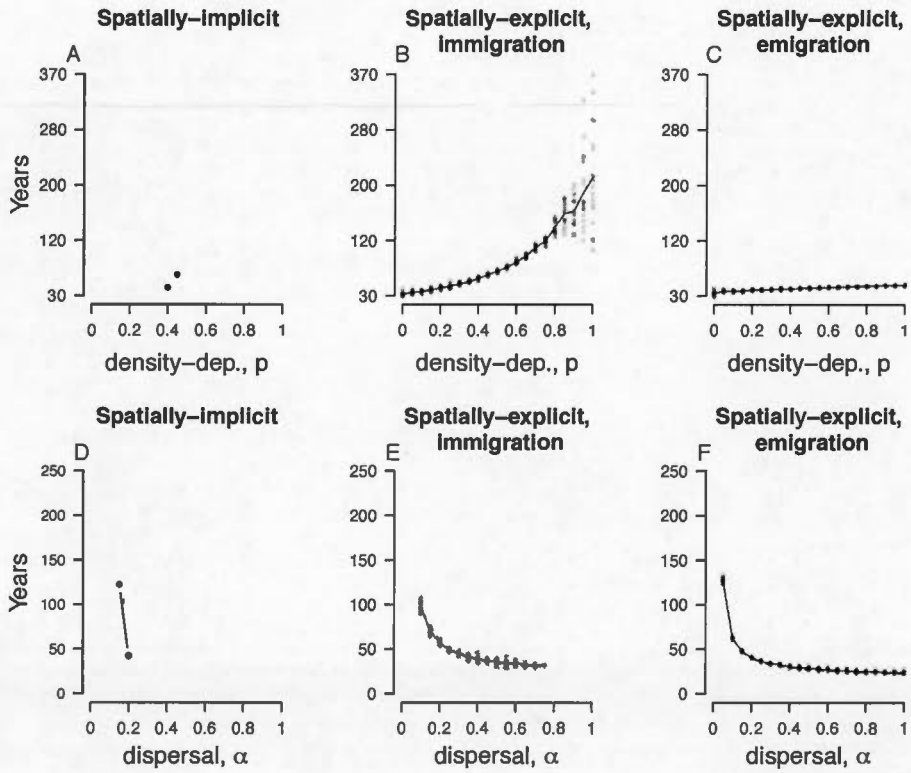

Figure 1.6 The length of outbreak return intervals as a function of density-dependence p (A-C) and dispersal α (D-F). Solid lines indicate averages from simulations with $\beta = 0.0001$ and points indicate values from each simulation. Dotted lines indicate $\beta = 0$. For clarity we do not show the values of each simulation when $\beta = 0$. Missing lines indicate that there is no periodicity. A, D, Spatially-implicit model. B, E, Spatially-explicit immigration-driven dispersal, C, F, Spatially-explicit emigration-driven dispersal. Other parameters are the same as in Fig. 1.3.

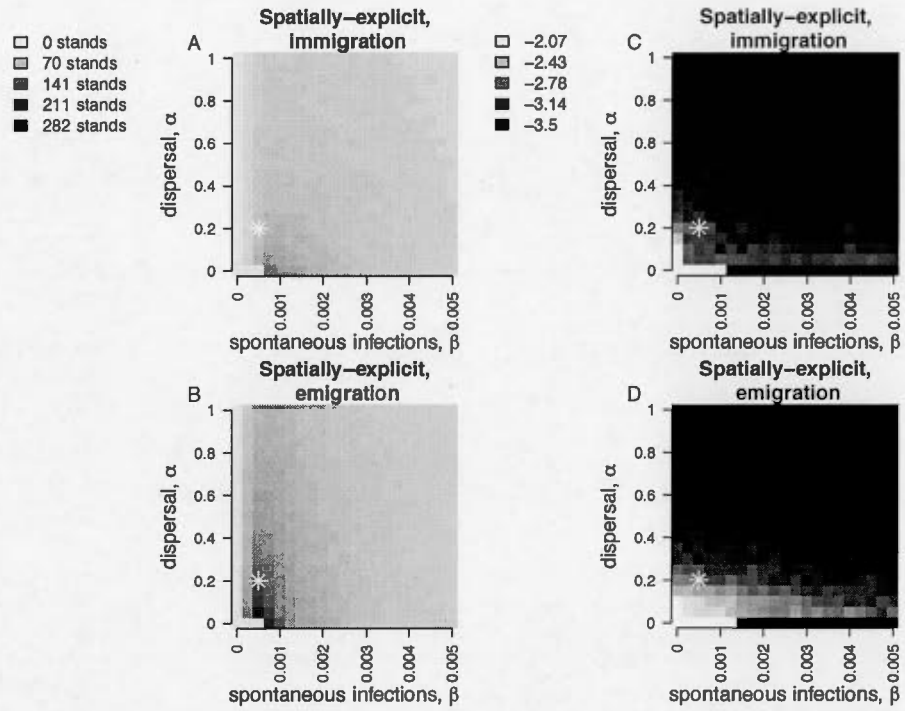

Figure 1.7 The average size of the largest infection patch (A, C, maximum number of stands per infection patch, average for 20 repetitions) and the average exponent of the power-law slope (C, D, average for 20 repetitions). A shallower slope indicates a higher proportion of larger infection patches, which would be expected when there are large outbreaks. The parameters used in Fig. 1.3 are indicated by the star.

Table 1.1 Conclusions from comparing the results from both spatially-implicit and -explicit FIRF models under different types of density-dependence. 'Yes' indicates that outbreaks occur under at least some parameter values. For the local stability analysis of the spatially-implicit model, outbreaks (damped or sustained oscillations) are indicated by the presence of complex eigenvalues. Outbreak cyclicity is assessed by numerical simulations.

Model	Density-dependence	One outbreak	Cyclic outbreaks	Patchy landscapes
Spatially-implicit	$p = 0$	yes	no	-
	$p > 0$	yes	yes	-
Spatially-explicit	$p = 0$	-	yes	yes
- immigration	$p > 0$	-	yes	yes
- emigration	$p > 0$	-	yes	yes

CHAPTER II

MORE THAN MORAN: COUPLING STATISTICAL AND SIMULATION MODELS TO UNDERSTAND HOW DISPERSAL AND CLIMATE VARIATION DRIVE OUTBREAK DYNAMICS

Hedvig K Nenzén, Pedro Peres-Neto, Dominique Gravel

Abstract

Understanding the processes that underlie species fluctuations is crucial to the development of efficient management strategies for outbreaks of destructive forest pests. Yet, despite many empirical and theoretical studies of species fluctuations, the role of biotic and abiotic factors as well as their interactions in driving large-scale outbreaks is far from well understood. Here, we set out a modelling framework to investigate how dispersal and autocorrelated climate variables relate to outbreaks of a major defoliator of North American boreal forest, the spruce budworm. We developed a model to represent the regional dynamics of spruce budworm and based the model on data collected from spatiotemporal aerial surveys of defoliation from 1968-2015 in Quebec, Canada. The effects of climate on local forest stand infection and dieback transitions, along with dispersal probability and distance, were estimated statistically. Simulations were run with these estimates to identify the effects of spatiotemporal climate autocorrelation on outbreaks. Dispersal together with all climate variables was found to best fit the observed outbreak size. Simulation models also revealed that positive temporal autocorrelation in climate promotes outbreaks, indicating that a series of suitable years could encourage outbreaks. Our models indicate that spatially-explicit management strategies may be effective in controlling outbreaks.

Keywords: landscape ecology, model, outbreaks, climate autocorrelation, dispersal

Introduction

Understanding the mechanisms underlying the spatiotemporal population dynamics of species is an ongoing ecological challenge (Liebhold et al., 2004). Outbreaks are high population densities of defoliating insects covering large areas and causing extensive tree mortality, making this phenomena of great concern for management decisions (Boyd et al., 2013). For example, spruce budworm (*Choristoneura fumiferana*) outbreaks profoundly structure the dynamics of North American boreal forests (Fleming, 2000). Defoliation is so synchronized that during the last outbreak, 80% of Quebec's (Canada) forests were infected at the same time (MFFP, 2014), destroying 200 million m^3 of wood and causing large economic and ecological impacts in the region (Morin et al., 2007). The multiple mechanisms hypothesized to synchronize budworm outbreaks have been so far studied separately, so their relative roles in driving outbreaks are not well understood, preventing efficient management actions. Here, we present a novel framework that couples statistical and simulation models to tease apart the drivers of synchronous outbreaks of forest defoliating insects.

Hypotheses underlying outbreaks can be broadly divided into abiotic (i.e. climate) or intrinsic (i.e. dispersal) drivers (Liebhold et al., 2004). According to the abiotic hypothesis, spatially autocorrelated environmental variation affecting population dynamics synchronizes the abundance of isolated populations (the Moran effect, Moran, 1953). Alternatively, the intrinsic hypothesis suggests that synchrony occurs when individuals from a single infected population disperse rapidly throughout the landscape (Williams & Liebhold, 2000). Previous empirical studies concentrated on single local populations, thus not considering the effect of possible dispersal from adjacent populations in driving population changes (Tian et al., 2011). Similarly, theoretical models may have underesti-

mated the effects of dispersal as they only used the same local population density data (Kendall et al., 1999). Such local population-level approaches provided only a partial understanding of the mechanisms underlying outbreaks that are driven by both regional climate fluctuations and dispersal (Gilbert & O'Connor, 2013). As such, it is necessary to use landscape-level data of species dynamics to investigate the effects of both environmental autocorrelation and dispersal.

An alternative approach to represent the dynamics of insect outbreaks at landscape-levels is to consider their population state as in either low (endemic) or high (epidemic) abundance. During endemic periods, budworm densities could be considered as 'absent' as they cause no detectable forest defoliation (Régnière & Nealis, 2007). During epidemic periods budworm densities are several orders of magnitude higher (Régnière & Nealis, 2007) and could be considered as 'present' because they cause visible forest defoliation. Large-scale dynamics thus emerge from the local infection (from absent to present) and dieback (from present to absent) transitions. Fortunately, large-scale, multi-year empirical defoliation data (e.g., aerial surveys) is readily available, yet rarely used to parameterize simulation models. We use defoliation data as a proxy for extreme insect population fluctuations. Because density fluctuations of defoliating insect species such as the budworm are so extreme, we propose that dynamics can be sufficiently expressed by presences/absences instead of abundances.

The spatial dynamics of endemic and epidemic occupancy in our proposed framework easily maps onto metapopulation and epidemiological models. Metapopulation theory (Levins, 1969) represents transitions between empty and occupied patches driven by colonization and extinction. Similarly, epidemiological models (Kermack & McKendrick, 1927) track either negligible or disease-causing densities of the infectious agent among individuals in a host population. The two methods are mathematically equivalent in some instances (Grenfell & Harwood, 1997) and

are supported by extensive theoretical development (Hanski, 1998). For example, spatially-explicit vaccination of the most vulnerable locations reduces the size of epidemics of infectious diseases (Keeling et al., 2003). Insights from epidemiological models could be used to develop more effective spatial management strategies of insect outbreaks.

We parameterize the metapopulation model with observed defoliation transitions in spatiotemporal aerial surveys. Transition from endemic to epidemic states is a binomial stochastic process whose drivers can be evaluated from empirical data. Stochastic cell occupancy, state-and-transition, and occupancy models, are all essentially parameterized metapopulation models of species dynamics in space (Moilanen, 2004; Buckland & Elston, 1993; Bestelmeyer et al., 2004). Statistical models have been used to determine how local stand transitions of various insect species depend on annual climate fluctuations and potential dispersal from already infected neighboring cells (Bouchard & Auger, 2014; Kärvemo et al., 2016). The transitions observed in aerial surveys could be used to parameterize a metapopulation model of insect defoliations according to simple rules of dispersal and environmental effects. According to metapopulation and epidemiological theory, the transition from endemic to epidemic is expected to be conditional on both dispersal and climate. Here, we propose that a metapopulation approach of insect outbreaks can be used to represent the effects of intrinsic and extrinsic drivers of outbreaks.

Climate is usually non-randomly distributed and is autocorrelated in space and time (Legendre, 1993). Positive autocorrelation, when climate values are more similar among adjacent temporal or spatial units than expected by chance, may affect population fluctuations and dispersal (Ruokolainen et al., 2009). Synchronous outbreaks may be produced by suitable climate in many locations (Moran effect, spatial autocorrelation). Recent theoretical and experimental studies suggest that

suitable climate conditions over consecutive periods further synchronize populations (temporal autocorrelation, Gonzalez & Holt, 2002; Massie et al., 2015), but this mechanism has never been demonstrated in nature. We expect that a simulation model parameterized from empirical transitions can assist in disentangling the relative importance and the interactions between drivers of outbreak dynamics.

The goal of our study is threefold: 1) determine how climate and dispersal variables drive observed budworm outbreak and dieback transitions; 2) quantify their relative importance; and 3) understand the effects of spatial and temporal climate autocorrelation on outbreak dynamics. We parameterized a metapopulation model from data on transitions in 6 446 10 km^2 cells of boreal forest observed over 46 years in Quebec, Canada. We predict that if the model reproduces the observed outbreaks using the observed autocorrelated climate variables, it suggests that the Moran effect drives budworm outbreaks. Alternatively, if the model reproduces the observed outbreaks with non auto-correlated climate, then it would suggest that dispersal is the most important driver. We used budworm as an example species but our coupled statistical-simulation metapopulation model is certainly applicable to any species that displays large-scale synchrony. The results from the unique combination of statistical and simulation model analysis developed here, provide strong support for an interaction between dispersal and climatic drivers of outbreak dynamics and new perspectives for forest management.

Materials and methods

Coupled statistical and simulation model framework

We considered a metapopulation approach in which a single spatial unit is a cell, and multiple cells together constitute a landscape (Fig. 2.1). Each cell can be in two different states: forest F with endemic budworm densities that do not cause defoliation, or infected forest I with epidemic budworm densities

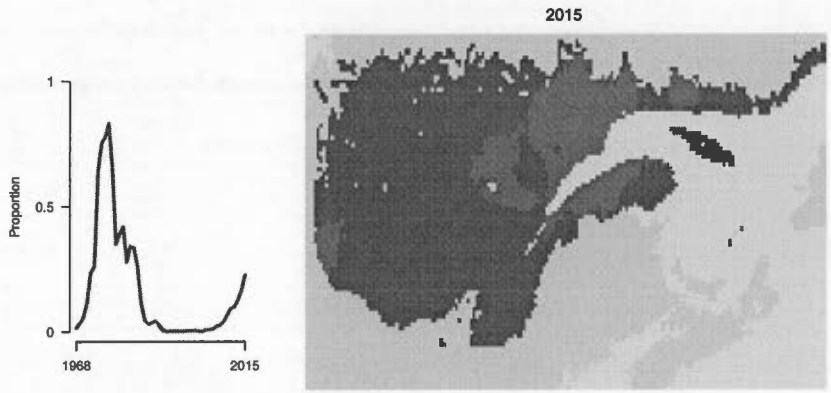

Figure 2.1 Left, the proportion of outbreaks over time, expressed as the proportion of cells in the infected state. Right, the geographic extent of the study area in Quebec province, Eastern Canada. Each square is a 'cell' (6 446 in total) and the colour indicates its state: Dark grey (red online) is defoliated/infected, grey (green online) is forest non-infected cell in 2015. Grey areas were never infected and excluded from the analysis.

that show signs of defoliation (as in chapter 1). As such, these two cell states correspond to observed endemic and epidemic population densities that vary over orders of magnitude (Cappuccino et al., 1998). We studied the transition from forest to infection (infection transition $F \rightarrow I$ or $F \rightarrow I$, colonization) and the transition from infection back to forest (dieback transition $I \rightarrow F$, extinction, Fig. 2.2). Stochastic state transitions ($F \rightarrow I$ and $I \rightarrow F$) across all cells (landscape) generate a fluctuating proportion of F and I cells over time.

Our modelling framework has two parts. We start by statistically estimating the transition probabilities of infection and dieback given dispersal constraints and climatic conditions, and then we use the transition probabilities as parameters in a simulation model to test the influence of autocorrelation on outbreaks. Infection of a single forest cell resulted from two processes corresponding to the following two hypotheses, respectively: 1) by increasing the insect population density due to favourable climate; 2) by dispersing individuals arriving from neighboring infected

cells (Fig. 2.2 arrows). A candidate set of statistical submodels were chosen *a priori* based on dispersal and climate hypotheses to assess the relative contribution of these two processes (i.e., climate and dispersal) in driving large-scale outbreaks. The probability of infection in cell i was modeled as a log-linear model of climate and dispersal:

$$Probability\{F \rightarrow I\}_i = \beta_0 + \beta_n E_i + \alpha_n K_i \tag{2.1}$$

where β_0 is the intercept, E_i is the set of climate variable, β_n is the set of parameters representing the effect of climate variables on the transition probability, K_i is the proportion of infected neighbors around cell i and α_n is the parameter representing this effect. We tested up to third degree polynomial, i.e. n up to 3 (eqn 2.1), for both climate and dispersal variables. This accounted for complex responses while obtaining parametric relationships for the simulation model. The transition probability of dieback from infection to forest is only dependent on climate and set by parameter γ:

$$Probability\{I \rightarrow F\}_i = \gamma E_i \tag{2.2}$$

First, we performed model comparison to select the best-fitting statistical model representing the observed transitions. Second, the statistical model of transition probabilities was used to carry out simulation 'experiments' to investigate the effect of spatiotemporal climate autocorrelation on outbreak dynamics. Our statistical models can only describe the effect of climate for single time steps and cells, whereas simulations integrate dynamics across the entire landscape and over time. We measured the total proportion of infected cells in the landscape through time generated by the simulation model and assessed if they were similar to observed outbreaks. We tested the influence of climate autocorrelation on outbreaks by randomizing climate variables E_i, which maintained climatic values

but removed autocorrelation structure.

Spatiotemporal data

Spruce budworm infection distribution

The Ministère des Forêts, Faune et Parc du Quebec (MFFP, 2014) have tracked the temporal (annual) and spatial distribution of budworm outbreaks based on aerial surveys and recorded mapped polygons indicating areas of defoliation in Quebec province, Eastern Canada. The data span 1968 through 2015, which include one full outbreak (1968-1995), along with the beginning of an ongoing outbreak which started around 2010 (Fig. 2.1).

We converted these polygons to a lattice of 10km x 10km geographical cells (patches, forest stands, from here on referred to as cells arranged in a continuous lattice, Fig. 2.1), which formed the basis for our coupled statistical-simulation model framework. Because recent polygons were mapped to a smaller scale than older data, data across all years were aggregated to the same cell size. We overlaid 1km x 1km spaced points on the original infected polygons, and then resampled this to a regular grid of 10km x 10km cells so if at least one of the points within the cell was infected, the cell was classified as infected (following Bouchard & Auger, 2014). This aggregation also minimized small-scale landscape variations. Any level of defoliation (light, moderate or serious defoliation) within polygons were registered as I. We assumed that non-defoliated areas were F. In total, the study area had 6 446 cells after removing cells that were never infected. Each cell was mapped for 46 years, yielding 283 272 transition events (Tables B.4, B.5).

After mortality from defoliation, forest regrowth usually takes around 40 years (Burns & Honkala, 1990), but occasionally a cell was observed to become reinfected before full regrowth. These fast transitions may have arisen because

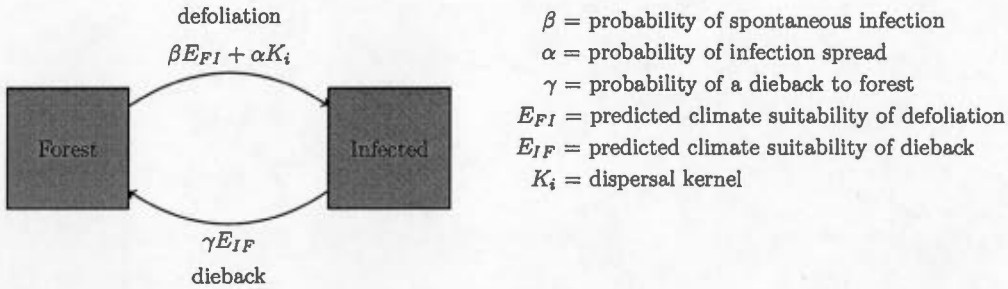

Figure 2.2 Schematic representation of a metapopulation approach to forest insect outbreaks, indicating the forest F and infected I states. The arrows indicate the parameters that set the state transitions infection $F \rightarrow I$ and dieback $I \rightarrow F$.

of detection errors and as such were not considered here as representative of the naturally observed infection and dieback processes we aim to model. To account for this issue, if a cell became infected, not infected and then re-infected within five years, we converted the intermediate years to the infected state.

Table 2.1 The potential climate variables used in the analysis and their time lags tested. The interpolated values covered each cell in the study area (Fig. 2.1 b) from 1965- 2013. From McKenney et al., 2011. Bottom five lines, the types of climate randomizations.

Climate Variable	Time lag
Max/min temperature of warmest/coldest period	1 year before
Max/min temperature of coldest month	2 years before
Max/min temperature of spring (April-May)	3 years before
Max/min temperature of summer (June-July)	
Length of growing season (Growing Degree Days)	
Total Precipitation	
Elevation (constant in time)	
	Original time, original space
	Random time, original space
	Original time, random space
	Random time, random space
	Average time and space (constant)

Climate variables

Historical climate variables covering the same spatiotemporal extent as the defoliation data were obtained from publicly available data. In this data set, climate station data were interpolated to continuous rasters using the ANUSPLIN method (McKenney et al., 2011). Multiple climate variables, in particular extreme temperatures, influence outbreak severity and occurrence (Candau & Fleming, 2005). We consequently selected eight potential annual and seasonal climate variables (and elevation, Table 2.1) for the analysis. Climate one, two and three years before each year t (E_{t-1}, E_{t-2} and E_{t-3}) were also included as climate variables may have a delayed effect on insect population growth and mortality (Aukema et al., 2008). All climate variables were standardized within the range $0-1$ (max-obs)/(max-min) to facilitate comparison between parameters.

Dispersal variables

The expansion of budworm infection to an endemic cell is more likely to occur if there are infected cells in the vicinity (Bouchard & Auger, 2014). Note that dispersal here was defined as the spread of defoliation. As defoliation was used as a proxy for infection, defoliation spread represented the successful dispersal of insect individuals. We considered neighborhood dispersal kernels K_i to represent propagule pressure around cell i. We compared K_{it-1} and K_{it-2} computed one and two years prior to the transition t and $t+1$ given that egg-laying adults produced a population increase the following year when larvae emerge. We used two methods and a range of neighborhood sizes in each method to evaluate dispersal kernels that characterize dispersal:

The autologistic kernel represented the proportion of infected cells within a certain distance (Yackulic et al., 2015). All cells within the neighborhood were

given equal weight. K_i of each potential donor cell i was the number of infected cells j within distance d. K_i is standardized by the total number of neighbors so that K is one if all neighbours are infected. We calculated K_i for $d = 2 - 30$ cells in increments of 1 because the maximum radius of 30 cells covered the majority of the landscape (89 x 176 cells).

The negative exponential kernel included all cells in the landscape but gave a higher weight to cells close to the focal cell, allowing long-distance dispersal (i.e. beyond the threshold distance in the autologistic kernel). The negative exponential kernel is the sum of the weighted distances between all cells (Moilanen, 1999):

$$K_i = \sum_{j \neq i} exp(-\delta d_{ij})$$

where δ is the average dispersal distance and d_{ij} is the distance in number of cells between cell i and j (in this equation α traditionally represents the effect of distance, but we use δ to avoid confusion with α probability of dispersal). We calculated dispersal variables varying $\delta = 2 - 30$ in increments of 2 because this range captured extremes of both short and long-distance dispersal (Table B.4). The values of negative exponential dispersal variable K_i were standardized to $0-1$ (max-obs)/(max-min) to be on the same scale as the autologistic kernel.

Statistical models

We determined how climate and dispersal influenced transition probabilities by tracking the state transitions of each cell in the observed defoliation data, and estimating how the probabilities were affected by climate and dispersal. We constructed separate statistical models for the infection $F \rightarrow I$ and dieback $I \rightarrow F$ state transition probabilities. Transition was modelled as a binomial process using logistic regression. The selected climate and dispersal variables described above

were used as predictors of forest transitions (equation 2.1 - 2.2).

Models were evaluated in two ways: model fit (accuracy) and predictive performance on independent data. Goodness-of-fit metrics to assess model fit were ΔAIC and pseudo r^2 for logistic regressions, $r^2 = 1-(residualdeviance/nulldeviance)$. Cross-validation to assess predictive performance was performed on a random subset of the data and on the second outbreak. Random cross-validation was performed by splitting the data in half, fitting the model on the subset and then estimating model performance on the remaining validation data. This was repeated 10 times and the average error calculated. Temporal cross-validation was performed by fitting the model to the first outbreak (1968-1992) and predicting the model on the second outbreak (1993-2015). We did not estimate temporal cross-validation in $I \rightarrow F$ transitions because there were little data from the second outbreak.

Model comparison

We tested which potential dispersal kernel K_i and kernel parameters d and δ best fitted the data. Given that the dispersal variables were highly correlated (first axis of a Principal Components Analysis on the correlation matrix explained 84% of the variation, Fig. B.1), we used forward stepwise model selection to rank models with each dispersal kernel separately. Only the best-supported kernel was retained for all subsequent analyses (according to AIC, Fig.s B.4).

The full regression model had one dispersal and all eight climate variables with three time delays as predictors (Table 2.2). We used the first and three best climate variables and interactions between them to construct submodels. To determine which candidate climate variable best explained the observed budworm infection and dieback transitions, we used backward stepwise model selection because climate variables were not collinear (the first PCA axis on the correlation

matrix explained 50% of the variation, Figs. B.2). We estimated a geographical null model to assess if outbreaks were independent of climate and directional in space (anisotropic). Latitude and longitude were used as predictors for the geographical null model. We also estimated a dispersal null model in which dispersal was not limited by distance (global dispersal). Proportion infected area in the previous year was the global dispersal predictor, and was compared to the best-fitting distance-based dispersal kernel.

Simulation model

We simulated outbreaks using the estimated infection and dieback transition probabilities from the full statistical model to investigate the effect of spatiotemporal autocorrelation of climate variables on the outbreak dynamics. We ran stochastic simulations with the statistical transition probabilities and the observed climatic fluctuations, so the simulations occurred in the same landscape and over the same years as the observed outbreaks. Uncertainty can propagate up and yield different large-scale dynamics even if the model successfully represents the local dynamics (here transitions, Peters et al., 2004a).

Simulations were initialized with the 1970 climate and run for 45 years. Depending on the state of chosen cell i (F or I), transition probabilities $Probability\{F \rightarrow I\}_i$ and $Probability\{I \rightarrow F\}_i$ were applied (as explained above, equations 2.1 and 2.2). The dispersal kernel K_i was calculated dynamically from the cells infected in the previous year. We added climate and dispersal parameters exactly as in the statistical model to obtain spatiotemporal transition probabilities (equation 2.1). The final probabilities were then compared to uniformly distributed random values $0 - 1$ to determine if a transition occurs, so transitions were stochastic but influenced by the probabilities. We used asynchronous updating of the landscape by randomly picking and updating 6 446 cells per time step in order to

approximate continuous spatial dynamics (Durrett & Levin, 1994).

We carried out simulations with and without autocorrelated climate to understand if structured climate variation drives outbreaks (Figure 2.1, panels in Fig. 2.4). We randomized climate variables, thus maintaining the frequency distribution of values but removing the autocorrelation structure. First, we randomized climate conditions across time-steps, within each cell, to remove temporal autocorrelation. Then we randomized climate conditions between cells, within each time-step, to remove spatial autocorrelation. We randomized climate in both space and time to remove both temporal and spatial autocorrelation. Simulations with average climate values from all years and locations were carried out to test how climate variation affects outbreak dynamics. Finally, to investigate if the estimated dispersal kernel was important in producing outbreaks, we also implemented global dispersal with the original climate variables.

We characterized simulated outbreaks (30 repetitions per spatiotemporal autocorrelation) in time and space to compare them to observed outbreaks. Simulated infections were stochastic and so cannot be compared cell-by-cell to observed infections. Instead, to examine if simulated outbreaks were as large, i.e. as spatially synchronous as observed outbreaks, we recorded the proportion of the landscape in state I per year. We also calculated the maximum, standard deviation, and temporal autocorrelation of proportion I. Real outbreaks are known to be spatially clustered (i.e. infected cells were often connected by their 8 closest neighbors when considering a rasterized landscape, Fig. 2.1 b), and so we determined if the simulation model was able to reproduce this property. We calculated the maximum cluster size and number of outbreak clusters per simulation to compare the spatial characteristics of observed and simulated landscapes.

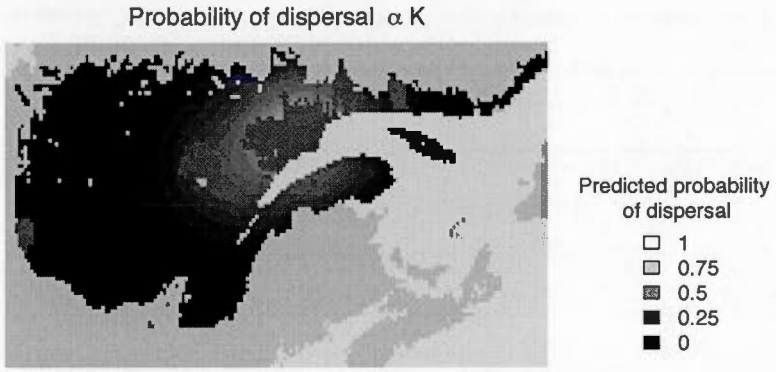

Figure 2.3 Map of αK calculated from the cells defoliated in 2013 (in dark grey, red online). The dispersal kernel K was calculated using the negative exponential kernel with $\delta = 10$.

Results

The statistical model identified that budworm dispersal most often occurs over short distances but there was occasional long-distance dispersal. We found that the negative exponential kernel best fit the observed infection transitions (Fig. B.4, Fig. 2.3 for example). The dispersal probabilities were generally below 0.5, indicating that dispersal was episodic and did not always occur. We identified that lagged spring and summer temperatures best explained the infection and dieback transitions. The three strongest climatic drivers of the $F \rightarrow I$ transition were in order of importance: maximum summer temperature three years before, summer minimum temperature three years before and number of growing degree days 2 years before (Fig. B.5, Table B.1). Climatic transition probabilities were low, around 0.1 for the most suitable conditions (Fig. B.7). Minimum spring temperature three years before, precipitation three years before, and minimum temperature of the coldest period two years before were the strongest predictors of dieback transitions (Fig. B.6, Table B.2).

The model comparison indicated that both climate and dispersal drivers af-

fected outbreaks, but their relative importance depended on how models were evaluated. Models with only climate variables were more accurate (according to AIC), while models with only dispersal predicted the second outbreak better (according to temporal cross-validation, Table 2.2, Table B.6). The full climate model, i.e. with all climatic variables and third degree response, was the most accurate model when predicting on randomly selected data from both outbreaks (cross-validation according to AIC, Table 2.2). However, the full model was less successful at predicting the second outbreak (according to temporal cross-validation, Table 2.2). The model with the best predictive performance was a submodel with three climate variables, dispersal and interactions between them (according to temporal cross-validation, Table 2.2). Dispersal was the best unique variable in terms of both accuracy and predictive performance (according to AIC and cross-validation, Table 2.2). Adding interactions between climate and dispersal increased model fit, though it decreased predictive power (according to AIC and temporal cross-validation, Table 2.2). Models with interaction so closely fit to the first outbreak are not general enough to predict the second outbreak (overfit). The geographical null model did not fit outbreaks well, indicating that climate was important in synchronizing outbreaks.

Simulations with the parameterized metapopulation model revealed that successive periods of temporally autocorrelated climate synchronized outbreaks. Retaining only the temporal climate autocorrelation produced outbreaks that covered 70% of the landscape, compared to the 90% observed (example simulations Fig. 2.4, Fig. 2.5 a). Simulations with the original autocorrelated climate also produced outbreaks that were as large as the observed outbreaks (Fig. 2.5, a, b). When retaining only spatial autocorrelation (i.e., removing temporal autocorrelation), outbreaks did not occur during the same years as observed outbreaks and were on average smaller (40-60%, Fig. 2.5 a), indicating that the model was less

sensitive to spatial autocorrelation. Simulations with constant climate had 10% landscape infection throughout the simulations with no variability.

Temporal dynamics were in general well captured, and spatial dynamics less so. Randomizing climate in time produced outbreaks with lower next-year temporal autocorrelation (correlations $0.7 - 0.9$ with 1 year time lag, Fig. 2.5 c), with long-range positive temporal autocorrelation (6-16 years, Fig. 2.5 d). Even spatially randomized climatic conditions occasionally resulted in outbreaks that were as temporally autocorrelated as observed outbreaks. The difference between spatially autocorrelated (random time) and completely random climate conditions was small, again indicating that spatial autocorrelation has a weak effect on outbreak dynamics. Simulated outbreaks were more fragmented in space than observed ones. Simulated outbreak clusters were more numerous and smaller in size than the observed ones (Fig. 2.1, 2.5 e, f). Simulations with global dispersal and observed spatiotemporal autocorrelation yielded landscapes with high proportions of infected cells but reflected neither the temporal nor the spatial characteristics of observed outbreaks (Fig. 2.5).

Table 2.2 Model selection results on defoliation FI transitions. The three best climate variables were summer maximum temperature $t-3$, summer minimum temperature $t-3$ and number of growing degree days $t-2$. The variables had third-degree response terms. K = the number of variables.

	K	AIC	deltaAIC	pseudo-r^2	random residuals	temporal residuals
all climate + dispersal	79	19475	0	0.425	2439	1375
all climate	76	24374	4899	0.300	2842	1582
3 climate + dispersal	13	27599	8124	0.214	3390	1387
1 climate x dispersal	16	28084	8609	0.186	3610	1395
1 climate + dispersal	7	28860	9386	0.175	3558	1384
dispersal	4	28889	9414	0.168	3610	1378
3 climate (with interactions)	64	29708	10234	0.156	3329	1575
global dispersal	4	30548	11073	0.120	3688	1490
3 climate	10	32076	12602	0.066	3721	1581
1 climate	4	33678	14203	0.015	3868	1572
latitude x longitude	16	34596	15121	0.013	3751	1562

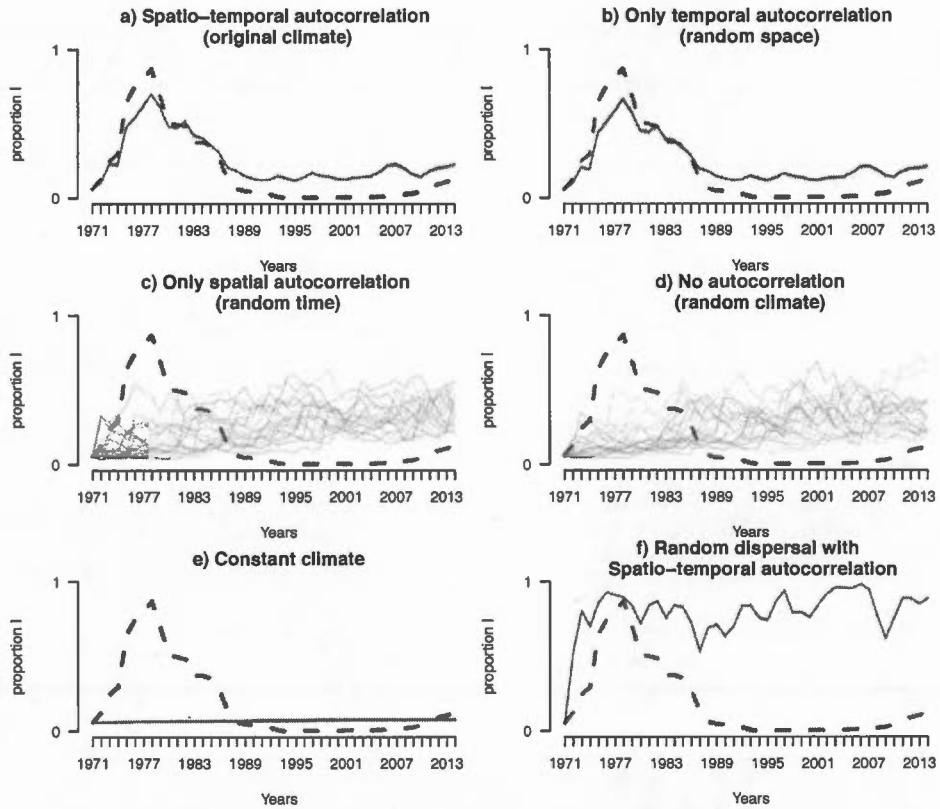

Figure 2.4 The simulated proportion of infected cells with different types of spatiotemporally autocorrelated climate. Dotted lines indicates the observed outbreaks, and each thin line indicates one simulated outbreak.

Discussion

We performed a coupled statistical and simulation analysis of 48 years of spruce budworm outbreak observations to understand how dispersal and climate drive the dynamics. The estimated parameters from the best statistical model were incorporated into a simulation model to investigate the role of spatiotemporal autocorrelation on the initial development of outbreaks and their spatial structure. The same framework can be applied to other insect species that are mapped by defoliation.

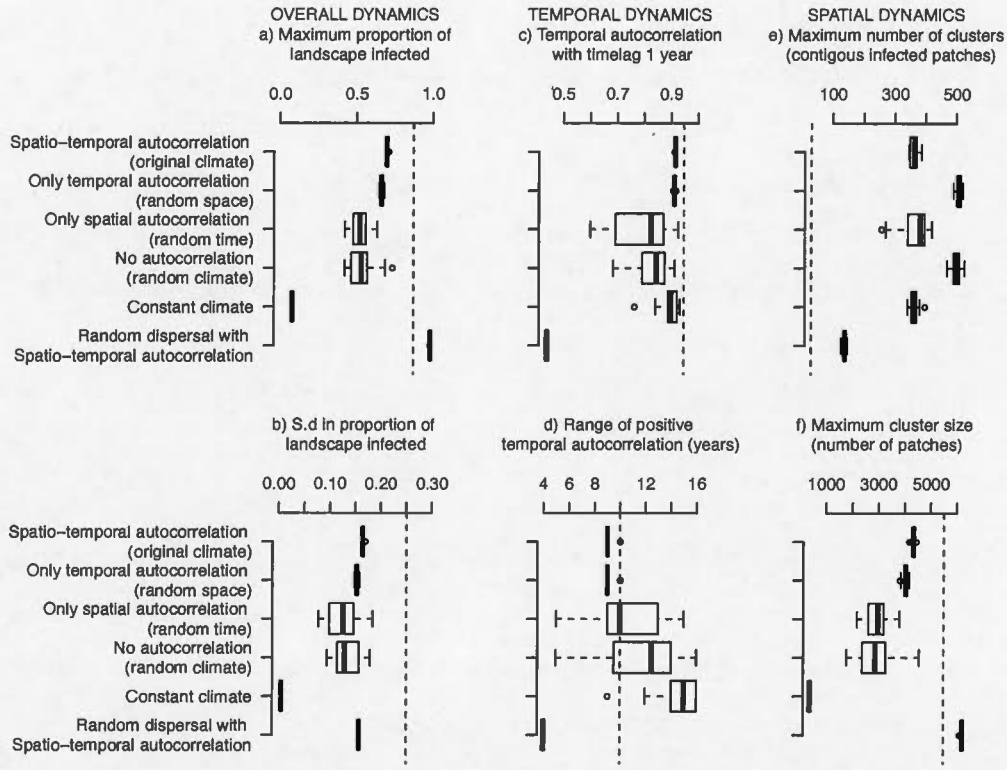

Figure 2.5 Summary results from simulation model. Horizontal dotted lines indicate the values in the observed outbreaks. Each plot shows the values from 100 simulations. Boxes encompass the 25% - 75% quartiles of the data, with the median indicated by the thick line through the centre of each box. Whiskers extending from the box encompass the 95% quartiles, and extreme observations are shown as circles. a, Maximum proportion of infected area. b, Standard deviation in the simulated proportion of infected area I. c, Temporal autocorrelation with a 1 year time lag. d, Range of positive temporal autocorrelation (in years). e, Maximum number of contiguous outbreak clusters per simulation. f, Largest contiguous outbreak cluster size per simulation (number of cells).

We found that infection spread between forest cells occurred occasionally over long distances, however short-distance dispersal was more common. Individual-based studies show that adult moths can efficiently travel 48 km (Anderson & Sturtevant, 2011), and the maximum recorded distance is 450 km (Greenbank, 1980). The greater importance of the negative-exponential kernel over the autologistic version indicates that dispersal was essentially driven by strong short-distance dispersal events and occasional long-distance dispersal events. For instance, the probability of dispersal was low though a cell was surrounded by infected cells in a suitable climate (Fig. B.4). The budworm population is genetically well-mixed (James et al., 2015), supporting effective long-distance dispersal. However, dispersal was still limited by distance as the dispersal null model with global dispersal badly fit the data (Table 2.2). Metapopulation models are often estimated from static (snapshot) distributions and individual dispersal observations (Moilanen, 1999). In contrast to these static methods and due to the detailed spatiotemporal nature of our data, we characterized effective dispersal. The strength and shape of dispersal is often the unknown factor in predictive models, and thus in understanding outbreaks (Myers & Cory, 2013). Our framework describes an effective method to quantify dispersal directly from spatiotemporal occupancy data.

We disentangled for the first time the effects of climate and dispersal with an innovative coupling of statistical analysis and simulation modelling. In the end, our results indicate that both climate and dispersal interact to drive outbreaks. Previous studies may have over-estimated the role of the Moran effect in driving population fluctuations because they did not test for the hypothesis of dispersal. Purely temporal analyses pool data across large regions (Tian et al., 2011), thus possibly confounding local dispersal events with climatic effects. Spatial analyses suggest that climate drives dynamics if the spatial autocorrelation of climate has a

longer range than the spatial autocorrelation of outbreaks (Peltonen et al., 2002). Models that exclude dispersal cannot characterize how climate drives infection transition events separately from dispersal. Recent process-based statistical studies testing both climate and dispersal (intrinsic and extrinsic) hypotheses have shown that dispersal is more important than climate in synchronizing outbreaks (Preisler et al., 2012; Veran et al., 2014). Similarly, we found that dispersal was an important factor in synchronizing infections in space, although it required an autocorrelated climate trigger (simulations with constant climate vs. simulations with climate, Figure 2.4).

Among the abiotic drivers, a suite of climate predictors best described the observed transitions. We found that delayed spring and summer temperatures influenced both infection and dieback transitions, suggesting that climate during the reproductive season had a delayed effect on insect population growth, similar to what Aukema et al. (2008) observed. Multiple climate variables are necessary to reproduce outbreak dynamics because these may affect insect development periods and life histories differently. In general, winter temperatures affect overwintering survival, maximum spring temperature affects larval emergence, and summer temperatures affect feeding rates (Régnière et al., 2012; Gray, 2013). The full model with all climate variables was more accurate, suggesting that a specific combination of climate characteristics was important ('a perfect storm', Wilmers et al., 2007). Moreover, interactions between predictors increased fit, and may indicate that climate and dispersal interact (e.g., dispersal is greater in warmer temperatures).

The difficulty in identifying a single climate driver may be explained statistically. First, it is difficult to fit autocorrelated predictor variables (Kissling & Carl, 2008). Spatiotemporal autoregressive models that account for spatiotemporal autocorrelation are not generalized to logistic regression with complex re-

sponse functions (Cressie & Wikle, 2011, but see Griffith & Peres-Neto, 2006). Moreover, our goal is not to remove autocorrelation, but to understand how it affects species dynamics. Cross-validation suggested that the full model overfit the data and included the maximum number of climate variables to produce a spurious relationship. Simpler models with fewer variables are generally preferred for prediction purposes (Cuddington et al., 2013).

The simulation model suggests that non-random climate variation produced outbreaks even though climate itself was a weak statistical predictor. Simulation models can draw such conclusions because they simulate several years, not just one year ahead. The model reproduced the emergent temporal characteristics of budworm outbreaks; 0.9 temporal autocorrelation with a one year lag, and 10 year range in positive autocorrelation (Fig. 2.5 c, d). We identified that temporal climate autocorrelation drives large-scale outbreaks, because retaining only temporal autocorrelation produced outbreaks that were similar to both spatial and temporal outbreak characteristics. Non-random temporal environmental variation has been shown to inflate the Moran effect in microcosm experiments (Gonzalez & Holt, 2002; Massie et al., 2015) and theoretical population models (Vasseur, 2007). For the budworm, several consecutive dry summers have been associated with infections (Greenbank, 1956). This simulation model allowed us to identify the importance of autocorrelated temporal climate variation at the landscape scale. However, since climate has a high spatial autocorrelation (analysis not shown), randomizing climate in space does not change dynamics and may have led us to underestimate the role of spatial autocorrelation.

Our simulation model showed that spatiotemporal autocorrelation affected outbreaks, but it did not completely reproduce the observed dynamics. Observed dispersal events are episodic in time and clustered in space, yielding a small number of large outbreak clusters (maximum 30 clusters and a single cluster covering

85% of the study area, Fig. 2.5 e, f). Dispersal is difficult to model because it is inherently stochastic and may be driven by unpredictable atmospheric conditions such as wind direction (Sturtevant et al., 2013). Since our model already contained all possible observed climatic spatial autocorrelation, it is possible that additional hypotheses are required to completely predict outbreak patterns (Liebhold et al., 2004). Spatially correlated distributions of natural enemies such as parasitoids may synchronize insect densities (Roland & Taylor, 1997), but there is little available empirical data. The effect of local environmental conditions such as forest composition may further mediate natural enemy interactions (Bouchard & Auger, 2014). However, Gray (2013) found that climate was a better predictor of outbreak duration and severity than forest composition. Detailed data on natural enemies and forest composition could improve predictions.

Conclusion

Dramatic spruce budworm outbreaks have inspired the development of many models, including statistical and simulation models. Here we reinterpreted outbreaks as a metapopulation process so that forest defoliation data could be employed as an indicator of low and high insect densities. It is beneficial to estimate parameters on the same scale at which outbreaks are observed, because emergent outbreak characteristics may not be predicted from local mechanisms (Fleming et al., 2002). Simple metapopulation models are as useful as complex local population models, especially when the ecological mechanisms are hard to parameterize or simply unknown (Harrison et al., 2011). Simple models are also more applicable because of their ease of use and generality, and can easily be extended to other species. The relative importance of dispersal is one of the main hurdles for understanding outbreaks (Myers & Cory, 2013) and here we present a method to quantify dispersal kernels from aerial survey data. The landscape-scale of our process-based metapopulation model makes it relevant for the development

of large-scale forestry management practices. Pest management considers pests as immobile, possibly preventing effective management (Tscharntke et al., 2007). Since metapopulation models are analogous to epidemiological models (Grenfell & Harwood, 1997), widely tested epidemiological techniques to minimize transmission can be considered. Our metapopulation model could be used to generate spatially-explicit management strategies that minimize dispersal and thus outbreaks. Moreover, to our knowledge, we have demonstrated for the first time that spatiotemporal autocorrelation in climate values may amplify insect population fluctuations.

Acknowledgements

Thank you to the organizers and participants of the UIFRO workshop 'Climate Induced Range-Shifts in Boreal Forest Pests,' and the organizers of the CJFR special issue. Funding was provided by the Forest Complexity Modelling programme, Natural Sciences and Engineering Research Council of Canada - Collaborative Research and Training Experience and Discovery programmes, Canada Research Chairs, Université du Quebec à Montréal and a Doctoral Research Fellowship from the Fonds de recherche du Quebec - Nature et technologies. Many thanks to Emily Tissier, Alyssa Butler, Mathieu Bouchard and reviewers for comments on the manuscript.

CHAPTER III

HERBIVORES HOSTING HOSTS: CAN PARASITOIDS CAUSE LARGE-SCALE OUTBREAKS?

Hedvig K Nenzén, Véronique Martel, Dominique Gravel

Synchronous population fluctuations occur for many species and have large economic impacts, but remain poorly understood. Dispersal, climate and natural enemies have been proposed to cause synchronous population fluctuations. Defoliating insect herbivores have many natural enemies that may cause landscape-scale changes in their densities and thus regional forest defoliation. One of the most common and effective natural enemy of herbivores are parasitoids that lay eggs in the herbivore, i.e. the herbivore is simultaneously a host to the parasitoid. During endemic herbivore/host periods the parasitoid-caused mortality is high. To study and effectively manage insect herbivore outbreaks we need spatial modelling approaches that include these natural enemies. However, predictions from classic host-parasitoid population models cannot be compared to commonly-observed parasitism mortality rates. We constructed a novel model from observed biological processes to study how natural enemies affect insect outbreaks on a

landscape-scale. It is a metacommunity model in which local control and exclusion of species were driven by interactions between the forest, hosts, primary parasitoids and their parasitoids (hyperparasitoids). Hyperparasitoids have a strong effect because they decrease both host and parasitoid densities which simultaneously disrupts their own potential to reproduce. Hyperparasitoids ultimately lead to the decrease of both parasitoid and hyperparasitoid populations which allows host outbreaks. Model simulations showed that the quantitative implementation of these observed natural enemies can reproduce outbreaks. The model also identified the testable prediction that hyperparasitoid-caused mortality should increase just before the onset of an outbreak because hyperparasitoid instability leads to outbreaks. If verified empirically, hyperparasitoid community dominance could provide a biotic early warning signal that an outbreak will occur.

3.1 Introduction

The causes of synchronous population dynamics, such as outbreaks of insect pests, are an enduring 'ecological mystery' (Elton, 1924) which has large ecosystem consequences. Insect outbreaks lead to high population densities and forest defoliation over large areas (Myers & Cory, 2013). Three main mechanisms that synchronize large-scale outbreaks have been proposed: dispersal, climate, and natural enemies (Liebhold et al., 2004; Berryman, 1996; Cooke et al., 2007). First, dispersal synchronizes outbreaks when individuals spread and initiate defoliation throughout the landscape. Second, climate variation that is spatially autocorrelated influences population dynamics of isolated populations in similar ways, thus synchronizing their fluctuations. Finally, synchronous fluctuations of natural enemies may produce large-scale outbreaks by modifying non-linear species interactions and dispersal (Tenow et al., 2012; Haynes et al., 2009). For defo-

liating (herbivorous) insects, parasitoids are the most common natural enemy, killing more individuals than predators and parasites combined (Hawkins et al., 1999). The relative importance of mechanisms behind outbreaks are unclear. Improving our understanding these mechanisms is necessary to develop management programs to reduce devastation of economically-important forests.

Parasitoids decrease densities of their host species and thus prevent forest defoliation, which suggests that defoliation may result from synchronous loss of 'parasitoid-control'. Such 'parasitoid-control' has been observed for various host species during their endemic, low-density periods (Myers & Cory, 2013; Rosenheim, 2001). For unknown reasons this parasitoid control is lost at the beginning of insect outbreaks (Myers & Cory, 2013). Parasitoids effectively control host population densities due to parasitoids' unique trophic-reproduction lifestyle (Godfray & Shimada, 1999). Parasitoids lay eggs on or inside host larvae, then the eggs develop and the hatched larvae feed on the host, ultimately killing it (Godfray & Shimada, 1999). As each parasitoid attack simultaneously increases parasitoid growth rates and causes a zero host fitness, host-parasitoid interactions are highly over-exploitative (Lafferty & Kuris, 2002). Host-parasitoid models based on population densities of these two species generally reflect this locally unstable relationship and can generate population oscillations of increasing amplitude that lead to the extinction of both species (Nicholson & Bailey, 1935; Mills & Getz, 1996). In nature, Parasitoids provide an ecosystem service by controlling insect pests, while hyperparasitoids may provide an 'ecosystem disservice' (Gagic et al., 2012) by interrupting this control. Biological pest management relies on effective parasitoid-control (Murdoch et al., 2005), yet traditional models cannot explain why in certain cases parasitoid-control fails leading to 'ecological surprises' (90%, Rosenheim, 2001; Tylianakis & Binzer, 2014).

It has been suggested that successful parasitoid-control can be inhibited be-

cause parasitoids are in turn a host to other parasitoid species that decrease their densities (Sullivan & Wolfgang, 1999). Parasitoids themselves are attacked by parasitoids, and such hyperparasitoids inhibit parasitoid-control and may thus cause host outbreaks (Rosenheim, 1998). Hyperparasitoids must deposit their eggs in primary parasitoid larvae that develop in hosts that have been parasitized (Sullivan & Wolfgang, 1999). The hyperparasitoid larvae are nourished by the developing parasitoid eggs. As hyperparasitoids cause parasitoid mortality and parasitoids cause host death, the outcome is that hyperparasitoid-control is also an intrinsically unstable ecological interaction (Figure 3.1). In experiments, hyperparasitoids lowered population densities of parasitoids and suppressed parasitoid-control on aphids (Van Veen et al., 2001; Schooler et al., 2011). Therefore, hyperparasitoids would explain why parasitoid-control decreases and biological control fails, as observed during host outbreaks. Traditional models present no consensus on hyperparasitoids and suggest that they either decrease or increase host densities (Nicholson & Bailey, 1935; Beddington et al., 1978; May & Hassell, 1981). So to explain observed host outbreaks without hyperparasitoids, theoretical population models have shown that spatial host-parasitoid dynamics may produce spatial coexistence when hosts escape mortality by dispersal (Hassell et al., 1991; Hirzel et al., 2007). However, two-species models are insufficient because models need to incorporate hyperparasitoids that are suggested inhibit parasitoid-control.

Multiple trophic levels of natural enemies have been observed in nature, and models are needed explore how these hyperparasitoids cause outbreaks in a landscape. Complex host-parasitoid-hyperparasitoid interaction networks with multiple trophic levels exist (Hawkins et al., 1999; Morris et al., 2014). For example, the spruce budworm has large outbreaks *Choristoneura fumiferana*, Boulanger et al., 2012) and a parasitoid community with more than three trophic levels that changes in prevalence during an outbreak cycle (Eveleigh et al., 2007). In a landscape

context, dispersal between populations may change host-parasitoid dynamics, as been shown both in nature (Maron & Harrison, 1997; Roland & Taylor, 1997) and experimentally (Huffaker, 1958; Bonsall & Hastings, 2004). Spatial dynamics may affect persistence of top predators (McCann, 2000; Gravel et al., 2011a) but it is unclear if hyperparasitoid dispersal contributes to their persistence thus outbreaks. Verbal tri-trophic models formulated for the spruce budworm suggest that biotic interactions are an important component of outbreaks (Royama, 1992; Fleming, 1996; Cooke et al., 2007). Quantitative models exist for other natural enemies such as predators (Turchin, 1999), pathogens (Dwyer et al., 2004) and parasites (Anderson & May, 1980). However, there is no general model that is built from and that matches observed host-parasitoid-hyperparasitoid dynamics.

Here we developed a quantitative theoretical model to explore how hyperparasitoids interrupt host suppression and synchronize insect outbreaks in a metacommunity context. To simplify the model and instead of tracking population densities, we constructed a trophic metacommunity model (Leibold et al., 2004; Gravel et al., 2011b). The model employed observed forest defoliation to indicate host-, parasitoid-, and hyperparasitoid-control, states that are analogous to presence-absence in a metapopulation model (Levins, 1969). In nature, host-parasitoid population ratios affect the forest state: forest defoliation occurs when host densities are high compared to parasitoid densities. A healthy forest is maintained when host (herbivore) densities are suppressed by parasitoids (i.e., strong parasitoid-control). Hyperparasitoids can in turn control parasitoid densities and maintain a healthy forest for a while, so the model includes dynamics of an additional trophic level (Figure 3.1). When hyperparasitoid-control is eventually lost, high host densities occur. Since we include forest defoliation and depletion, we include a realistic resource feedback that population models usually ignore (but see Ludwig et al., 1978; Turchin et al., 2003; Økland & Bjørnstad, 2006). The

model assumes that defoliation is sufficient to represent the underlying population fluctuations and density ratios, and due to this simplification, the model can represent four interacting trophic levels with fewer parameters: resource, host, parasitoid and hyperparasitoid.

To study under what conditions outbreaks occur, the model is inspired by the spruce budworm, a classic non-equilibrium spatial system with a parasitoid community composed of three trophic levels. Here we define stability as being the absence of outbreaks, i.e. spatially-synchronized defoliation, and a stable system has constant, low rates of defoliation. Our goal is to investigate how natural enemies affect synchronous forest defoliation by constructing a theoretical model where parasitoid interactions drive host densities. Specifically we asked if little-studied hyperparasitoids are the mechanism that interrupts natural enemy control and allow host populations to increase. To determine if hyperparasitoid-control is a plausible hypothesis for outbreaks, we investigate whether hyperparasitoid dynamics can generate simulated outbreaks that better fit observed outbreaks. Outbreaks should be larger if parasitoid densities are lower in hyperparasitoid-controlled forest than parasitoid-controlled forests, as expected if hyperparasitoids cannot attack the hosts without the parasitoid present. Therefore we also test the hypothesis that outbreaks should be larger if hosts can spread faster into hyperparasitoid- than parasitoid-controlled forest. To explore metacommunity dynamics we asked under what conditions (local colonization and extinction rates, dispersal) the system dynamics were stable. The goals were to identify: 1. What species characteristics, i.e. parameters in which interaction webs are necessary to produce outbreaks? 2. How do host and parasitoid prevalence change during an outbreak? Therefore the model would be useful for management to understand when the metacommunity might cause outbreaks. Specifically, the model predicts that the fraction of parasitism rates caused by hyperparasitoids should increase

just before parasitism rates fall and outbreaks occur.

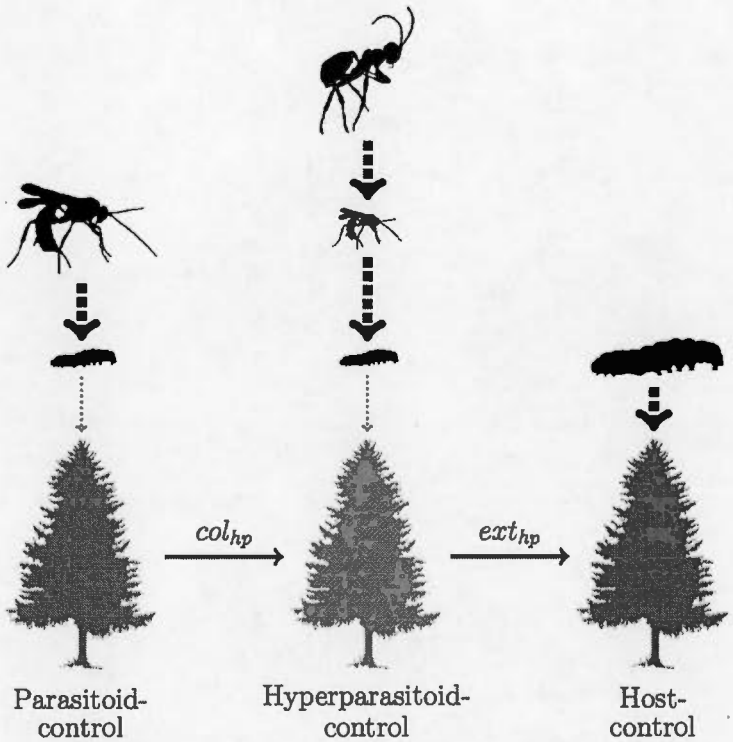

Figure 3.1 Effect of each trophic level on underlying trophic levels. Vertical line thickness indicates interaction strength. Horizontal arrows indicate time. Species sizes is proportional to the density of each trophic level (not body size). The forest appears defoliated only in the host-controlled state, and both parasitoid- and hyperparasitoid-controlled forest is healthy, non-defoliated. Note that hyperparasitoids have a strong effect on both parasitoid and host, in contrast to trophic relationships where a stronger effect on one trophic level leads to a weaker effect on the next trophic level (alternating not additive).

3.2 Methods

3.2.1 Spruce budworm metacommunity

We based our metacommunity model on observed interactions between budworm and its natural enemies. Parasitoids strongly reduce host (herbivorous

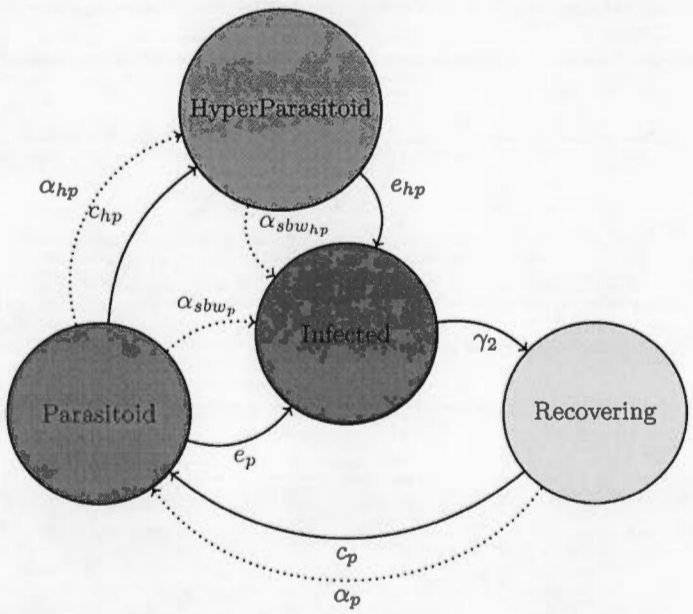

Figure 3.2 Metacommunity model with the three trophic levels with host-controlled, parasitoid-controlled and hyperparasitoid-controlled states, showing states and transitions. Dotted lines indicate second-order rates that depend on the concentration of both states. See Table 3.1 for description of states and parameters.

budworm) survival rates and may ultimately inhibit outbreaks (Royama, 1992; Berryman, 1996). Multiple studies have shown that the budworm experiences high parasitism rates during endemic periods (i.e. the proportion of individuals that were killed by parasitism, 50-90% in Seehausen et al., 2014, 40-70% in Cappuccino et al., 1998 and all primary parasitoids, 62-75% Dowden et al., 1950), 80% by one species, Cusson et al., 1998). These high parasitism rates show how effective parasitoids are as natural control agents. High parasitism rates also indicates the resource available to hyperparasitoids during endemic periods. Parasitism rates during epidemics are likely lower, but data are scarce (Régnière & Nealis, 2007). Parasitoids can contribute to host mate-finding Allee effect (Régnière et al., 2013) by further decreasing low host populations. Parasitism rates are

however higher towards the end of an epidemic, possibly because host densities have already been reduced due to resource depletion and not parasitoid-caused mortality (Régnière & Nealis, 2007). Outbreaks of other defoliating insect pests are also terminated by resource depletion (Hagen et al., 2010; Schott et al., 2010).

We then translated observations of host-parasitoid-hyperparasitoid dynamics to a theoretical metacommunity model representing multiple stands (patches, cells) within a landscape. Metapopulation models express the presence and absence of a single species in habitat patches as the result of colonization and extinction events (Levins, 1969). In this metacommunity model we expressed the replacement of low and high species densities as the result of control and exclusion events. Each patch (1-10km^2) contained a forest stand that can be in only one state (parasitoid-controlled, hyperparasitoid-controlled, infected or recovering) according to the present insect species. The model represents one species per trophic level, but can easily be extended to multiple species with known interactions (Gravel et al., 2011b). We expressed dynamics in both a differential equation model with spatially-implicit (global) dispersal and a cellular automata with spatially-explicit dispersal between neighbouring stands. Comparing results from spatially-explicit and -implicit simulations allows us to explore the role of local dispersal in outbreaks.

3.2.2 Description of stand states

Each stand represents a forest stand whose condition is controlled by hosts, parasitoids or hyperparasitoids and stand state indicates how forest condition is affected by underlying species ratios (Figures 3.1, 3.2 boxes). Even though a host population can be largely suppressed by parasitoids (high parasitism rates), some host individuals will survive and parasitoid-control is not complete. Insect hosts (i.e. defoliators) such as budworm are present at very low, barely detectable, den-

sities during endemic periods (Sanders, 1996; Régnière et al., 2013). Stand state is determined by population density ratios, thus indirectly representing population fluctuations of classic Nicholson-Bailey host-parasitoid models.

A stand in infected state I indicates epidemic host densities and infected, defoliated forest. The host experiences little parasitoid-caused mortality, leading to high, epidemic host densities and low parasitoid densities. Parasitoid-controlled forest P indicates endemic host densities and a healthy forest condition. Parasitism leads to mortality of host individuals, which means that they are maintained at low densities. The parasitoid-controlled state is separated into two states depending on source of host mortality: parasitoid- or hyperparasitoid-controlled. During endemic periods, high parasitism rates can also be caused by hyperparasitoids, state HP. This state has low densities of both host and parasitoids because the hyperparasitoid kills parasitoids that have already infected the host, so total parasitism rates remains high. We assume that both P and HP states produce healthy forest in which the host is controlled by primary parasitoids and hyperparasitoids. Total parasitism rates are therefore the sum of these two states with low host densities, $P + HP$. Severe defoliation causes complete forest death, and eventually results in R recovering forest. Young forest can only support low host densities, so there is no visible defoliation.

3.2.3 Description of state transitions

Rates of c control and e exclusion describe changes in parasitoid dominance. c and e are analogous to colonization and extinction in the metapopulation model but we rename them to emphasize that they occur due to biotic interactions (Figure 3.2 arrows). Control and exclusion processes occur at rates proportional to themselves because the parasitoid is present in the forest at low densities (dispersal from another stand is not required). Dispersal of hosts occurs only between

neighbouring stands (α).

A recovering forest grows to mature parasitoid-controlled forest ($R- > P$ with probability c_p). During forest recovery, parasitoids locate and attack scattered host individuals, increasing in density and establishing dominance. Parasitized hosts are the main resource in the parasitoid-controlled forest, therefore hyperparasitoids reproduce and gradually control parasitoids ($P- > HP$ with probability c_{hp}). Small hyperparasitoids are weaker dispersers so the transition from parasitoid-controlled to hyperparasitoid-controlled forest only depends on the proportion of its state (not on proportion of another state). Hyperparasitoid-control is unstable because hyperparasitoids ultimately cause mortality of both hosts and parasitoids (simultaneous strong effects on two trophic levels, Figure 3.1). Over time, parasitoid mortality by hyperparasitoids feeds back to hyperparasitoid mortality because there are no parasitized hosts required to complete its life cycle (obligate hyperparasitoids can only attack already parasitized hosts). The hyperparasitoid is excluded locally because hyperparasitoid-control is an unstable state and causes a top-down collapse of the host-parasitoid-hyperparasitoid chain. When hyperparasitoids are excluded, low host densities experience no natural enemy attack and reproduce without natural enemies. Host densities increase exponentially because parasitoids cannot increase fast enough, and cause defoliation ($HP- > I$ with probability e_{hp}). Parasitoid-control is also unstable because parasitoids overexploit hosts. When parasitoids are excluded, hosts reproduce without natural enemies, causing defoliation ($P- > I$ with probability e_p).

Dispersal between neighbouring stands allows hosts to spread from infected to parasitoid- controlled forest ($HP- > I$ if neighbours are infected, dispersal transition with probability $\alpha_{sbw_{hp}}$, mass action). Hyperparasitoid-controlled stands have a low parasitoid density. Because the hyperparasitoid cannot lay eggs in the budworm without the parasitoid intermediate, the budworm experiences

no mortality there. Host dispersal can also take place into parasitoid-controlled forest because host densities are several orders of magnitudes higher in infected states ($P- > I$ dispersal transition with probability α_{sbw_p}, mass action). Parasitoid and hyperparasitoid disperse to the four closest stands, controlled by α_p and α_{hp} respectively. We assume that defoliation dieback is caused by resource depletion and not parasitoids ($I- > R$ transition with probability γ_2).

3.2.4 Spatially-implicit metacommunity model formulation

We express the above verbal description of the host-parasitoid- model in a system of mean-field equations to quantify landscape dynamics. Here we implement the novel biotic mechanism that the hyperparasitoid inhibits parasitoid-control and initiates a defoliation event. Without hyperparasitoids ($c_{hp} = 0$) the metacommunity model reduces to a parasitoid model. Each variable represents the proportion of stands in each forest state, and the landscape contains a fixed number of stands, so $R + P + HP + I = 1$ and $R = 1 - (P + HP + I)$. We represent the dynamics with the following system of differential equations:

$$\frac{dP}{dt} = c_p R + \alpha_p PR - e_p P - (1 - (1 - \alpha_{sbw_p} I^8))P - c_{hp} P - \alpha_{hp} PHP \quad (3.1a)$$

$$\frac{dI}{dt} = e_p P + (1 - (1 - \alpha_{sbw_p} I^8))P + e_{hp} HP + (1 - (1 - \alpha_{sbw_{hp}} I^8))HP - \gamma_2 I \quad (3.1b)$$

$$\frac{dHP}{dt} = c_{hp} P + \alpha_{hp} PHP - e_{hp} HP - (1 - (1 - \alpha_{sbw_{hp}} I^8))HP \quad (3.1c)$$

$$\frac{dR}{dt} = \gamma_2 I - c_p R - \alpha_p PR \quad (3.1d)$$

Rates c and e are (hyper)parasitoid-control and exclusion rates, γ_2 is infection dieback (Table 3.1). Because forest stands are immobile, α_p corresponds to

host dispersal into parasitoid-controlled forest and α_{hp} corresponds to host dispersal into hyperparasitoid-controlled forest. In a landscape model each stand is potentially surrounded by multiple infected stands yet a single successful dispersal event is sufficient to cause infection. Therefore, we need to modify I in the equation. $1 - I$ sets the rate that no dispersal occurs from a given neighbor. The neighborhood of each stand is the closest 8 stands, and the rate at which a no-dispersal event occurs from all of them is thus $(1 - I)^8$. Finally, rate of dispersal from *at least one* neighbor is $1 - (1 - I)^8$ (as Fukś & Lawniczak, 2001; Guichard et al., 2003). This approximation allows us to implicitly consider space and introduces a more realistic non-linearity in the system making it susceptible to instability (Nenzen et al. submitted). A high proportion of infected forest stands means a high density of insects and population growth, and indirectly a higher rate of infection.

3.2.5 Spatially-explicit metacommunity model formulation

A spatially-explicit model is used to investigate the effect of spatially-explicit dispersal by tracking the neighbours of each forest stand. It is a cellular automaton where each stand can be in *only* one of four potential states: parasitoid-controlled forest, P, hyperparasitoid-controlled forest HP, infected, I, or recovering, R. Therefore, the *total* proportion of each state is equivalent to the proportion modeled by the mean-field model. The transition rules to each focal stand (and from

each infected neighbor in case of dispersal) are the following:

$$R \rightarrow P \text{ if parasitoid species present } (c_p) \tag{3.2a}$$

$$P \rightarrow HP \text{ if hyperparasitoid species controls and parasitoid absent } (c_{hp}) \tag{3.2b}$$

$$HP \rightarrow I \text{ if hyperparasitoid species is excluded and parasitoid absent } (e_{hp}) \tag{3.2c}$$

$$P \rightarrow I \text{ if } \alpha_p \geq h \tag{3.2d}$$

$$HP \rightarrow I \text{ if } \alpha_{hp} \geq h \tag{3.2e}$$

$$I \rightarrow R \text{ if } \gamma_2 \geq h \tag{3.2f}$$

In our spatially-explicit model, the transition depends on the same parameters as in the spatially-implicit model, but rates from the deterministic spatially-implicit model here become probabilities of transition. Probabilities are stochastic because they are compared to uniformly distributed random numbers h between $0-1$.The algorithm simulates a separate dispersal event from each infected neighbor with a random h drawn for each infected neighbor (maximum 8 neighbouring stands). A susceptible stand can potentially be infected multiple times but one successful dispersal event is enough to cause an infection.

3.2.6 Model implementation and analysis

We investigated the spatially-implicit and -explicit metacommunity model with numerical simulations, and specifically the impact of hyperparasitoid control rate and host dispersal on occurrence of outbreaks.

To explore parameter space, we tested 20 values of c_{hp} in the range $0.00001-$

0.1, and 2 values of e_{hp}, 0.00001 and 0.002. We also tested the effect of distinct host dispersal rates into parasitoid- and hyperparasitoid-controlled forest, α_p and α_{hp} (0-1 in increments of 0.05, equations 3.1a-3.1d, 3.2a-3.2f). Other parameters are considered constant and so they were not investigated here (Table 3.1). The minimum time to reach mature forest in North American boreal forests is 40 years (Burns & Honkala, 1990), therefore we set c_p to 1/40. Stand mortality usually begins in the fifth year of infection, and full mortality occurs after roughly 10 years when the stand is completely defoliated and unable to photosynthesize (MacLean, 1980). We therefore set γ_2 to 1/3, based on the number of years infection lasts before killing a forest stand.

We analyzed the spatially-implicit model (equations 3.1a-3.1d) with both local stability analysis and numerical simulations. Local stability analysis was conducted to identify the critical conditions required for the occurrence of damped or sustained oscillations at different parameter values (Soetaert, 2009). Local stability analysis estimates the Jacobian matrix numerically at the positive equilibrium points. Oscillations occur if the eigenvalues of the Jacobian are complex (have imaginary parts). We numerically simulated the spatially-implicit model with a Runge-Kutta fourth-order integration with a time step of 0.1. We ran simulations for 5000 years and discarded the first 100 years as transients.

The spatial simulations (equations 3.2a-3.2f) occurred in a square lattice of X^2 forest stands with periodic boundary conditions (torus, X = 200). We used a large landscape to allow landscape dynamics to emerge, and present results from a subset of 10 x 10 stands. In each time step (year) the model randomly selected X^2 stands and updated their states. A stand may therefore have no or multiple state changes per stand in a single time step. This method approximates continuous mean-field dynamics (asynchronous updating, Durrett & Levin, 1994). The initial state was an equal proportion of all states (0.25) distributed randomly in space.

Table 3.1 Model states and default parameters used in simulations.

Process	Symbol	Value	Description
States	P		Parasitoid-controlled forest
	HP		Hyperparasitoid-controlled forest
	I		Infected forest
	R		Recovering forest
Parameters	γ_2	1/3	Infection dieback
	c_p	1/40	Forest regrowth to P
	e_p	0	Parasitoid exclusion, loss of control
	c_{hp}	0.0001	Hyperparasitoid-control
	e_{hp}	0.001	Hyperparasitoid exclusion, loss of control
	α_p	0	Parasitoid dispersal
	α_{hp}	0.3	Hyperparasitoid dispersal
	α_{sbw_p}	0.0	Probability of host dispersal into P
	$\alpha_{sbw_{hp}}$	0.4	Probability of host dispersal into HP

We ran 10 stochastic simulations for each parameter set.

We analyzed the simulation results to determine if large-scale outbreaks occurred, and their spatial distribution. We recorded maximum proportion of infected stands I during each simulation as outbreak size. Average parasitism rates were represented by the combined proportions of P and HP states, since this indicates the proportion of stands where host densities are low.

3.3 Results

Model simulations indicated that hyperparasitoids destabilized community dynamics and caused hosts to have large, cyclic outbreaks. Outbreaks occurred as hyperparasitoids gradually controlled a larger proportion of the previously parasitoid-controlled landscape and their inherent instability caused them to drop and an outbreak occur (Figure 3.3 C, F). Even though the model was formulated so there were no hyperparasitoids in defoliated forest, on a landscape-scale hyperparasitoids remained during the epidemic period. Hyperparasitoid-control peaked just before and during outbreaks.

The spatially-implicit model generated outbreaks at the beginning of simulations, while the spatially-implicit model generated outbreaks that were sustained for longer periods. In the spatially-implicit model, with only the presence of hyperparasitoids there were damped oscillations (Figure 3.3 C). In the spatially-explicit model, with hyperparasitoids there were large outbreaks that covered almost 50% of the landscape. Outbreaks initiated by only hyperparasitoids were 10% larger than those produced under the assumption both hyperparasitoids and parasitoids (Figure 3.3 F vs. E). If there were no hyperparasitoids and only parasitoids caused outbreaks, defoliation was constant and there were no large-scale outbreaks (in both spatially-implicit and -explicit models, Figure 3.3 A, D).

Hyperparasitoid control and exclusion rates controlled the outbreak dynamics. Higher hyperparasitoid control rates c_{hp} removed hyperparasitoid-control faster and increased outbreak size (0.4 of landscape infected at low hyperparasitoid exclusion e_{hp} rates, Figure 3.4). Higher hyperparasitoid control and exclusion rates allowed the hyperparasitoid to quickly control hosts throughout the landscape, so outbreaks occurred constantly and were therefore smaller (0.07 of landscape infected, Figure 3.4).

Simulation results supported the hypothesis that hosts should be capable of spreading more into hyperparasitoid-controlled forest. The reason is that in forest controlled by hyperparasitoids, parasitoid densities are lower so hosts experience less parasitism and outbreaks are larger. With no host dispersal, outbreaks covered <0.01 of the landscape (α_{sbw_p} and $\alpha_{sbw_{hp}} < 0.1$, Figure 3.5). Larger outbreaks occurred when hosts dispersed faster into hyperparasitoid-controlled forests than into parasitoid-controlled forest (in terms of % landscape infected, above the white diagonal, Figure 3.5).

3.4 Discussion

Insect outbreaks have large ecosystem and economic impacts so to better predict and anticipate them, we investigated how natural enemies may cause outbreaks. Our metacommunity model replicated unstable and over-exploitative host-parasitoid interactions and results suggested that natural enemies destabilize host dynamics and generate outbreaks. Parasitoid and hyperparasitoid densities build up until all natural enemies are excluded and host population rapidly increases (Figure 3.3). The spatially-implicit version did not generate sustained outbreaks, while the outbreaks in spatially-explicit version suggest that local dispersal is essential to generate outbreaks in nature (Figure 3.3 C vs. F). Hyperparasitoids especially destabilize host dynamics because they control the densities of two trophic levels simultaneously; both hosts and parasitoids (Figure 3.1). Only parasitoids could not explain why total parasitoid-control decreases, so if hyperparasitoids were not observed, parasitoids could not explain outbreaks alone. We showed that modelling 2 species (host and parasitoid) is insufficient and that tri-trophic metacommunity model was capable of reproducing outbreaks. Higher trophic levels such as hyperparasitoids potentially add instability to forest pest ecosystems and cause outbreaks.

We constructed a metacommunity model that quantitatively supported observations that hyperparasitoids may cause outbreaks (Rosenheim, 1998). Hyperparasitoid impacts are generally underestimated because they are little studied. Hyperparasitoids are difficult to rear in laboratories and few studies are explicitly designed to sample them when emerging at the end of the season (Hawkins, 1994; Rosenheim, 1998). Studies that quantified their effects indicate that modelling dynamics of additional trophic levels is necessary. For example, single-species metapopulation models did not capture dynamics of hosts that are attacked by

parasitoids (Kean & Barlow, 2000). Rosenheim (2001) observed empirically that parasitoids controlled aphid host densities in cotton fields. Parasitoid densities increased when they were protected from hyperparasitoid predation, suggesting that hyperparasitoids can disrupt the top-down control.

Without investigating hyperparasitoids, studies may attribute outbreaks to other mechanisms, such as bottom-up control or climate. The model helps to illuminate the top-down mechanisms that cause observed parasitoid-control to decrease just before an outbreak (Myers & Cory, 2013). During epidemic periods of spruce budworm the observed natural enemy community had more hyperparasitoid species. Eveleigh et al. (2007) interpreted this as a 'bird feeder effect', in which higher budworm densities attract a higher parasitoid and hyperparasitoid species richness. Here, hyperparasitoids were more prevalent just before and during epidemic periods because they actually add additional instability and cause outbreaks. The top-down hypothesis that natural enemies drive outbreaks fits observed budworm outbreaks well because there were long endemic periods punctuated by fast increases in epidemic densities (Figure 3.3). Once the host has increased in density in one location, higher dispersal rates into hyperparasitoid-controlled forest further favoured large outbreak sizes (as expected because it encounters no natural enemies without the primary parasitoid (Figure 3.5). Model results suggested that top-down control can also explain the occurrence of outbreaks.

The model can be validated with landscape-level data such as defoliation and parasitism rates because it models parasitoid-control. We assumed that defoliation is a proxy for high host:parasitoid density ratios, and that healthy forest indicates high parasitoid- and hyperparasitoid-control rates. This assumption allows us to build a presence-absence metacommunity model instead of a population density model. While these assumptions might simplify the ecology too much, metacom-

munity models are advantageous because they require fewer parameters so are more are transparent. An additional advantage of using defoliation as a proxy for species-control is that the model can be directly compared to available data on parasitoid-caused host mortality (i.e. percentage parasitism rates on hosts caused by all parasitoids, Myers & Cory, 2013; Klemola et al., 2010). This is useful because in the field it is easier to quantify parasitism rates than estimate population densities (as required by population models, among other parameters, Hassell, 2000). We suggest the model is flexible enough to illuminate dynamics of other parasitoid systems.

3.5 Conclusion

The metapopulation concept was originally developed to improve biological control of pests (Levins, 1969), but has rarely been used in biological pest management because it did not explicitly include biotic interactions. Here, we extend the metapopulation models to metacommunity model that can represent realistic interactions between multiple trophic levels. This metacommunity model is more transparent and tractable compared to similar population models that represent multiple trophic levels with a greater number of parameters. Results suggest that future empirical and theoretical studies should also consider natural enemies from higher trophic levels, as they may have destabilizing effects on host dynamics. The model made the testable prediction that hyperparasitoid-control rates should increase (and consequently parasitism rates drop) just before an outbreak occurs. If empirical data reveal the same gradual increase of hyperparasitoid-control rates, hyperparasitoids could could serve as an early warning signal of outbreaks.

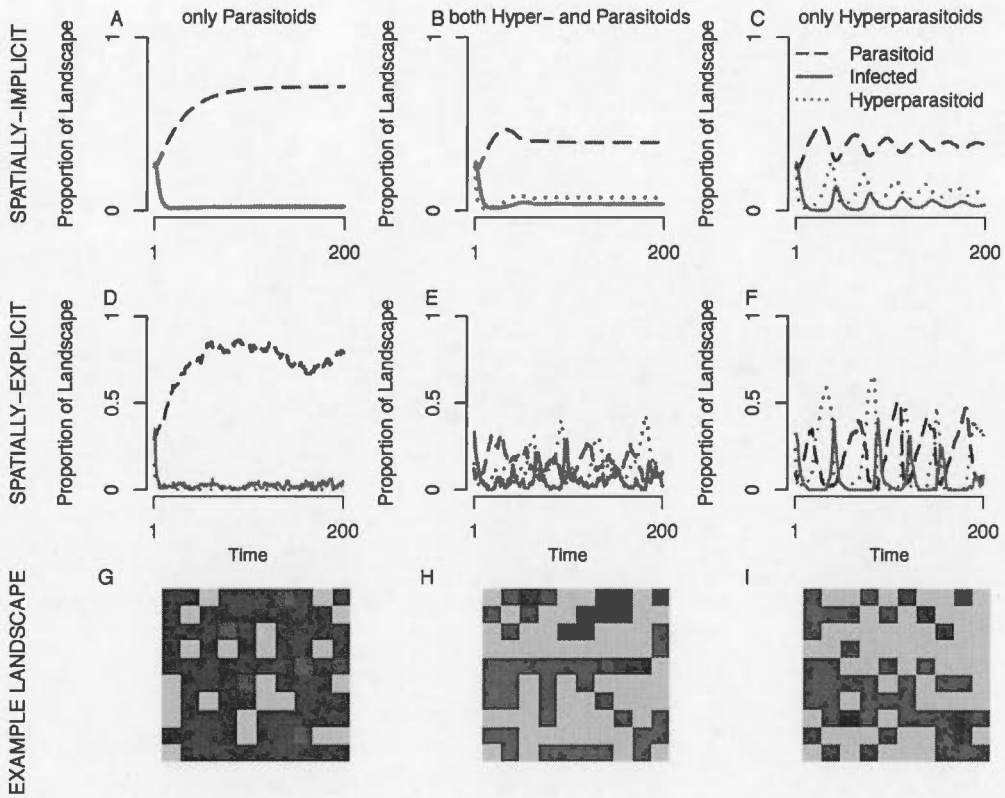

Figure 3.3 Example simulations with only parasitoids (left column, A, D, G), both parasitoids and hyperparasitoids (middle column, B, E, H), and only hyperparasitoids (right column, C, F, I), in both spatially-implicit (top row) and -explicit models (middle row). The bottom row shows an example landscape from the spatially-explicit simulations. If a (hyper-)parasitoid was present, its exclusion rate e_p (e_{hp}) was 0.001. All other parameters are as in Table 3.1.

3.6 Acknowledgements

Funding was provided by the Forest Complexity Modelling programme, Natural Sciences and Engineering Research Council of Canada - Collaborative Research and Training Experience and Discovery programmes, Canada Research Chairs, Université du Québec à Montréal and a Doctoral Research Fellowship from the Fonds de recherche du Québec - Nature et technologies. Thanks to Lukas

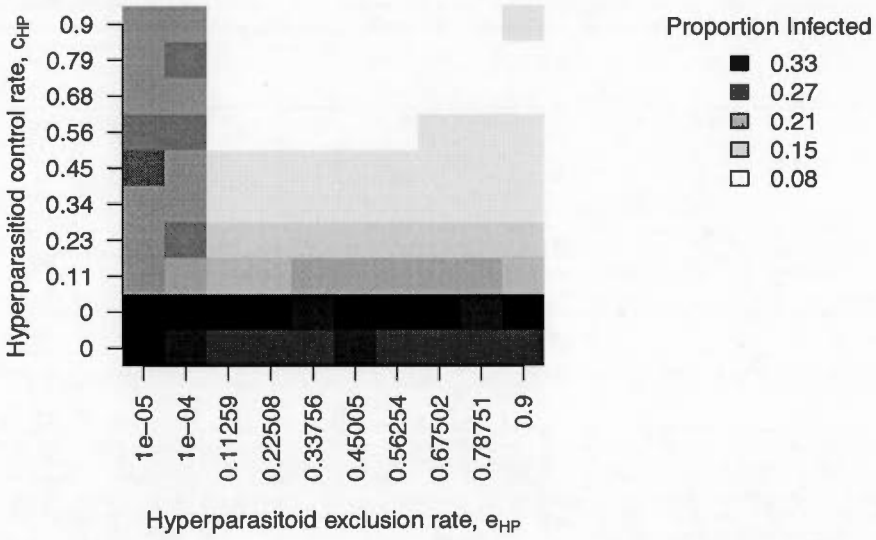

Figure 3.4 Effect of hyperparasitoid control c_{hp} and exclusion e_{hp} rates on outbreak size, i.e. proportion landscape in state I. Each value indicates the average maximum infected proportion from all simulations with that parameter combination. Simulations were carried out with other parameters as in Table 3.1.

Seehausen for introduction to budworm parasitoids. Thanks to Emily Tissier for editing the manuscript.

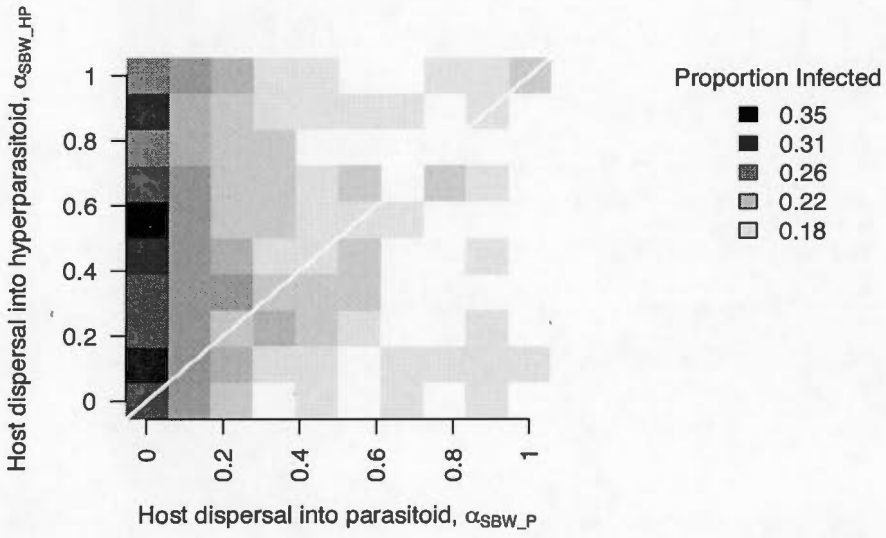

Figure 3.5 Effect of host dispersal rates into parasitoid-controlled and hyperparasitoid-controlled forest on outbreak size, i.e. proportion landscape in state I. The diagonal white line indicates $\alpha_{sbw_p} = \alpha_{sbw_{hp}}$. Simulations were carried out with all other parameters as in Table 3.1.

CONCLUSION

In chapter 1, I constructed a metapopulation model inspired by spruce budworm to assess how insect dispersal affects outbreaks by tracking defoliation. Transitions between mature (non-defoliated) and infected (defoliated) forest mirrored the local cycle of the budworm resource depletion and regeneration. Results showed that nonlinear dispersal between patches synchronized these local cycles and generated outbreaks. The Allee effect decreases budworm population growth rates during low densities (Régnière & Nealis, 2007); the result suggest that this local process may propagate up to influence landscape dynamics. My modelling framework compared spatially-implicit and -explicit model implementations; the difference between these results is the presence of spatial variability in dispersal. I found that spatially-explicit simulations produced outbreaks over a wider set of parameters, and that stronger dispersal produced larger outbreaks in terms of infected landscape. The emergent simulation results matched the 35-year periodicity of budworm outbreaks in our region, but simulated infections never covered more than a third of the landscape. While certain parameter values reproduced observed outbreaks, those parameter values may not be realistic in nature. In this theoretical chapter, I identified that nonlinear dispersal can synchronize fluctuations, however what triggers the initial 'epicenter' remained unknown.

In chapter 2, observed landscape data was used to parameterize the model framework developed in chapter 1. Confronting my model with data allowed me to test the second synchronizing mechanism; the Moran effect. A statistical model was fitted to data to explore if infection epicentres and dispersal were driven by climate fluctuations. I found outbreaks were driven by a suite of climate variables.

Coupling statistical models to simulation models showed that temporal autocorrelation was important to synchronize outbreaks (Figure B.8, Figure 2.4). At the beginning of both outbreaks, defoliation probabilities were high and dieback probabilities were low, which generated many epicentres that stayed infected for many years (asynchronous probabilities, Figure B.8). Consecutive years with suitable climate conditions affected local population growth and mortality rates so that the species remained at epidemic densities longer and were able to disperse. Temporal autocorrelation 'enhanced' the Moran effect by indirectly favoured dispersal which, in turn, synchronized outbreaks. It was dispersal that synchronized outbreaks and not the spatial Moran effect, because the spatial autocorrelation did not contribute to better reproducing outbreaks. An interaction between climate and dispersal was also identified statistically (submodels with interactions fit observed data better, Table 2.2).

The Moran effect alone cannot explain why budworm outbreaks recur every 35 years (Royama, 1992), so other processes might be acting upon these outbreaks. Temporal autocorrelation is important, but climate does not cycle regularly and therefore cannot cause outbreaks with regular intervals. Local cycles may be explained by the forest resource slowly growing back after previous mortality. However, these resource cycles are not sufficient to explain large-scale outbreaks because they cannot synchronize defoliation in space. Empirical studies have shown that stand age alone only partially explained variation in stand mortality (Bergeron et al., 1995). On the basis of this, I did not consider stand age as a synchronizing mechanism. I tested this assumption, and stand age was not an accurate predictor of the observed defoliation dynamics (according to AIC, Section B.3). Stand age was not considered as a mechanism in my model, instead local cycles were determined solely by landscape-level drivers that can synchronize outbreaks (dispersal, climate and natural enemies).

My simulation model reproduced the temporal patterns of budworm defoliation but was less successful at reproducing spatial and spatiotemporal patterns. The dispersal kernel, parameterized from the spatiotemporal spread of defoliation, indicated that budworms disperse over long distances (Figure 2.3). The observed kernel had a much larger range than the neighbourhood kernel in chapter 1, and should have generated the spatially clustered defoliation. However, defoliation 'clusters' were too small and fragmented and did not closely resemble observed outbreaks (Figure 2.5). Moreover, the model did not reproduce the episodic transitions in observed data (Figure 0.4). Episodic defoliation occurs when multiple neighbouring stands become infected in the same year. The model already accounted for spatiotemporal climate variation and so we can rule out climate as a causal factor. Forest type as a predictor also did not reproduce the observed defoliation dynamics in my work (according to AIC, Section B.3). Intuitively, this result is expected as forest type does not change annually. Moreover, these episodic transitions occur throughout large regions (Sturtevant et al., 2015). It is possible that episodic transitions are data artefacts if aerial surveys were not detailed enough. Because my estimated dispersal kernel, climate and forest type cannot fully explain the observed patterns of dispersal, additional mechanisms should be explored.

The dispersal kernel can be altered to represent underlying population processes. In presence-absence models, dispersal represents both successful migration from a patch as well as establishment in another patch. In population models on the other hand, density-dependent dispersal from a patch is proportional to population size, where population size varies in response to climate. The interaction between climate in one location and successful dispersal elsewhere was not explicit in our framework. To represent how climate affects local population size, one could add a spatially-explicit mechanism that uses climate as a proxy for lo-

cal population density (Lande et al., 1999; Gravel et al., 2010). For example, the dispersal kernel to a patch could be further modified to depend on the climate in the donor patch. The dispersal probability to patch i from patch j would be $exp(-\delta d_{ij} E_j)$ where E_j is the climate in patch j, δ is the parameter to estimate and d_{ij} is the distance between cells (instead of $exp(-\delta d_{ij})$ in chapter 2). Thus, population dynamics could be approximated to possibly provide a more realistic model.

In chapter 3, I tested the third synchronizing mechanism: biotic interactions. If climate is not responsible for initiating outbreaks, possibly interactions with natural enemies can destabilize budworm dynamics. To rigorously investigate this, I developed a metacommunity model in which host-parasitoid interactions drive species distribution. My model reflected the intuition of Royama (1992) that multiple levels of natural enemies build up over time: "Because many (probably all) primary parasitoids in the field are attacked by their own enemies, their efficacy to control spruce budworm is greatly reduced." Thus, the forest - budworm - natural enemy complex oscillates slowly with high amplitude. This formulation also followed the tritrophic verbal model of Cooke et al. (2007), but instead, I included four trophic levels; resource, host, parasitoid and hyperparasitoid. My model is similar to the double equilibria model (Ludwig et al., 1978) in that natural enemies affect host densities. Our model was capable of representing multiple trophic interactions without becoming intractable by representing species ratios (control or not controlled) instead of densities.

To explore the hypothesis of biotic interaction, I reformulated the landscape model of previous chapters so the healthy forest stage can be controlled by two different trophic levels (parasitoid and hyperparasitoid). This is a valid assumption because parasitoids and hyperparasitoids both suppress host densities, but hyperparasitoids are more difficult to detect (Rosenheim, 1998). The addition of this

state changed the underlying model structure, as well as emergent outbreak patterns. In epidemiology, disease patterns were better understood when states that are difficult to detect were included in the SIR model. For example, cholera may cause inapparent (assymptomatic) infections in individuals, but those individuals do not transmit the disease and change the overall disease pattern (King et al., 2008). The formulation of a mechanistic model must account for all important states and underlying mechanisms to be able to predict outbreak dynamics (King et al., 2008). In my study system, I suggest that the hyperparasitoid-controlled forest is an inapparent state which is rarely measured but its presence changes outbreak patterns.

Previous chapters showed that dispersal is episodic, so the logical next step is developing a spatially-explicit version of the metacommunity model. Parasitoids generally have smaller body sizes than hosts because there is less available energy at the top of the food chain (since only one trophic interaction occurs during their lifetime, Brodeur, 2000). Smaller parasitoids are less mobile than their hosts, and hyperparasitoids are occasionally wingless (Harvey, 2008). In trophic networks, predators disperse more than their prey which links patches in space and reduces spatial heterogeneity (McCann et al., 2005; Gravel et al., 2011b; Tunney et al., 2012). However, I expect less mobile natural enemies such as parasitoids, to increase the patchiness in the landscape. A spatially-explicit model can assess whether hyperparasitoids reproduce the spatial patchiness and episodic transitions of observed defoliation. Parasitoids have unique coexistence and dispersal dynamics, compared to predators, and these characteristics are reflected in the design of the metacommunity model.

Current host-parasitoid models rarely incorporate multiple species at each trophic level, but the metacommunity model can easily be extended to represent multispecies dynamics. Ecologists do not completely understand dynamics

of observed complex host-parasitoid interaction networks (Hawkins et al., 1999; Morris et al., 2014). Host-parasitoid networks show which species are generalists and attack multiple hosts, or specialists that only attack one host. The identity of species, and proportion of specialists and generalists that attack the budworm, changes during an outbreak cycle. For example, during the end of epidemic budworm densities, there was a higher number of generalist parasitoid and hyperparasitoid species than during endemic periods (Eveleigh et al., 2007). To investigate if specialist and generalist species play different roles in outbreaks, model simulations could test how interaction networks observed during endemic and epidemic periods influence outbreak size. Do certain specialists or generalists, at the parasitoid or hyperparasitoid level, encourage or discourage outbreaks? A metacommunity model would provide the mechanisms to study spatiotemporal community assembly, and could explore how the interactions between species affects outbreaks (Eveleigh et al., 2007; McCann & Rooney, 2009).

3.7 Management to minimize outbreaks

The metapopulation model was developed explicitly to guide pest management (Levins, 1969), but it has rarely been applied to real pest management situations. Even though research shows that species disperse, pest control is handled as if pests were immobile (Stinner et al., 1983; Tscharntke et al., 2007). The metapopulation model could be very useful to explore novel management practices because it is formulated at the landscape scale: the scale at which management is decided (Cuddington et al., 2013). In order for ecological theory to have a wider influence on society, the spatiotemporal scales of population experiments and models should match management scales (Stevens et al., 2007). The improved understanding of landscape-scale drivers of outbreaks achieved in this thesis can aid in management of budworm outbreaks. By knowing how dispersal and natural enemies synchronize outbreaks, we can develop novel management

methods to desynchronize outbreaks.

Various control strategies have been employed to stop the destruction of economically-important forests, but budworm outbreaks have proven remarkably resistant to control efforts. When outbreaks have already started, short-term strategies against spruce budworm are through biological and chemical controls. Large-scale DDT aerial spraying was common until the end of the last big outbreak (Morin et al., 2007; Ludwig et al., 1978). Such indiscriminate pest interventions can harm the metacommunity, and DDT application possibly killed budworm's natural enemies and further prolonging outbreaks (Cooke et al., 2007). Presently, a bacterial insecticide *Bacillus thuringensis* is used to control defoliation (Fournier et al., 2010). However, spraying one stand is futile, because dispersal from other locations will increase local host densities anyway (Sturtevant et al., 2015). Trying to stop an outbreak through population suppression is 'practically impossible' (Liebhold, 2012), so past control efforts may have been ineffective because they did not consider the landscape. The goal is not to stop outbreaks, but to desynchronize them so that defoliation is constant in time.

Since the metapopulation model is analogous to epidemiological models (Grenfell & Harwood, 1997; Earn et al., 1998), the model developed here can integrate epidemiological strategies to bolster management strategies. Given that the goal of epidemiology is to contain outbreaks, epidemiology has a large toolbox of vaccination techniques (Anderson & May, 1992; Keeling & Rohani, 2008). Epidemiological models can open new possibilities of forest management by 'vaccinating' the landscape against insect outbreaks. In the metapopulation model, logging removes forest that is susceptible to outbreaks, just like in epidemiology, vaccination removes susceptible individuals to limit transmission (Riley, 2007). Currently, forestry management sets total levels of harvesting in the form of 'annual allowable cuts', but does not direct in which locations the harvesting should

be implemented. As shown in epidemiology, targeting the individuals most likely to spread the disease leads to more effective vaccination (Keeling & Eames, 2005). For diseases within a landscape, targeted vaccination corresponds to spatial vaccination. For instance, Beyer et al. (2011) constructed a spatially-explicit metapopulation model of rabies and determined which locations should be targeted to produce effective vaccinations. The budworm dispersal kernel estimated here could be transformed into management tools for setting spatiotemporally-explicit harvesting guidelines. I showed that the Allee effect has landscape-scale effects on outbreak size. By logging to fragment large areas of mature forest, the Allee effect could be used to reduce effective dispersal and thus outbreaks (Johnson et al., 2006; Blackwood et al., 2012).

A second approach to improve management is through biological control that uses the characteristics of higher-level hyperparasitoids. Biocontrol methods presently focus on how characteristics of single parasitoid species may influence parasitoid control (Murdoch et al., 2003; Briggs & Hoopes, 2004) and rarely if the parasitoid is suppressed by hyperparasitoids. Research efforts have possibly ignored hyperparasitoids because they inhibit parasitoid control and threaten biocontrol (Rosenheim, 1998). However, ecologists have to understand why parasitoid control fails. As Royama (1992) cautioned, what happens in the system will be difficult to predict unless we know the composition and status of the food web. The model suggests that a rising proportion of hyperparasitism constitutes an early warning signal (Scheffer et al., 2009) for imminent loss of parasitoid control and eventual outbreak.

3.8 Conclusion: Space-time interactions in forest metacommunities

In this thesis, I reinterpreted insect pest outbreaks as a metapopulation process, which closely integrated data with modelling, and bridged inductive and

deductive models (Coulson et al., 2004). Articulating our biological knowledge in mechanistic models forces us to clearly express the dynamics and acknowledge our assumptions. I formulated a single model from the defoliation data that incorporated the three main mechanisms of outbreaks, instead of a separate model for each hypothesis. The metapopulation model is flexible enough to be applied to other species with spatiotemporal presence-absence data, and the resulting parameter values corresponds to drivers of each species. Successful management strategies depend on knowing the parameters that affect species dynamics (Levins, 1969). In conclusion, the metacommunity model is a way to produce simple, semi-mechanistic and data-rich models (Cooke et al., 2007).

Validation is a challenge with more complex models (Scheller & Mladenoff, 2007), however my minimal framework could be validated in four ways. For the statistical model, I compared model accuracy and predictive ability (AIC vs. independent cross-validation). The two evaluation measures provide complementary information, showing that climate accurately describes outbreaks but is not general enough to predict future outbreaks. Second, I used a simulation model to fit emergent properties such as outbreak frequency and amplitude, instead of statistical accuracy. Third, to assess if model type influences results, the simulation model in chapter 1 was implemented with two different mathematical methods (ordinary differential equations and cellular automata) which makes robust results (Levins, 1966; Scheller & Mladenoff, 2007; Harrison et al., 2011). Finally, the metacommunity model reflected the same unstable coexistence as host-parasitoid models (Nicholson & Bailey, 1935) but in a presence-absence formulation. Reformulating the model from the same biological observations avoids assumptions inherent in population models. In the end however, models are no more, and no less, than our best understanding of the system (Levins, 1966).

In this thesis I investigated the three main mechanisms hypothesized to syn-

chronize outbreaks by developing a novel modelling framework that allows direct comparison to empirical data on the same scale as outbreaks. I demonstrated that spatiotemporal autocorrelation in climate values may amplify insect population fluctuations, and that dispersal and natural enemies interact to spatially cluster distributions. I also presented an original, quantitative theory and testable predictions of how higher-order natural enemies can influence outbreaks. Thus, local processes of budworm and natural enemy interactions produce slow oscillations in one location. When dispersal was enhanced by the Moran effect, it synchronized the oscillations in multiple locations causing a widespread, periodic outbreak to occur. I studied multiple scales of outbreaks and was able to show that different drivers control local and regional dynamics. Although I might have sacrificed precision by not modelling population densities, I gained realism and generality (Levins, 1966), and a model useful to improve future management. In short, I demonstrated that temporal climate autocorrelation may amplify insect population fluctuations in time and that dispersal and natural enemies interact to spatially cluster distributions.

APPENDIX A

EPIDEMIOLOGICAL LANDSCAPE MODELS REPRODUCE CYCLIC INSECT OUTBREAKS

A.1 Local stability analysis of the mass-action approximation

Here we show the analytical results for the local stability analysis of the equations with mass action dispersal αFI. Here we use mass action dispersal because the dispersal equation $\beta F+\alpha f(I)[1-(1-I)^{24}]F$ and $f(I) = I^p$ (equivalent to the cellular automata) is not tractable. We used the mass-action approximation αFI of dispersal to be able to solve the equations algebraically. The equations are:

$$\frac{dF}{dt} = \gamma_1(1 - F - I) - \beta F - \alpha IF \tag{A.1}$$

$$\frac{dI}{dt} = \beta F + \alpha IF - \gamma_2 I \tag{A.2}$$

Without the assumption of spontaneous infections ($\beta = 0$), there are two equilibria (analysis in sage code, Section A.2 below). In one unstable equilibrium there is no spruce budworm so we do not analyse it further. For the second equilib-

rium, $\overline{F}$ indicates the proportion of mature forest in the landscape at equilibrium:

$$\overline{F} = \frac{\gamma_2}{\alpha}$$

$\overline{I}$ indicates the proportion of infected forest in the landscape at equilibrium:

$$\overline{I} = \frac{(\alpha * \gamma_1 - \gamma_1 * \gamma_2)}{(\alpha * \gamma_1 + \alpha * \gamma_2)}$$

We evaluate the Jacobian of the system of equations at the non-trivial equilibrium point. We determine the stability of this equilibrium point based on the eigenvalues of the Jacobian. The parameter values determine the stability of the system, as indicated by the sign of the real parts of the eigenvalues and if the eigenvalues are complex. We evaluate the eigenvalues under several parameter values α, γ_1 and γ_2. With $\alpha = 0.6, \gamma_1 = 1/3$ and $\gamma_2 = 1/3$ the eigenvalues λ are:

$$\lambda_1 = -0.03 - i0.09$$

$$\lambda_2 = -0.03 + i0.09$$

Eigenvalues are complex conjugates with negative real parts. The equilibrium point is a stable spiral: trajectories undergo damped oscillations toward the equilibrium.

With $\alpha = 0.1, \gamma_1 = 1/3$ and $\gamma_2 = 1/3$ the eigenvalues are:

$$\lambda_1 = -0.09$$

$$\lambda_2 = 0.08$$

One eigenvalue has negative real parts and the other has positive real parts. Therefore the equilibrium is a saddle point, which is always unstable.

With the assumption that spontaneous infections occur ($\beta > 0$, sage code in Section A.2 below), the same method of analysis indicates that there are two equilibria. For the first equilibrium, the eigenvalues and the condition for oscillations indicate that it does not have oscillations (negative and positive real eigenvalues). We evaluate the eigenvalues under several parameter values α. For example, with $\beta = 0.0015, \alpha = 0.1, \gamma_1 = 1/3$ and $\gamma_2 = 1/3$ the eigenvalues are:

$$\lambda_1 = 0.10$$

$$\lambda_2 = -0.09$$

With $\beta = 0.0015, \alpha = 0.6, \gamma_1 = 1/3$ and $\gamma_2 = 1/3$ the eigenvalues are:

$$\lambda_1 = 0.30$$

$$\lambda_2 = -0.03$$

Therefore, for both low and high dispersal rates the equilibrium is a saddle point (unstable).

For the second equilibrium, there are damped oscillations under high dispersal values ($\alpha = 0.6$, complex conjugates eigenvalues with negative real parts).

$$\lambda_1 = -0.04 - i0.095$$

$$\lambda_2 = -0.04 + i0.095$$

Therefore, with spontaneous infections and high rates of mass-action dispersal there are damped outbreaks (i.e. $\beta > 0$, produces oscillations that disappear over time).

A.2 Code for symbolic mathematical analysis

Here we show analysis of the FIRF model without $\beta = 0$ and with spontaneous infections $\beta > 0$ in sage (The Sage Developers, 2015). Results are preceded by #.

```
######################
# without spontaneous infections
# b = 0
reset()
var('a,g1,g2,F,In')

dFdt = g1*(1-F-In) - a*F*In
dIndt = a*F*In - g2*In

solutions = solve([dFdt==0, dIndt==0], [F,In])
solutions
# two solutions, one no Infected forest
# [[F == 1, In == 0], [F == g2/a, In == (a*g1 - g1*g2)/(a*g1 + a*g2)]]

J = jacobian([dFdt, dIndt], [F, In])
J
# [-In*a - g1  -F*a - g1]
```

```
# [      In*a   F*a - g2]

# evaluate the J Jacobian matrix at equilibria.
# second equilibrium
# substitute sequentially to get rid of F
J1 = J.substitute(solutions[1][0])
# substitute sequentially to get rid of In
J2 = J1.substitute(solutions[1][1])

eigs = J2.eigenvalues()
# test parameter values
eigvals0 = eigs[0](a = 0.6, g1 = 0.033, g2 = 0.33)
eigvals0
# -0.0287727272727273 - 0.0899006683250423*I
eigvals1 = eigs[1](a = 0.6, g1 = 0.033, g2 = 0.33)
eigvals1 # both eigenvalues are complex
# with negative parts = damped oscillations
# -0.0287727272727273 + 0.0899006683250423*I

# with lower dispersal a
eigvals0 = eigs[0](a = 0.1, g1 = 0.033, g2 = 0.33)
eigvals0
# -0.0933755611562973
eigvals1 = eigs[1](a = 0.1, g1 = 0.033, g2 = 0.33)
eigvals1
# unstable without oscillations (positive real parts)
# 0.0812846520653882
```

```
# condition for oscillations (complex eigenvalues)
tr = J2.trace()
dete = J2.det()
condition = tr^2 - 4*dete
condition
# ((a*g1 - g1*g2)*a/(a*g1 + a*g2) + g1)^2 -
# 4*(a*g1 - g1*g2)*a*(g1 + g2)/(a*g1 + a*g2)
condition(a = 0.6, g1 = 0.033, g2 = 0.33)
# condition is negative, there are oscillations
# -0.0323285206611570

# with lower dispersal a
condition(a = 0.1, g1 = 0.033, g2 = 0.33)
# the condition is positive,
# there are no oscillations (real eigenvalues)
# 0.0305061900826446


########################
# with spontaneous infections
# b > 0
reset()
var('a,b,g1,g2,F,In')

dFdt = g1*(1-F-In) - a*F*In - b*F
dIndt = a*F*In + b*F - g2*In
```

```
solutions = solve([dFdt==0, dIndt==0], [F,In])
solutions
# two long solutions
# [[F == -((b + g1)*g2^2 - ((a - b)*g1 - sqrt(a^2*g1^2 + 2*a*b*g1^2 +
# b^2*g1^2 + 2*a*b*g1*g2 + 2*b^2*g1*g2 - 2*a*g1^2*g2 + 2*b*g1^2*g2 +
# b^2*g2^2 + 2*b*g1*g2^2 + g1^2*g2^2))*g2)/((a^2 + a*b)*g1 +
# (a*b - a*g1)*g2 - sqrt(a^2*g1^2 + 2*a*b*g1^2 + b^2*g1^2 + 2*a*b*g1*g2 +
# 2*b^2*g1*g2 - 2*a*g1^2*g2 + 2*b*g1^2*g2 + b^2*g2^2 + 2*b*g1*g2^2 +
# g1^2*g2^2)*a),
# In == 1/2*((a - b)*g1 - (b + g1)*g2 - sqrt((a^2 + 2*a*b + b^2)*g1^2 +
# (b^2 + 2*b*g1 + g1^2)*g2^2 - 2*((a - b)*g1^2 - (a*b + b^2)*g1)*g2))/
# (a*g1 + a*g2)],
# [F == -((b + g1)*g2^2 - ((a - b)*g1 + sqrt(a^2*g1^2 + 2*a*b*g1^2 +
# b^2*g1^2 + 2*a*b*g1*g2 + 2*b^2*g1*g2 - 2*a*g1^2*g2 + 2*b*g1^2*g2 +
# b^2*g2^2 + 2*b*g1*g2^2 + g1^2*g2^2))*g2)/((a^2 + a*b)*g1
# + (a*b - a*g1)*g2 +
# sqrt(a^2*g1^2 + 2*a*b*g1^2 + b^2*g1^2 + 2*a*b*g1*g2 +
# 2*b^2*g1*g2 - 2*a*g1^2*g2 + 2*b*g1^2*g2 + b^2*g2^2 +
# 2*b*g1*g2^2 + g1^2*g2^2)*a),
# In == 1/2*((a - b)*g1 - (b + g1)*g2 + sqrt((a^2 + 2*a*b + b^2)*g1^2 +
# (b^2 + 2*b*g1 + g1^2)*g2^2 - 2*((a - b)*g1^2 - (a*b + b^2)*g1)*g2))
# /(a*g1 + a*g2)]]

J = jacobian([dFdt, dIndt], [F, In])
# evaluate the J Jacobian matrix at equilibria.

# first equilibrium
J1 = J.substitute(solutions[0][0])
```

```
J2 = J1.substitute(solutions[0][1])

eigs = J2.eigenvalues()
# test parameter values

eigvals0 = eigs[0](a = 0.6, b = 0.0015, g1 = 0.033, g2 = 0.33)
eigvals0
# 0.307590192814325
eigvals1 = eigs[1](a = 0.6, b = 0.0015, g1 = 0.033, g2 = 0.33)
eigvals1
# -0.0345756472563504
# both real eigenvalues with negative and positive parts,
# so saddle node without oscillations

# with lower dispersal a
eigvals0 = eigs[0](a = 0.1, b = 0.0015, g1 = 0.033, g2 = 0.33)
eigvals0
# 0.0984874692918797
eigvals1 = eigs[1](a = 0.1, b = 0.0015, g1 = 0.033, g2 = 0.33)
eigvals1
# -0.0869643497927223
# both real eigenvalues with negative and positive parts,
#  so saddle node without oscillations


# condition for oscillations (complex eigenvalues)
tr = J2.trace()
dete = J2.det()
```

```
condition = tr^2 - 4*dete
condition(a = 0.6, b = 0.0015, g1 = 0.033, g2 = 0.33)
# condition is positive, there are no oscillations
# 0.117077462111258

condition(a = 0.1, b = 0.0015, g1 = 0.033, g2 = 0.33)
# condition is positive, there are no oscillations
# 0.0343923772017880

# second equilibrium ############
J1 = J.substitute(solutions[1][0])
J2 = J1.substitute(solutions[1][1])

eigs = J2.eigenvalues()
# test parameter values
eigvals0 = eigs[0](a = 0.6, b = 0.0015, g1 = 0.033, g2 = 0.33)
eigvals0 # complex eigenvalues
# -0.0392800000517154 - 0.0953530891067237*I
eigvals1 = eigs[1](a = 0.6, b = 0.0015, g1 = 0.033, g2 = 0.33)
eigvals1 # complex eigenvalues
# with negative parts = damped oscillations
# -0.0392800000517154 + 0.0953530891067237*I

# with lower dispersal a
eigvals = eigs[1](a = 0.1, b = 0.0015, g1 = 0.033, g2 = 0.33)
eigvals # stable without oscillations
# (positive real parts)
# -0.0364156343768909
```

```
# condition for oscillations (complex eigenvalues)
tr = J2.trace()
dete = J2.det()
condition = tr^2 - 4*dete
condition(a = 0.6, b = 0.0015, g1 = 0.033, g2 = 0.33)
# condition is positive, there are no oscillations
# 0.117077462111258

condition(a = 0.1, b = 0.0015, g1 = 0.033, g2 = 0.33)
# condition is positive, there are no oscillations
# 0.0343923772017880

# second equilibrium ############
J1 = J.substitute(solutions[1][0])
J2 = J1.substitute(solutions[1][1])

eigs = J2.eigenvalues()
# test parameter values
eigvals0 = eigs[0](a = 0.6, b = 0.0015, g1 = 0.033, g2 = 0.33)
eigvals0 # complex eigenvalues
# -0.0392800000517154 - 0.0953530891067237*I
eigvals1 = eigs[1](a = 0.6, b = 0.0015, g1 = 0.033, g2 = 0.33)
eigvals1 # complex eigenvalues
# with negative parts = damped oscillations
# -0.0392800000517154 + 0.0953530891067237*I
```

```
# with lower dispersal a
eigvals = eigs[1](a = 0.1, b = 0.0015, g1 = 0.033, g2 = 0.33)
eigvals # stable without oscillations
# (positive real parts)
# -0.0364156343768909
```

Table A.1 Parameters of full model.

Process	Symbol	Value	Description
States	F		Mature forest
	I		Infected forest
	R		Recovering forest
Rates	α	$0-1$, by 0.05 steps	Probability of spread
	β	$0-0.005$, by 0.00025 steps	Probability of spontaneous outbreaks
	γ_1	40^{-1}	Regrowth
	γ_2	3^{-1}	Dieback
	p	$0-1$, by 0.05	Strength of nonlinear density dependent dispersal

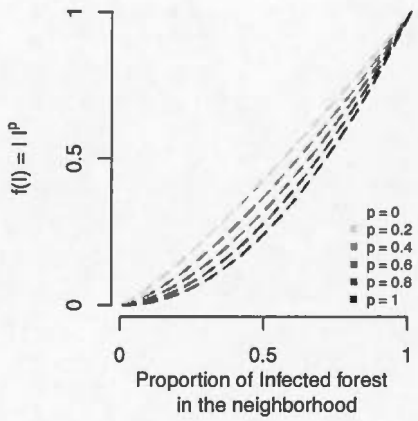

Figure A.1 Illustration of the density-dependent dispersal function. The lines show the nonlinear dispersal function $f(I) = I^p I$ under different values of p and $\alpha = 1$.

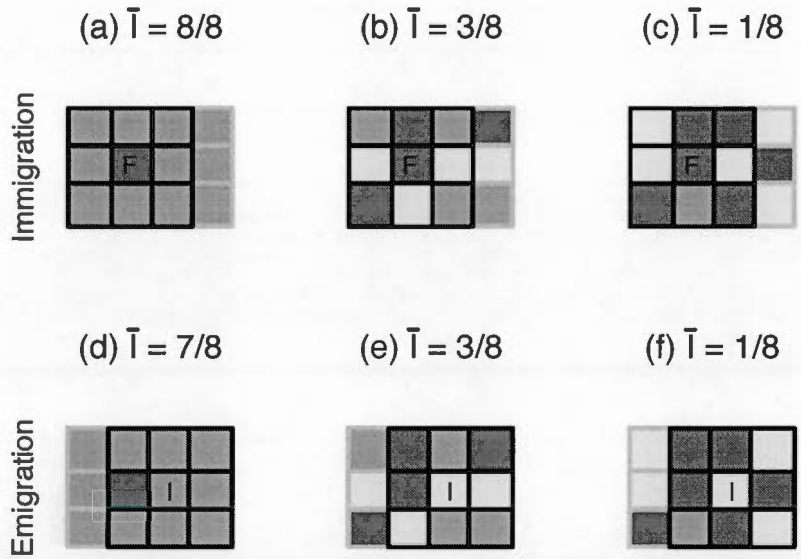

Figure A.2 Neighborhood considered for the calculation of the density-dependent dispersal function f(I) for immigration and emigration models (delineated by black lines). For immigration (a-c), the neighborhood consists of the 8 stands surrounding the arrival stand F. I_F counts the relative number of infected stands in the neighborhood. For emigration (d-f), the neighborhood consists of the 8 stands surrounding the origin stand I. $\overline{I}_I$ counts the relative number of infected stands in the neighborhood.

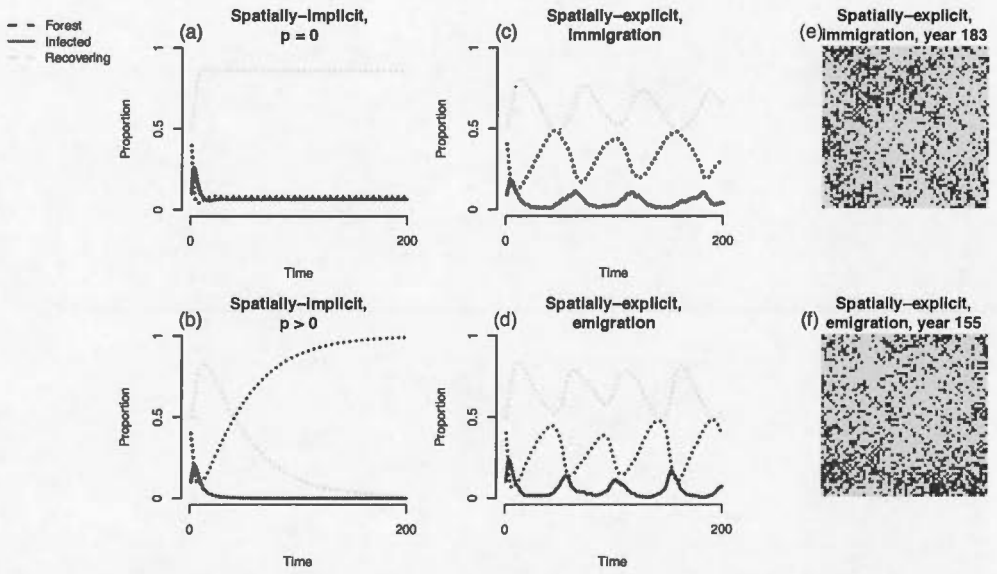

Figure A.3 Examples of FIRF model simulations without spontaneous outbreaks ($\beta = 0$). The same figure as Figure 2 in the manuscript. *a*, Spatially-implicit model with density-independent dispersal ($p = 0$). *b*, Spatially-implicit model with density-dependent dispersal ($p > 0$). *c*, spatially-explicit immigration model with density-dependent dispersal ($p > 0$). *d*, spatially-explicit emigration model with density-dependent dispersal ($p > 0$). *e* and *f* show the spatial distribution of stands from the simulation runs in c and d. The parameters used are $\alpha = 0.2$, $\beta = 0$, $\gamma_1 = 1/40$, $\gamma_2 = 1/3$ and $p = 0.4$.

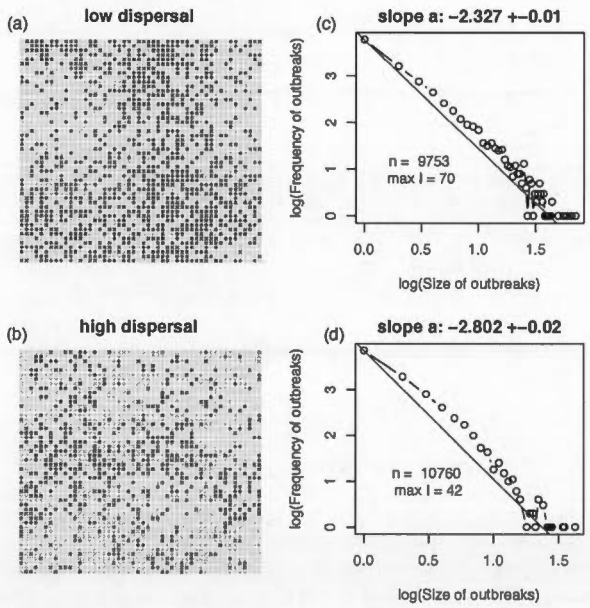

Figure A.4 Examples of spatially-explicit FIRF model simulations with low and high emigration-driven dispersal (α). *a*, spatial distribution of stands with low dispersal $\alpha = 0.2$ and *b* high dispersal $\alpha = 0.5$. The corresponding power-law slopes (solid line) from high *c* and low dispersal *d*. The parameters used are $\beta = 0.0001$, $\gamma_1 = 1/40$, $\gamma_2 = 1/3$ and $p = 0.4$.

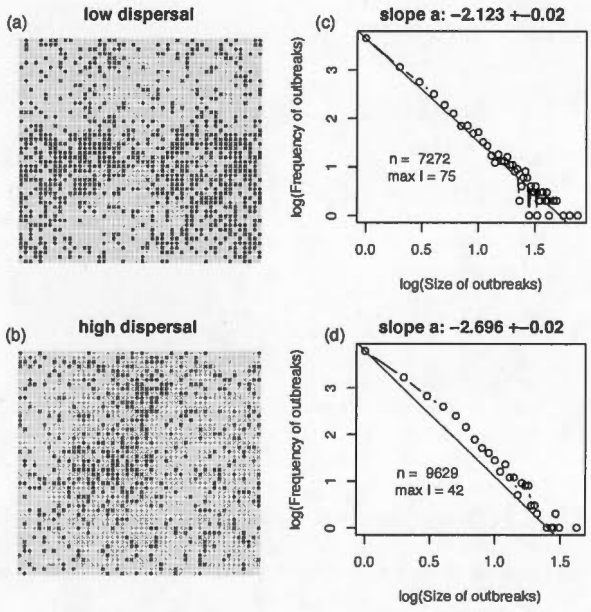

Figure A.5 Examples of spatially-explicit FIRF model simulations with low and high immigration-driven dispersal (α). *a*, spatial distribution of stands with low dispersal $\alpha = 0.2$ and *b* high dispersal $\alpha = 0.5$. The corresponding power-law slopes (solid line) from high *c* and low dispersal *d*.

APPENDIX B

MORE THAN MORAN: COUPLING STATISTICAL AND SIMULATION MODELS TO UNDERSTAND HOW DISPERSAL AND CLIMATE VARIATION DRIVE OUTBREAK DYNAMICS

Parameter results

The climate prediction E_{FI} was low even in the most suitable climates ($\beta = 0.008$, Figure B.7).

The mean climate prediction of infections E_{FI} was higher along the coast and in the south. In models with only the best climate variable, the probability of spontaneous outbreaks was highest at moderate maximum summer temperatures, two years previously (Figure B.7c).

The mean infection dieback to forest E_{IF} was more probable on the geographic range edges, meaning that the outbreaks die back faster in unsuitable climates closer to the range edges (γ, Figure B.7b). In unsuitable climates, (i.e. in extreme spring maximum temperatures) the probability of an infected forest becoming forest in the next year was close to one (Figure B.7 d).

Dispersal probabilities were highest at around $K_i = 0.5$ (Figure B.7 e). Dispersal probabilities were also affected by climate, so in suitable climates the probability of dispersal can reach 1 (thin lines in Figure B.7 e).

Multiple climate variables influence the transition of outbreaks. Summer and spring temperatures generally had a large effect on infection probabilities. Temperature during the growth period determines the insect-temperature response curves in the laboratory (Régnière, 1987). In contrast to a similar smaller-scale study with linear climate relationships, precipitation and elevation variables were not selected (Bouchard & Auger, 2014). Temperature variables were selected here because our study spanned a wide environmental gradient, to which nonlinear temperature responses fit better. Non-parametric models have suggested that temperature determines cumulative budworm damage (Candau & Fleming, 2011; Gray, 2013), and here we show that temperature also affects infection transitions.

Analysis of spatial autocorrelation in the statistical model

It was necessary to separate the relative contribution of dispersal and (multiple) climate variables to outbreaks, so predictions were divided up to dispersal- and climate-dependent partial predictions. Climate predictions E_{FI} represented the contribution of multiple climate variables to the probability of transition. The total probability of transition comes from adding the climate predictions E_{FI} and neighbourhood infection K:

$$Probability\{F \rightarrow I\}_i = E_{FI} + \alpha_1 K + \alpha_2 K^2 + \alpha_3 K^3$$

We analyzed if a higher autocorrelation in E_{FI} was associated with more successful infection transitions. We examined the effect of autocorrelation in E_{FI} in time. We assessed if a series of years with suitable climate for outbreaks occurred during large-scale outbreaks, i.e. in years with temporally autocorrelated predictions. To calculate the temporal autocorrelation of predictions, we first calculated the annual mean of infection E_{FI} and dieback E_{IF} predictions. We then

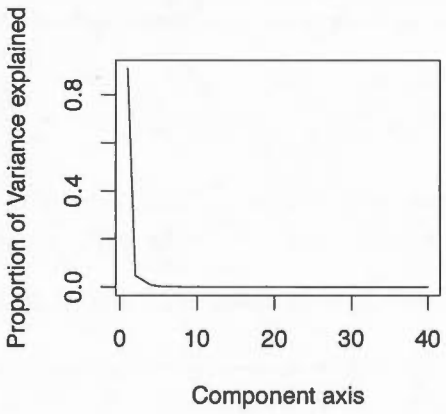

Figure B.1 Proportion of variance explained by the first 25 axes of a PCA on the dispersal variables K.

estimated during which years the predictions were asynchronous (phase coherence in wavelet cross-correlation, R-package biwavelet, Gouhier & Grinsted, 2012).

The effect of temporal autocorrelation in climate predictions E on infections shows that the outbreak in 1971-1980 occurred at the same time as a high climate predictions E_{FI}, and low average climate predictions E_{FI}. This combination led to many new infection transitions that stayed infected longer (Figure B.8 a). Infection and dieback transition probabilities were asynchronous for several years at the beginning of the outbreak (not significant, Figure B.8 b). However, the probabilities were also asynchronous between outbreaks.

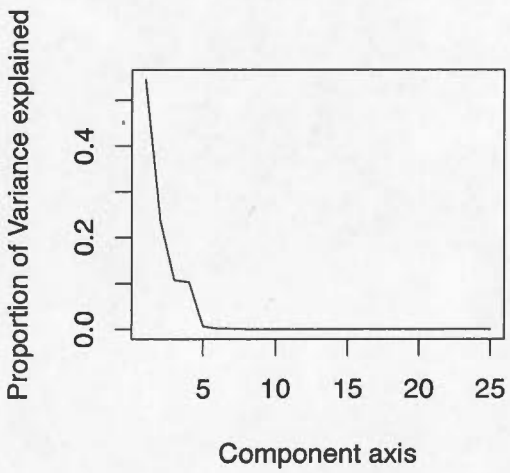

Figure B.2 Proportion of variance explained by the first 25 axes of a PCA on the climate variables.

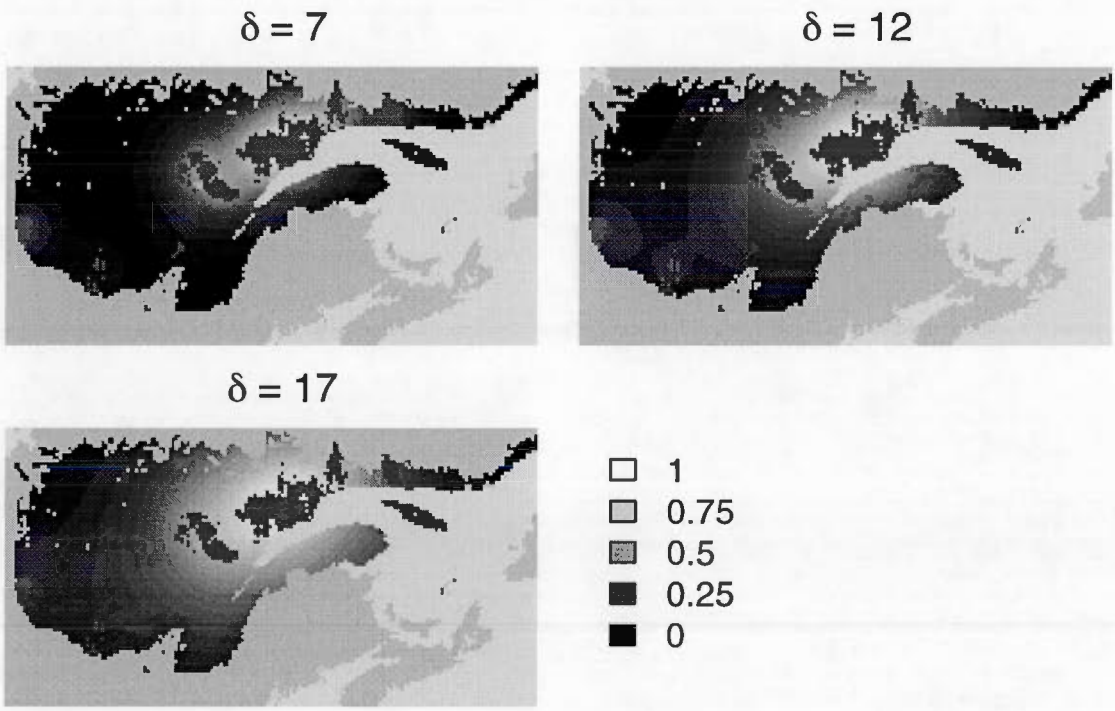

Figure B.3 Examples of K with different values for δ, the effect of distance to defoliated cells.

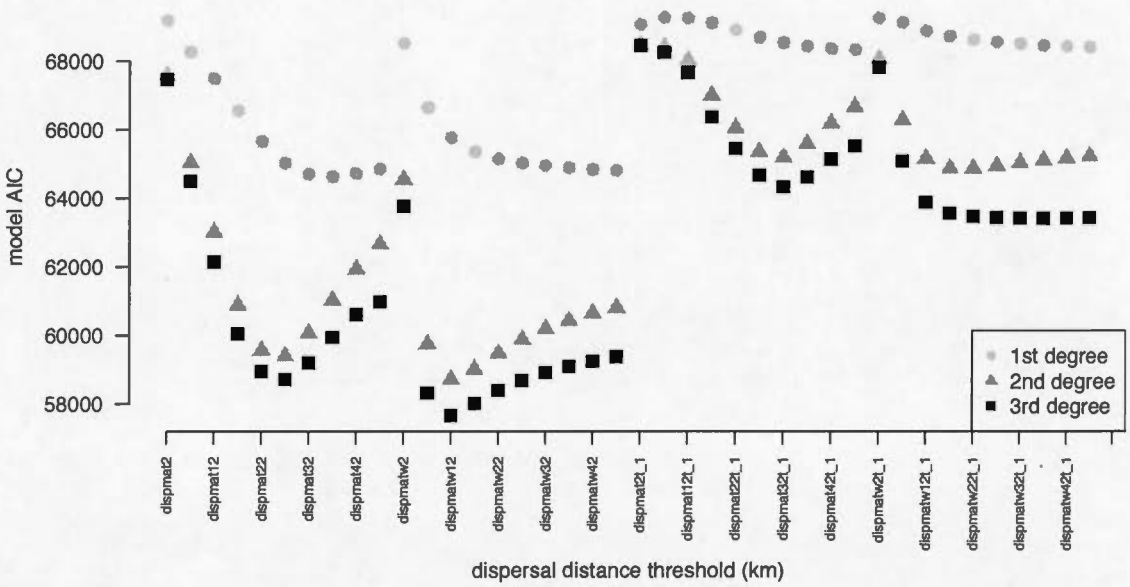

Figure B.4 The likelihood profile from selection of the best dispersal kernel K_i with first, second and third degree response functions. The estimated AIC with dispersal kernels calculated with different δ values, from a forwards stepwise logistic regression. The autologistic and negative exponential kernels are both tested with infection distributions from one and two years previously.

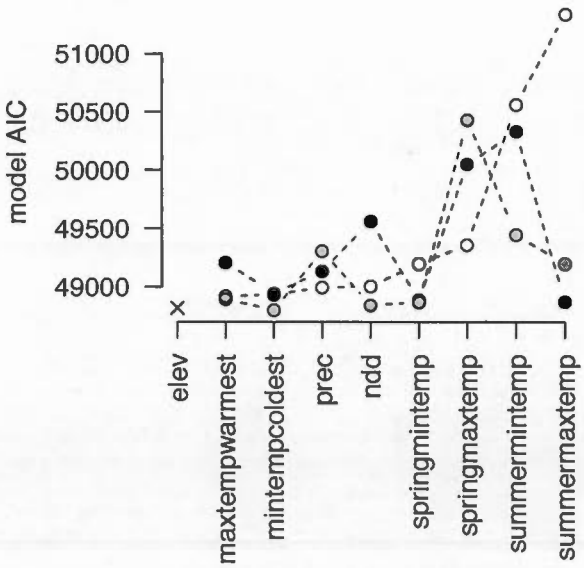

Figure B.5 Selection of best climate variable. AIC results of backward model selection results on FI infection transitions, third-degree response terms.

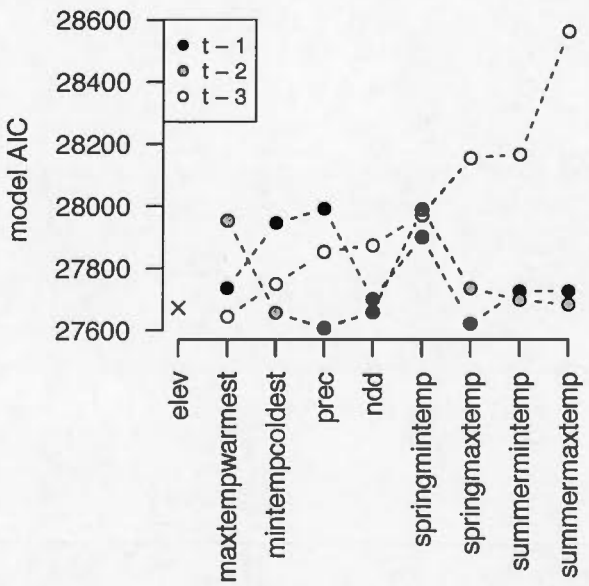

Figure B.6 AIC results, backward selection. Model selection results on IM transitions, response terms with 3 degrees and estimated on all data.

Table B.1 AIC results, backward selection. Model selection results on MI transitions, with 1,2 and 3-degree response terms and estimated on all data. Each AIC is obtained when carrying out a glm with all climate variables except that one. The variable when removed results in the highest AIC is the most important variable.

	AIC, degree 1	deltaAIC, degree 1	AIC, degree 2	deltaAIC, degree 2	AIC, degree 3	deltaAIC, degree 3
summermaxtempt_3	61162	0	54267	0	51339	0
summermintempt_3	59273	1889	53039	1228	50561	778
nddt_2	58068	3094	52490	1777	50429	910
summermintempt_1	59091	2071	53315	952	50325	1014
nddt_1	58654	2508	52693	1574	50048	1291
springmaxtempt_1	58012	3150	51784	2483	49561	1778
summermintempt_2	57908	3254	51704	2563	49443	1896
nddt_3	57819	3342	51791	2476	49357	1982
maxtempwarmestt_2	58884	2278	52058	2209	49307	2032
springmintempt_1	57835	3327	51746	2521	49209	2130
prect_3	57774	3387	51603	2664	49197	2142
summermaxtempt_2	58039	3122	51702	2565	49196	2143
maxtempwarmestt_1	58861	2301	52130	2138	49135	2204
springmaxtempt_3	57807	3355	51391	2876	49003	2336
maxtempwarmestt_3	59459	1703	52166	2101	48994	2345
mintempcoldestt_1	57891	3271	51691	2577	48943	2396
mintempcoldestt_3	57793	3369	51554	2713	48933	2406
springmintempt_3	57767	3395	51815	2452	48919	2419
springmintempt_2	57840	3321	51557	2711	48892	2447
prect_1	57775	3387	51463	2804	48888	2451
summermaxtempt_1	57816	3345	51634	2633	48870	2469
prect_2	57872	3290	51524	2743	48865	2474
springmaxtempt_2	57932	3230	51451	2817	48842	2497
elev	57768	3394	51509	2758	48818	2521
mintempcoldestt_2	57929	3233	51536	2731	48799	2540

Table B.2 AIC results, backward selection. Model selection results on IM transitions, with 1,2 and 3-degree response terms and estimated on all data. Each AIC is obtained when carrying out a glm with all climate variables except that one. The variable when removed results in the highest AIC is the most important variable.

	AIC, degree 1	deltaAIC, degree 1	AIC, degree 2	deltaAIC, degree 2	AIC, degree 3	deltaAIC, degree 3
springmintempt_3	34641	1618	29896	0	28564	0
prect_3	34744	1515	28992	904	28166	397
mintempcoldestt_3	36259	0	29393	503	28155	408
summermintempt_1	35301	958	29249	647	27992	572
maxtempwarmestt_2	34638	1621	29200	696	27989	574
maxtempwarmestt_3	34804	1455	29060	837	27972	592
summermaxtempt_2	34633	1626	29009	887	27955	609
nddt_1	35141	1118	29059	837	27945	619
maxtempwarmestt_1	34778	1481	29256	641	27901	663
springmaxtempt_3	34659	1600	29015	881	27875	688
summermintempt_3	34649	1610	28955	941	27853	711
nddt_3	34641	1618	29078	818	27750	814
summermaxtempt_1	34718	1542	28970	926	27737	826
mintempcoldestt_2	34813	1446	28938	958	27736	828
prect_1	34679	1581	28837	1059	27726	837
springmintempt_1	34633	1627	28973	923	27726	837
springmaxtempt_1	34635	1624	28780	1116	27701	863
prect_2	34684	1575	28836	1060	27698	865
springmintempt_2	34985	1274	28880	1016	27684	880
elev	34925	1334	28885	1011	27673	891
springmaxtempt_2	34911	1348	28776	1120	27659	904
nddt_2	34662	1598	28768	1128	27657	907
summermaxtempt_3	34661	1598	28782	1115	27645	919
mintempcoldestt_1	34761	1498	28783	1113	27623	941
summermintempt_2	34661	1598	28780	1116	27608	956

Table B.3 Model selection results on defoliation FI transitions also testing submodels of the effect of forest type and years since outbreaks. We removed all data points where the number of years since the last outbreak and the forest type was unknown, which resulted in a smaller data set (192 056 instead of 235 744 observations). The three best climate variables were summer maximum temperature $t-3$, summer minimum temperature $t-3$ and number of growing degree days $t-2$. The variables had third-degree response terms. K = the number of variables.

	K	AIC	deltaAIC	pseudo-r^2	random residuals	temporal residuals
all climate + dispersal	79	7232	0	0.300	13	0
all climate	76	8171	939	0.234	0	83
3 climate + dispersal	13	8764	1532	0.140	75	132
3 climate (with interactions)	64	8861	1629	0.145	53	105
dispersal	4	9072	1840	0.091	109	153
1 climate x dispersal	16	9107	1875	0.127	44	136
latitude x longitude	16	9179	1947	0.111	73	158
1 climate + dispersal	7	9183	1951	0.108	68	143
3 climate	10	9469	2237	0.056	100	171
global dispersal	4	9721	2489	0.045	93	172
years since outbreaks	4	10010	2778	0.048	50	176
1 climate	4	10163	2931	0.013	81	185
forest type	4	10238	3006	0.000	87	187
3 climate x dispersal	256	133008	125776	-6.919	935	186

	Forest_K1	I	Forest_K0
Infected	7821	47368	93
Forest	161975	6913	65855

Table B.4 The total transition events, when t0 is either Infected or Forest with no outbreaks ($K < 0.01$) and with outbreaks ($K > 0.01$).

	Forest_K1	I	Forest_K0
Infected	0.04606	0.87264	0.00141
Forest	0.95394	0.12736	0.99859

Table B.5 The total transition probabilities, when t0 is either Infected, Forest with no outbreaks ($K < 0.01$) and with outbreaks ($K > 0.01$).

Table B.6 Model selection results on dieback IF transitions. The predictors had third-degree response terms. K = the number of variables. The random residuals are estimated on half of the data selected randomly, and repeated 10 times.

	K	AIC	deltaAIC	pseudo-r^2	rand. res.
all climate	76	13700	0	0.337	19
3 climate x dispersal	256	14539	839	0.314	0
latitude x longitude	16	18787	5087	0.087	44
3 climate	10	18230	4530	0.111	48
1 climate	4	18207	4507	0.104	65

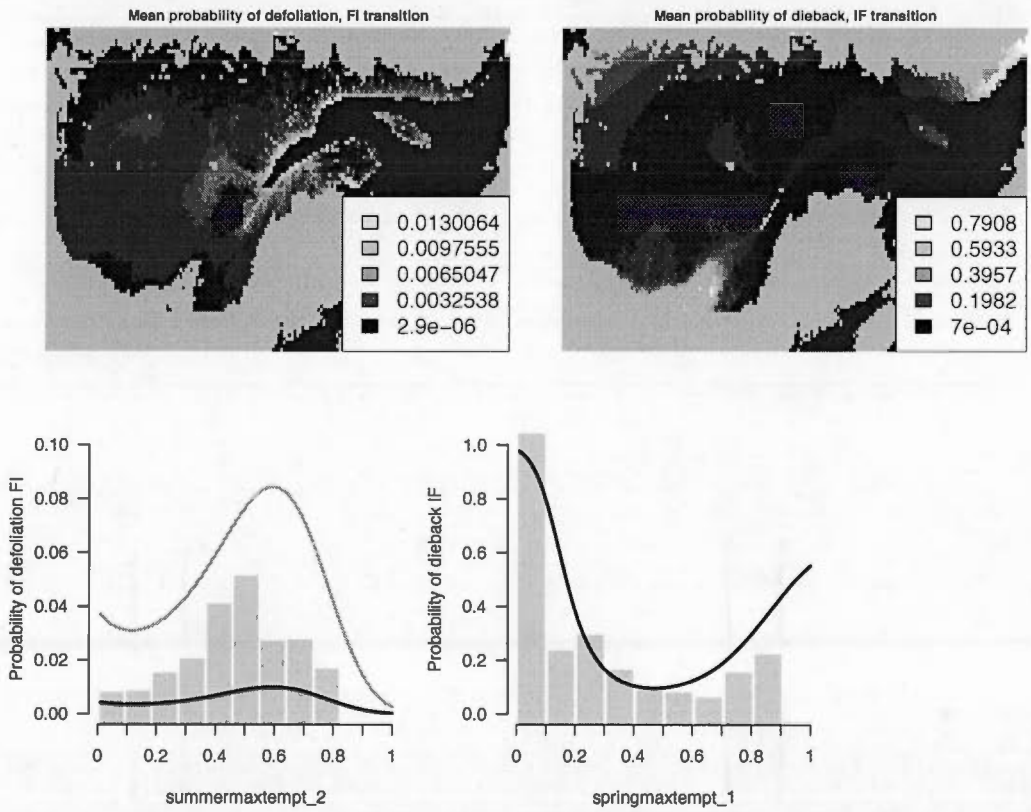

Figure B.7 The predicted climate predictions E estimated with a logistic regression with third-degree relationships. Top left, E_{FI}, mean probability of forest infection, calculated from all years. White colours indicate a high probability of a forest cell transitioning from the forest state F to infected I, and black colours indicates a low probability of transition (the forest stays as forest). These probabilities are only based on climate and do not include the effect of dispersal. Top right, E_{IF}, mean probability of dieback, calculated from all years. White colours indicate a high probability of a forest cell transitioning from the infected state I to the forest state F, and black colours indicates a low probability of transition (the infected area stays infected). Bottom left, The effect of one climate variable (selected by backward AIC) on the probability of FI infection. The black line shows the probability of spontaneous infection ($K_i = 0.0$) and the grey line shows the probability of infection when the dispersal kernel $K_i > 0.1$. The grey bars show the observed transitions. Bottom right, The effect of one climate variable (selected by backwards AIC) on the probability of IF dieback. The grey bars show the observed transitions.

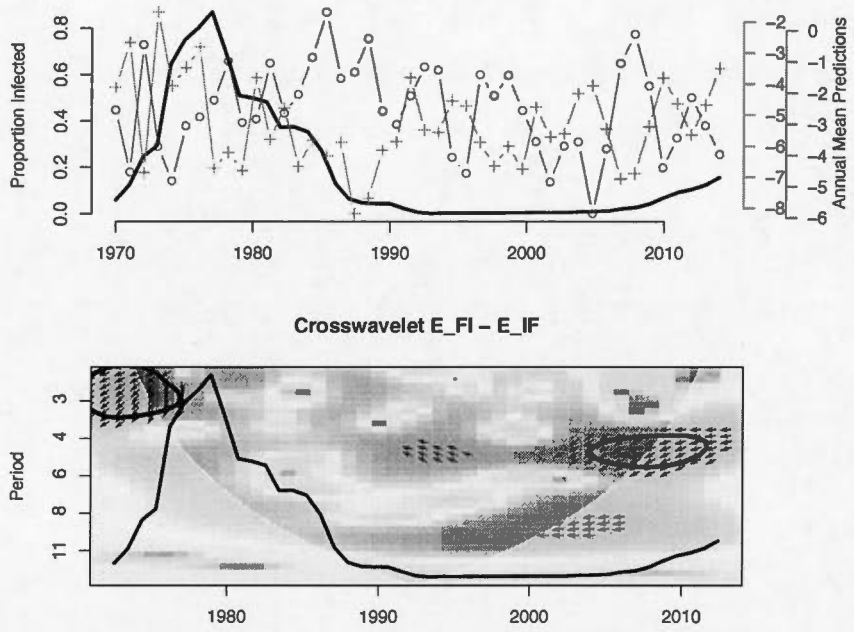

Figure B.8 The predicted climate predictions E and dispersal parameters. Bottom, the mean predicted probabilities of infection E_{FI} (red lines) and dieback E_{IF} (green lines), in all cells. The solid red line is the annual observed total proportion of infected forest. Top, cross-correlation wavelet between E_{FI} and E_{IF}. The colours represent the power of the period of the fluctuations, from dark blue (low values), to dark red (high values). The arrows show the phase angles between the fluctuations in the climatic predictions. Arrows pointing left indicate asynchrony in values and arrows pointing down indicate that the E_{FI} fluctuates before the E_{IF} by a quarter period (90°).

BIBLIOGRAPHY

Allstadt, A. J., Haynes, K. J., Liebhold, A. M. & Johnson, D. M. (2013). Long-term shifts in the cyclicity of outbreaks of a forest-defoliating insect. *Oecologia*, *172*, 141–151. http://dx.doi.org/10.1007/s00442-012-2474-x

Anderson, D. P. & Sturtevant, B. R. (2011). Pattern analysis of eastern spruce budworm Choristoneura fumiferana dispersal. *Ecography*, *34*(3), 488–497. http://dx.doi.org/10.1111/j.1600-0587.2010.06326.x

Anderson, R. M. & May, R. M. (1979). Population biology of infectious disease: Part I. *Nature*, *280*, 361–367.

Anderson, R. M. & May, R. M. (1980). Infectious Diseases and Population Cycles of Forest Insects. *Science*, *210*(4470), 658–661. http://dx.doi.org/10.1126/science.210.4470.658

Anderson, R. M. & May, R. M. (1992). *Infectious Diseases of Humans Dynamics and Control*. Oxford University Press.

Aukema, B. H., Carroll, A. L., Zheng, Y., Zhu, J., Raffa, K. F., Dan Moore, R., Stahl, K. & Taylor, S. W. (2008). Movement of outbreak populations of mountain pine beetle: Influences of spatiotemporal patterns and climate. *Ecography*, *31*, 348–358. http://dx.doi.org/10.1111/j.0906-7590.2007.05453.x

Baskerville, G. & Kleinschmidt, S. (1980). A dynamic model of growth in defoliated fir stands. *Can. J. For. Res.*, *11*(2), 206–214

Beddington, J. R., Free, C. A. & Lawton, J. H. (1978). Characteristics of successful natural enemies in models of biological control of insect pests. *Nature*, *273*(5663), 513–519. http://dx.doi.org/10.1038/273513a0

Benincà, E., Huisman, J., Heerkloss, R., Jöhnk, K. D., Branco, P., Van Nes, E. H., Scheffer, M. & Ellner, S. P. (2008). Chaos in a long-term experiment with a plankton community. *Nature*, *451*(7180), 822–5. http://dx.doi.org/10.1038/nature06512

Bergeron, Y., Leduc, A., Morin, H. & Joyal, C. (1995). Balsam fir mortality following the last spruce budworm outbreak in northwestern Quebec. *Can. J. For. Res.*, *25*, 1375–1384. http://dx.doi.org/10.1139/x95-150

Berryman, A. A. (1996). What causes population cycles of forest Lepidoptera? *Trends Ecol. & Evol.*, *11*(I), 28–32. http://dx.doi.org/10.1016/0169-5347(96)81066-4

Bestelmeyer, B. T., Herrick, J. E., Brown, J. R., Trujillo, D. A. & Havstad, K. M. (2004). Land management in the American southwest: a state-and-transition approach to ecosystem complexity. *Environ. Manage.*, *34*, 38–51. http://dx.doi.org/10.1007/s00267-004-0047-4

Beyer, H. L., Hampson, K., Lembo, T., Cleaveland, S., Kaare, M. & Haydon, D. T. (2011). Metapopulation dynamics of rabies and the efficacy of vaccination. *Proc. R. Soc. B-Biological Sci.*, *278*(1715), 2182–90. http://dx.doi.org/10.1098/rspb.2010.2312

Bjørnstad, O. N. & Grenfell, B. T. (2001). Noisy Clockwork: Time Series Analysis of Population Fluctuations in Animals. *Science*, *293*(5530), 638–643. http://dx.doi.org/10.1126/science.1062226

Bjørnstad, O. N., Ims, R. A. & Lambin, X. (1999). Spatial population dynamics: analyzing patterns and processes of population synchrony. *Trends Ecol. & Evol.*, *14*(11), 427–432. http://dx.doi.org/10.1016/S0169-5347(99)01677-8

Bjørnstad, O. N., Peltonen, M., Liebhold, A. M. & Baltensweiler, W. (2002). Waves of larch budmoth outbreaks in the European alps. *Science*, *298*(5595), 1020–3. http://dx.doi.org/10.1126/science.1075182

Blackwood, J. C., Berec, L., Yamanaka, T., Epanchin-Niell, R. S., Hastings, A. & Liebhold, A. M. (2012). Bioeconomic synergy between tactics for insect eradication in the presence of Allee effects. *Proc. R. Soc. B-Biological Sci.*, *279*(1739), 2807–15. http://dx.doi.org/10.1098/rspb.2012.0255

Blais, J. R. (1958). The vulnerability of balsam fir to spruce budworm attack in northwestern Ontario, with special reference to the physiological age of the tree. *For. Chronicles*, *34*(4), 405–422.

Blasius, B., Huppert, A. & Stone, L. (1999). Complex dynamics and phase synchronization in spatially extended ecological systems. *Nature*, *399*(6734), 354–359. http://dx.doi.org/10.1038/20676

Bonsall, M. B. & Hastings, A. (2004). Demographic and environmental stochasticity in predator-prey metapopulation dynamics. *J. Anim. Ecol.*, *73*(1963), 1043–1055. http://dx.doi.org/10.1111/j.0021-8790.2004.00874.x

Bouchard, M. & Auger, I. (2014). Influence of environmental factors and spatio-temporal covariates during the initial development of a spruce budworm outbreak. *Landsc. Ecol.*, *29*(1), 111–126. http://dx.doi.org/10.1007/s10980-013-9966-x

Boulanger, Y., Arseneault, D., Morin, H., Jardon, Y., Bertrand, P. & Dagneau, C. (2012). Dendrochronological reconstruction of spruce budworm (Choristoneura

fumiferana) outbreaks in southern Quebec for the last 400 years. *Can. J. For. Res.*, *42*, 1264–1276. http://dx.doi.org/10.1139/X2012-069

Bowler, D. E. & Benton, T. G. (2005). Causes and consequences of animal dispersal strategies: relating individual behaviour to spatial dynamics. *Biol. Rev.*, *80*(2), 205–25

Boyd, I. L., Freer-Smith, P. H., Gilligan, C. A. & Godfray, H. C. J. (2013). The consequence of tree pests and diseases for ecosystem services. *Science*, *342*(2013), 1235773. http://dx.doi.org/10.1126/science.1235773

Briggs, C. J. & Hoopes, M. F. (2004). Stabilizing effects in spatial parasitoid–host and predator–prey models: a review. *Theor. Popul. Biol.*, *65*(3), 299–315. http://dx.doi.org/10.1016/j.tpb.2003.11.001

Brodeur, J. (2000). Host specificity and trophic relationships of hyperparasitoids. In M. E. Hochberg & A. R. Ives (eds.), *Parasit. Popul. Biol.* pp. 163–183. Princeton University Press, Princeton.

Buckland, S. T. & Elston, D. A. (1993). Empirical Models for the Spatial Distribution of Wildlife. *J. Appl. Ecol.*, *30*(3), 478. http://dx.doi.org/10.2307/2404188

Burns, R. M. & Honkala, B. H. (1990). *Silvics of North America: 1. Conifers; 2. Hardwoods. vol.2.* Washington, DC: Agriculture Handbook 654. U.S. Department of Agriculture, Forest Service.

Candau, J.-N. & Fleming, R. A. (2005). Landscape-scale spatial distribution of spruce budworm defoliation in relation to bioclimatic conditions. *Can. J. For. Res.*, *35*, 2218–2232. http://dx.doi.org/10.1139/X05-078

Candau, J.-N. & Fleming, R. A. (2011). Forecasting the response of spruce budworm defoliation to climate change in Ontario. http://dx.doi.org/10.1139/x11-134

Cappuccino, N., Lavertu, D., Bergeron, Y. & Régnière, J. (1998). Spruce budworm impact, abundance and parasitism rate in a patchy landscape. *Oecologia*, *114*(2), 236–242. http://dx.doi.org/10.1007/s004420050441

Cash, B. A., Rodó, X., Ballester, J., Bouma, M. J., Baeza, A., Dhiman, R. & Pascual, M. (2013). Malaria epidemics and the influence of the tropical South Atlantic on the Indian monsoon. *Nat. Clim. Chang.*, *3*(5), 502–507. http://dx.doi.org/10.1038/nclimate1834

Cattadori, I. M., Haydon, D. T. & Hudson, P. J. (2005). Parasites and climate synchronize red grouse populations. *Nature*, *433*(7027), 737–741. http://dx.doi.org/10.1038/nature03276

Cazelles, B., Chavez, M., Berteaux, D., Ménard, F., Vik, J. O., Jenouvrier, S. & Stenseth, N. C. (2008). Wavelet analysis of ecological time series. *Oecologia*, *156*(2), 287–304. http://dx.doi.org/10.1007/s00442-008-0993-2

Clauset, A., Shalizi, C. & Newman, M. E. J. (2009). Power-law distributions in empirical data. *SIAM Rev.*, *51*(4), 661–703. http://dx.doi.org/10.1137/070710111

Cooke, B. J., Nealis, V. G. & Régnière, J. (2007). Insect defoliators as periodic disturbances in northern forest ecosystems. In E. Johnson & K. Miyanishi (eds.), *Plant Disturb. Ecol. Process Response* pp. 487–525. Burlington, Massachusetts, USA.: Elsevier.

Costantino, R., Desharnais, R., Cushing, J. & Dennis, B. (1997). Chaotic

Dynamics in an Insect Population. *Science*, *275*(1997), 389–391. http://dx.doi.org/10.1126/science.275.5298.389

Coulson, T. N., Rohani, P. & Pascual, M. (2004). Skeletons, noise and population growth: the end of an old debate? *Trends Ecol. & Evol.*, *19*(7), 359–64. http://dx.doi.org/10.1016/j.tree.2004.05.008

Cressie, N. & Wikle, C. (2011). *Statistics for Spatio-Temporal Data*. Wiley.

Cuddington, K. M., Fortin, M.-j., Gerber, L. R., Hastings, A., Liebhold, A. M., O'Connor, M. & Ray, C. (2013). Process-based models are required to manage ecological systems in a changing world. *Ecosphere*, *4*(2), 1–12. http://dx.doi.org/10.1890/ES12-00178.1

Cusson, M., Barron, J. R., Goulet, H., Regniere, J. & Doucet, D. (1998). Biology and status of Tranosema rostrale rostrale (Hymenoptera : Ichneumonidae), a parasitoid of the eastern spruce budworm (Lepidoptera : Tortricidae). *Ann. Entomol. Soc. Am.*, *91*(1), 87–93.

Dowden, P. B., Carolin, V. M. & Dirks, C. O. (1950). Natural Control Factors Affecting the Spruce Budworm in the Adirondacks During 1946-1948. *J. Econ. Entomol.*, *43*(6), 774–783. http://dx.doi.org/10.1093/jee/43.6.774

Durrett, R. & Levin, S. A. (1994). The importance of being discrete (and spatial). *Theor. Popul. Biol.*, *46*(3), 363–394. http://dx.doi.org/10.1006/tpbi.1994.1032

Dwyer, G., Dushoff, J. & Yee, S. H. (2004). The combined effects of pathogens and predators on insect outbreaks. *Nature*, *430*, 341–345. http://dx.doi.org/10.1038/nature02700.1.

Earn, D. J. D., Rohani, P., Bolker, B. M. & Grenfell, B. T. (2000). A Simple Model for Complex Dynamical Transitions in Epidemics. *Science*, *287*(5453), 667–670. http://dx.doi.org/10.1126/science.287.5453.667

Earn, D. J. D., Rohani, P. & Grenfell, B. T. (1998). Persistence, chaos and synchrony in ecology and epidemiology. *Proc. R. Soc. B-Biological Sci.*, *265*, 7–10

Eisinger, D. & Thulke, H. (2008). Spatial pattern formation facilitates eradication of infectious diseases. *J. Appl. Ecol.*, *45*(2), 415–423. http://dx.doi.org/10.1111/j.1365-2664.2007.01439.x

Elton, C. S. (1924). Periodic fluctuations in the number of animals: their causes and effects. *J. Exp. Biol.*, *2*, 119–163.

Erdle, T. A. & Maclean, J. E. (1999). Stand growth model calibration for use in forest pest impact assessment. *For. Chron.*, *75*(1), 141–152. http://dx.doi.org/10.5558/tfc75141-1

Evans, M. R., Norris, K. J. & Benton, T. G. (2012). Predictive ecology: systems approaches. *Philos. Trans. R. Soc. B Biol. Sci.*, *367*(1586), 163–169. http://dx.doi.org/10.1098/rstb.2011.0191

Eveleigh, E. S., McCann, K. S., McCarthy, P. C., Pollock, S. J., Lucarotti, C. J., Morin, B., McDougall, G. A., Strongman, D. B., Huber, J. T., Umbanhowar, J. & Faria, L. D. B. (2007). Fluctuations in density of an outbreak species drive diversity cascades in food webs. *Proc. Natl. Acad. Sci.*, *104*(43), 16976–81. http://dx.doi.org/10.1073/pnas.0704301104

Filipe, J. A. N., Cobb, R. C., Meentemeyer, R. K., Lee, C. A., Valachovic, Y. S., Cook, A. R., Rizzo, D. M. & Gilligan, C. A. (2012). Landscape Epidemiology

and Control of Pathogens with Cryptic and Long-Distance Dispersal: Sudden Oak Death in Northern Californian Forests. *PLoS Comput. Biol.*, *8*(1), e1002328. http://dx.doi.org/10.1371/journal.pcbi.1002328

Filipe, J. A. N. & Maule, M. (2004). Effects of dispersal mechanisms on spatio-temporal development of epidemics. *J. Theor. Biol.*, *226*(2), 125–141. http://dx.doi.org/10.1016/S0022-5193(03)00278-9

Fleming, R. A. (1996). A mechanistic perspective of possible influences of climate change on defoliating insects in North America's boreal forests. *Silva Fenn.*, *30*(2-3), 281–294

Fleming, R. A. (2000). Climate change and insect disturbance regimes in Canada's boreal forests. *World Resour. Rev.*, *12*(3), 521–555

Fleming, R. A., Barclay, H. J. & Candau, J.-N. (2002). Scaling-up an autoregressive time-series model (of spruce budworm population dynamics) changes its qualitative behavior. *Ecol. Modell.*, *149*(1-2), 127–142. http://dx.doi.org/10.1016/S0304-3800(01)00519-1

Fournier, C., Bauce, É., Dupont, A. & Berthiaume, R. (2010). Wood losses and economical threshold of Btk aerial spray operation against spruce budworm. *Pest Manag. Sci.*, *66*(3), 319–324. http://dx.doi.org/10.1002/ps.1878

Fuentealba, a. & Bauce, É. (2012). Carry-over effect of host nutritional quality on performance of spruce budworm progeny. *Bull. Entomol. Res.*, *102*(3), 275–84. http://dx.doi.org/10.1017/S0007485311000617

Fuentes, M., Kuperman M.N. & Fuentes M.A. (1999). Cellular automata and epidemiological models with spatial dependence. *Physica A*, *267*(3), 471–486. http://dx.doi.org/10.1016/S0378-4371(99)00027-8

Fukś, H. & Lawniczak, A. T. (2001). Individual-based lattice model for spatial spread of epidemics. *Discret. Dyn. Nat. Soc.*, *6*(3), 191–200. http://dx.doi.org/10.1155/S1026022601000206

Gagic, V., Hänke, S., Thies, C., Scherber, C., Tomanović, Ž. & Tscharntke, T. (2012). Agricultural intensification and cereal aphid-parasitoid-hyperparasitoid food webs: Network complexity, temporal variability and parasitism rates. *Oecologia*, *170*, 1099–1109. http://dx.doi.org/10.1007/s00442-012-2366-0

García-Valdés, R., Gotelli, N. J., Zavala, M. A., Purves, D. W. & Araújo, M. B. (2015). Effects of climate, species interactions, and dispersal on decadal colonization and extinction rates of Iberian tree species. *Ecol. Modell.*, *309*, 118–127. http://dx.doi.org/10.1016/j.ecolmodel.2015.04.003

Gilbert, B. & O'Connor, M. I. (2013). Climate change and species interactions: Beyond local communities. *Ann. N. Y. Acad. Sci.*, *1297*, 98–111. http://dx.doi.org/10.1111/nyas.12149

Godfray, H. C. J. & Shimada, M. (1999). Parasitoids as model organisms for ecologists. *Res. Popul. Ecol. (Kyoto).*, *41*, 3–10. http://dx.doi.org/10.1007/PL00011980

Gonzalez, A. & Holt, R. D. (2002). The inflationary effects of environmental fluctuations in source-sink systems. *Proc. Natl. Acad. Sci.*, *99*(23), 14872–14877

Gouhier, T. C. & Grinsted, A. (2012). biwavelet: Conduct univariate and bivariate wavelet analyses. R package version 0.12. Retrieved from http://cran.r-project.org/package=biwavelet

Gravel, D., Canard, E., Guichard, F. & Mouquet, N. (2011a). Persistence increases with diversity and connectance in trophic metacommunities. *PLoS One*, *6*(5), e19374. http://dx.doi.org/10.1371/journal.pone.0019374

Gravel, D., Massol, F., Canard, E., Mouillot, D. & Mouquet, N. (2011b). Trophic theory of island biogeography. *Ecol. Lett.*, *14*(10), 1010–1016. http://dx.doi.org/10.1111/j.1461-0248.2011.01667.x

Gravel, D., Mouquet, N., Loreau, M. & Guichard, F. (2010). Patch dynamics, persistence, and species coexistence in metaecosystems. *Am. Nat.*, *176*(3), 289–302. http://dx.doi.org/10.1086/655426

Gray, D. R. (2008). The relationship between climate and outbreak characteristics of the spruce budworm in eastern Canada. *Clim. Change*, *87*(3-4), 361–383. http://dx.doi.org/10.1007/s10584-007-9317-5

Gray, D. R. (2013). The influence of forest composition and climate on outbreak characteristics of the spruce budworm in eastern Canada. *Can. J. For. Res.*, *1195*, 1181–1195

Greenbank, D. (1956). The role of climate and dispersal in the inititiation of outbreaks of the spruce budworm in New Brunswick. 1. The role of climate. *Can. J. Zool.*, *34*, 453–476.

Greenbank, D. (1980). Spruce budworm (Lepidoptera: Tortricidae) moth flight and dispersal: new understanding from canopy observations, radar, and aircraft. *Mem. Entomol. Soc. Canada*, *112*, 1–49. http://dx.doi.org/10.4039/entm112110fv

Grenfell, B. T. & Harwood, J. (1997). (Meta)population dynamics of infectious diseases. *Trends Ecol. & Evol.*, *12*, 395–399.

Grenfell, B. T., Wilson, K., Finkenstädt, B., Coulson, T. N., Murray, S., Albon, S. D., Pemberton, J., Clutton-Brock, T. H. & Crawley, M. (1998). Noise and determinism in synchronized sheep dynamics. *Nature*, *394*(6694), 674–676

Griffith, D. A. & Peres-Neto, P. R. (2006). Spatial modeling in Ecology: the flexibility of the eigenfunction spatial analyses. *Ecology*, *87*(10), 2603–2613. http://dx.doi.org/10.1890/0012-9658(2006)87[2603:SMIETF]2.0.CO;2

Guichard, F., Halpin, P. M., Allison, G. W., Lubchenco, J. & Menge, B. A. (2003). Mussel disturbance dynamics: signatures of oceanographic forcing from local interactions. *Am. Nat.*, *161*(6), 889–904. http://dx.doi.org/10.1086/375300

Gustafson, E. J. (2013). When relationships estimated in the past cannot be used to predict the future: using mechanistic models to predict landscape ecological dynamics in a changing world. *Landsc. Ecol.*, *28*(8), 1429–1437. http://dx.doi.org/10.1007/s10980-013-9927-4

Hagen, S. B., Jepsen, J. U., Schott, T. & Ims, R. A. (2010). Spatially mismatched trophic dynamics: cyclically outbreaking geometrids and their larval parasitoids. *Biol. Lett.*, *6*, 566–569

Hanski, I. (1998). Metapopulation Dynamics. *Nature*, *396*(6706), 41–49. http://dx.doi.org/10.1038/23876

Hardy, Y., Lafond, A. & Hamel, L. (1983). The Epidemiology of the Current Spruce Budworm Outbreak in Quebec. *For. Sci.*, *29*, 715–725.

Harrison, P. J., Hanski, I. & Ovaskainen, O. (2011). Bayesian state-space modeling of metapopulation dynamics in the Glanville fritillary butterfly. *Ecol. Monogr.*, *81*(4), 581–598. http://dx.doi.org/10.1890/11-0192.1

Harvey, J. A. (2008). Comparing and contrasting development and reproductive strategies in the pupal hyperparasitoids Lysibia nana and Gelis agilis (Hymenoptera: Ichneumonidae). *Evol. Ecol.*, *22*, 153–166. http://dx.doi.org/10.1007/s10682-007-9164-x

Hassell, M. P. (2000). Host - parasitoid population dynamics. *J. Anim. Ecol.*, *69*, 543–566.

Hassell, M. P., Comins, H. N. & May, R. M. (1991). Spatial structure and chaos in insect population dynamics. *Nature*, *353*, 255–258. http://dx.doi.org/10.1038/353255a0

Hastings, A. (2004). Transients: the key to long-term ecological understanding? *Trends Ecol. & Evol.*, *19*(1), 39–45. http://dx.doi.org/10.1016/j.tree.2003.09.007

Hastings, A., Hom, C. L., Ellner, S. P., Turchin, P. & Godfray, H. C. J. (1993). Chaos in ecology: Is Mother Nature a strange attractor? *Annu. Rev. Ecol. Syst.*, *24*(1), 1–33. http://dx.doi.org/10.1146/annurev.es.24.110193.000245

Hawkins, B. A. (1994). *Pattern and Process in Host-Parasitoid Interactions*. Cambridge University Press.

Hawkins, B. A., Mills, N. J., Jervis, M. A. & Price, P. W. (1999). Is the biological control of insects a natural phenomenon? *Oikos*, *86*(3), 493–506. http://dx.doi.org/10.2307/3546654

Haynes, K. J., Liebhold, A. M., Fearer, T. M., Wang, G., Norman, G. W. & Johnson, D. M. (2009). Spatial synchrony propagates through a forest food web via consumer-resource interactions. *Ecology*, *90*(11), 2974–83

Hennigar, C. R., Maclean, J. E., Quiring, D. T. & Kershaw, J. A. (2008). Differences in Spruce Budworm Defoliation among Balsam Fir and White, Red, and Black Spruce. *For. Sci.*, *54*(2), 158–166

Hethcote, H. W. (1976). Qualitative analyses of communicable disease models. *Math. Biosc.*, *28*(3), 335–356.

Hethcote, H. W. & Levin, S. A. (1989). Periodicity in epidemiological models. In L. Gross, T. G. Hallam, & S. A. Levin (eds.), *Appl. Math. Ecol.* pp. 193–211. Berlin: Springer.

Hirzel, A. H., Nisbet, R. & Murdoch, W. W. (2007). Host-parasitoid spatial dynamics in heterogeneous landscapes. *Oikos*, *116*, 2082–2096. http://dx.doi.org/10.1111/j.2007.0030-1299.15976.x

Houseweart, M. (1980). Parasitic mites (Acari: Erythraeidae) on spruce budworm moths (Lepidoptera: Tortricidae). *Can. Entomol.*, *112*(02), 193–197. http://dx.doi.org/10.4039/Ent112193-2

Huber, J., Eveleigh, E. S., Pollock, S. & McCarthy, P. (1996). The Chalcidoid Parasitoids and Hyperparasitoids (Hymenoptera: Chalcidoidea) of Choristoneura Species (Lepidoptera: Tortricidae) in America north of Mexico. *Can. Entomol.*, *128*(06), 1167–1220. http://dx.doi.org/10.4039/Ent1281167-6

Huffaker, C. (1958). Experimental Studies on Predation: Dispersion Factors and Predator - Prey Oscillations. *Hilgardia A J. Agric. Sci.*, *27*, 795–834.

Ims, R. A. & Andreassen, H. P. (2000). Spatial synchronization of vole population dynamics by predatory birds. *Nature*, *408*(6809), 194–6. http://dx.doi.org/10.1038/35041562

Ims, R. A., Yoccoz, N. G. & Hagen, S. B. (2004). Do sub-Arctic winter moth populations in coastal birch forest exhibit spatially synchronous dynamics? *J. Anim. Ecol.*, *73*(6), 1129–1136. http://dx.doi.org/10.1111/j.0021-8790.2004.00882.x

James, P. M. A., Cooke, B. J., Brunet, B. M. T., Lumley, L. M. & Felix, A. (2015). Life-stage differences in spatial genetic structure in an irruptive forest

insect : implications for dispersal and spatial synchrony. *Mol. Ecol.*, *24*, 296–309. http://dx.doi.org/10.1111/mec.13025

James, P. M. A., Fortin, M.-j., Sturtevant, B. R., Fall, A. & Kneeshaw, D. (2010). Modelling Spatial Interactions Among Fire, Spruce Budworm, and Logging in the Boreal Forest. *Ecosystems*, *14*(1), 60–75. http://dx.doi.org/10.1007/s10021-010-9395-5

Jepsen, J. U., Hagen, S. B., Høgda, K. a., Ims, R. A., Karlsen, S. R., Tømmervik, H. & Yoccoz, N. G. (2009). Monitoring the spatio-temporal dynamics of geometrid moth outbreaks in birch forest using MODIS-NDVI data. *Remote Sens. Environ.*, *113*(9), 1939–1947. http://dx.doi.org/10.1016/j.rse.2009.05.006

Johnson, D. M., Liebhold, A. M., Tobin, P. C. & Bjørnstad, O. N. (2006). Allee effects and pulsed invasion by the gypsy moth. *Nature*, *444*(7117), 361–3. http://dx.doi.org/10.1038/nature05242

Kärvemo, S., Johansson, V., Schroeder, M. & Ranius, T. (2016). Local colonization-extinction dynamics of a tree-killing bark beetle during a large-scale outbreak. *Ecosphere*, *7*(3), 1–14. http://dx.doi.org/10.1002/ecs2.1257

Kausrud, K. L., Okland, B., Skarpaas, O., Grégoire, J.-C., Erbilgin, N. & Stenseth, N. C. (2011). Population dynamics in changing environments: the case of an eruptive forest pest species. *Biol. Rev.*, *87*, 34–51. http://dx.doi.org/10.1111/j.1469-185X.2011.00183.x

Kean, J. M. & Barlow, N. D. (2000). Can host-parasitoid metapopulations explain successful biological control? *Ecology*, *81*(8), 2188–2197. http://dx.doi.org/10.1890/0012-9658(2000)081[2188:CHPMES]2.0.CO;2

Keane, R. E., McKenzie, D., Falk, D., Smithwick, E., Miller, C. & Kellogg, L.-K. (2015). Representing climate, disturbance, and vegetation interactions in landscape models. *Ecol. Modell.*, *309-310*, 33–47.

Keeling, M. J. (1999). The effects of local spatial structure on epidemiological invasions. *Proc. R. Soc. B-Biological Sci.*, *266*(1421), 859–67. http://dx.doi.org/10.1098/rspb.1999.0716

Keeling, M. J. & Eames, K. T. D. (2005). Networks and epidemic models. *J. R. Soc. Interface*, *2*(4), 295–307. http://dx.doi.org/10.1098/rsif.2005.0051

Keeling, M. J. & Rohani, P. (2008). *Modeling infectious diseases in humans and animals.* Princeton, NJ: Princeton University Press.

Keeling, M. J., Woolhouse, M. E. J., May, R. M., Davies, G. & Grenfell, B. T. (2003). Modelling vaccination strategies against foot-and-mouth disease. *Nature*, *421*(6919), 136–42. http://dx.doi.org/10.1038/nature01343

Kéfi, S., Rietkerk, M., Alados, C., Pueyo, Y., Papanastasis, V. P., ElAich, A. & De Ruiter, P. C. (2007). Spatial vegetation patterns and imminent desertification in Mediterranean arid ecosystems. *Nature*, *449*(7159), 213–217. http://dx.doi.org/10.1038/nature06111

Kendall, B. E., Briggs, C. J., Murdoch, W. W., Turchin, P., Ellner, S. P., McCauley, E., Nisbet, R. M. & Wood, S. N. (1999). Why do populations cycle? A synthesis of statistical and mechanistic modeling approaches. *Ecology*, *80*, 1789–1805. http://dx.doi.org/10.1890/0012-9658(1999)080[1789:WDPCAS]2.0.CO;2

Kermack, W. O. & McKendrick, A. G. (1927). A Contribution to the Mathematical Theory of Epidemics. *Proc. R. Soc. A Math. Phys. Eng. Sci.*, *115*(772), 700–721. http://dx.doi.org/10.1098/rspa.1927.0118

King, A. A., Ionides, E. L., Pascual, M. & Bouma, M. J. (2008). Inapparent infections and cholera dynamics. *Nature*, *454*(August), 877–80. http://dx.doi.org/10.1038/nature07084

Kissling, W. D. & Carl, G. (2008). Spatial autocorrelation and the selection of simultaneous autoregressive models. *Glob. Ecol. Biogeogr.*, *17*, 59–71. http://dx.doi.org/10.1111/j.1466-8238.2007.00334.x

Kleczkowski, A., Gilligan, C. A. & Bailey, D. J. (1997). Scaling and Spatial Dynamics in Plant-Pathogen Systems: From Individuals to Populations. *Proc. R. Soc. B-Biological Sci.*, *264*(1384), 979–984. http://dx.doi.org/10.2307/51003

Klemola, N., Andersson, T., Ruohomäki, K. & Klemola, T. (2010). Experimental test of parasitism hypothesis for population cycles of a forest lepidopteran. *Ecology*, *91*(9), 2506–2513. http://dx.doi.org/10.1890/09-2076.1

Koelle, K., Rodó, X., Pascual, M., Yunus, M., Mostafa, G., Koelle, K. & Rodo, X. (2005). Refractory periods and climate forcing in cholera dynamics. *Nature*, *436*(7051), 696–700. http://dx.doi.org/10.1038/nature03820

Krebs, C. J., Boonstra, R., Boutin, S. & a.R.E. Sinclair (2001). What Drives the 10-year Cycle of Snowshoe Hares? *Bioscience*, *51*(1), 25. http://dx.doi.org/10.1641/0006-3568(2001)051[0025:WDTYCO]2.0.CO;2

Lafferty, K. D. & Kuris, A. M. (2002). Trophic strategies, animal diversity and body size. *Trends Ecol. & Evol.*, *17*(11), 507–513.

Lande, R., Engen, S. & Sæther, B.-E. (1999). Spatial Scale of Population Synchrony: Environmental Correlation versus Dispersal and Density Regulation. *Am. Nat.*, *154*(3), 271–281. http://dx.doi.org/10.1086/303240

Legendre, P. (1993). Spatial autocorrelation: trouble or new paradigm? *Ecology*, *74*(6), 1659–1673

Leibold, M. A., Holyoak, M., Mouquet, N., Amarasekare, P., Chase, J. M., Hoopes, M. F., Holt, R. D., Shurin, J. B., Law, R., Tilman, D., Loreau, M. & Gonzalez, A. (2004). The metacommunity concept: a framework for multi-scale community ecology. *Ecol. Lett.*, *7*(7), 601–613. http://dx.doi.org/10.1111/j.1461-0248.2004.00608.x

Levins, R. (1966). The strategy of model building in population biology. *Am. Nat.*, *54*, 421–431. http://dx.doi.org/10.2307/27836590

Levins, R. (1969). Some Demographic and Genetic Consequences of Environmental Heterogeneity for Biological Control. *Bull. Ecol. Soc. Am.*, *15*(3), 237–240.

Liebhold, A. M. (2012). Forest pest management in a changing world. *Int. J. Pest Manag.*, *58*(3), 289–295. http://dx.doi.org/10.1080/09670874.2012.678405

Liebhold, A. M. & Kamata, N. (2000). Introduction - Are population cycles and spatial synchrony a universal characteristic of forest insect populations? *Popul. Ecol.*, *42*, 205–209. http://dx.doi.org/10.1007/PL00011999

Liebhold, A. M., Koenig, W. D. & Bjørnstad, O. N. (2004). Spatial Synchrony in Population Dynamics. *Annu. Rev. Ecol. Evol. Syst.*, *35*(1), 467–490. http://dx.doi.org/10.1146/annurev.ecolsys.34.011802.132516

Lucuik, G. (1984). Effect of climatic factors on post-diapause emergence and survival of spruce budworm larvae (Lep- idoptera: Tortricidae). *Can. Entomol.*, *116*, 1077–1083.

Ludwig, D., Aronson, D. G. & Weinberger, H. F. (1979). Spatial patterning of the spruce budworm. *J. Math. Biol.*, *8*(3), 217–258. http://dx.doi.org/10.1007/BF00276310

Ludwig, D., Jones, D. D. & Holling, C. S. (1978). Qualitative Analysis of Insect Outbreak Systems: The Spruce Budworm and Forest. *J. Anim. Ecol.*, *47*(1), 315–332. http://dx.doi.org/10.2307/3939

Lysyk, T. (1990). Relationships between spruce budworm (Lepidoptera: Tortricidae) egg mass density and resultant defoliation of balsam fir and white spruce. *Can. Entomol.*, *122*, 253–262

MacLean, D. A. (1980). Vulnerability of fir-spruce stands during uncontrolled spruce budworm outbreaks: A review and discussion. *For. Chron.*, *56*(October), 213–221. http://dx.doi.org/10.5558/tfc56213-5

Maclean, J. E. & Olstaff, D. P. (1989). Pattern of balsam fir mortality caused by an uncontrolled budworm outbreak. *Can. J. For. Res.*, *19*, 1087–1095.

Malamud, B. D., Morein, G. & Turcotte, D. L. (1998). Forest fires: An example of self-organized critical behavior. *Science*, *281*(5384), 1840–2

Maron, J. L. & Harrison, S. P. (1997). Spatial Pattern Formation in an Insect Host-Parasitoid System. *Science*, *278*(1916), 1619–1621. http://dx.doi.org/10.1126/science.278.5343.1619

Massie, T. M., Weithoff, G., Kuckländer, N., Gaedke, U. & Blasius, B. (2015). Enhanced Moran effect by spatial variation in environmental autocorrelation. *Nat. Commun.*, *6*, 5993. http://dx.doi.org/10.1038/ncomms6993

May, R. M. & Hassell, M. P. (1981). The Dynamics of Multiparasitoid-Host Interactions. *Am. Nat.*, *117*(3), 234–261

McCann, K. S. (2000). The diversity-stability debate. *Nature*, *405*(6783), 228–233. http://dx.doi.org/10.1038/35012234

McCann, K. S., Rasmussen, J. B. & Umbanhowar, J. (2005). The dynamics of spatially coupled food webs. *Ecol. Lett.*, *8*(5), 513–23. http://dx.doi.org/10.1111/j.1461-0248.2005.00742.x

McCann, K. S. & Rooney, N. (2009). The more food webs change, the more they stay the same. *Philos. Trans. R. Soc. Lond. B. Biol. Sci.*, *364*(1524), 1789–801. http://dx.doi.org/10.1098/rstb.2008.0273

McCullough, D. G., Werner, R. A. & Neumann, D. (1998). Fire and insects in northern and boreal forest ecosystems of North America. *Annu. Rev. Entomol.*, *43*(6 3), 107–27. http://dx.doi.org/10.1146/annurev.ento.43.1.107

McKenney, D. W., Hutchinson, M. F., Papadopol, P., Lawrence, K., Pedlar, J., Campbell, K., Milewska, E., Hopkinson, R. F., Price, D. & Owen, T. (2011). Customized Spatial Climate Models for North America. Publicly available at gmaps.nrcan.gc.ca/cl_p/climatepoints.php. *Bull. Am. Meteorol. Soc.*, *92*(12), 1611–1622. http://dx.doi.org/10.1175/2011BAMS3132.1

Meentemeyer, R. K., Haas, S. E. & Václavík, T. (2012). Landscape Epidemiology of Emerging Infectious Diseases in Natural and Human-Altered Ecosystems. *Annu. Rev. Phytopathol.*, *50*, 379–402. http://dx.doi.org/10.1146/annurev-phyto-081211-172938

MFFP (2014). Forestiers Ministère des Forêts de la Faune et des Parcs Direction de la protection des forêts. Service de la gestion des Ravageurs. Donnees sur les perturbations naturelles: Tordeuse des bourgeons de l'épinette. Données ouvertes

Mills, N. J. & Getz, W. (1996). Modelling the biological control of insect pests: a review of host-parasitoid models.

Moilanen, A. (1999). Patch occupancy models of metapopulation dynamics: efficient parameter estimation using implicit statistical inference. *Ecology*, *80*(3), 1031–1043

Moilanen, A. (2004). SPOMSIM: Software for stochastic patch occupancy models of metapopulation dynamics. *Ecol. Modell.*, *179*, 533–550. http://dx.doi.org/10.1016/j.ecolmodel.2004.04.019

Moran, P. A. P. (1953). The statistical analysis of the Canadian lynx cycle. I. Structure and prediction. *Aust. J. Zool.*, *1*(2), 291–298.

Morin, H., Jardon, Y. & Gagnon, R. (2007). Relationship Between Spruce Budworm Outbreaks and Forest Dynamics in Eastern North America. In E. Johnson & K. Miyanishi (eds.), *Plant Disturb. Ecol. Process Response* pp. 555–577. New York: Elsevier.

Morris, R. J., Gripenberg, S., Lewis, O. T. & Roslin, T. (2014). Antagonistic interaction networks are structured independently of latitude and host guild. *Ecol. Lett.*, *17*(3), 340–9. http://dx.doi.org/10.1111/ele.12235

Murdoch, W. W., Briggs, C. J. & Nisbet, R. M. (2003). *Consumer-Resource Dynamics*. Princeton University Press.

Murdoch, W. W., Briggs, C. J. & Swarbrick, S. (2005). Host suppression and stability in a parasitoid-host system: experimental demonstration. *Science*, *309*(5734), 610–3. http://dx.doi.org/10.1126/science.1114426

Myers, J. H. & Cory, J. S. (2013). Population Cycles in Forest Lepidoptera Revisited. *Annu. Rev. Ecol. Evol. Syst.*, *44*(1), 565–592. http://dx.doi.org/10.1146/annurev-ecolsys-110512-135858

Narzo, A. D. & Narzo, F. D. (2010). Package 'tseriesChaos': Analysis of non-linear time series. R package version 0.1-13. Retrieved from `https://cran.r-project.org/package=tseriesChaos`

Nealis, V. G. & Régnière, J. (2004a). Fecundity and recruitment of eggs during outbreaks of the spruce budworm. *Can. Entomol.*, *136*(04), 591–604. `http://dx.doi.org/10.4039/n03-089`

Nealis, V. G. & Régnière, J. (2004b). Insect host relationships influencing disturbance by the spruce budworm in a boreal mixedwood forest. *Can. J. For. Res.*, *34*, 1870–1882. `http://dx.doi.org/10.1139/X04-061`

Nealis, V. G. & Régnière, J. (2009). Risk of dispersal in western spruce budworm. *Agric. For. Entomol.*, *11*(2), 213–223. `http://dx.doi.org/10.1111/j.1461-9563.2008.00414.x`

Neri, F. M., Bates, A., Füchtbauer, W. S., Pérez-Reche, F. J., Taraskin, S. N., Otten, W., Bailey, D. J. & Gilligan, C. a. (2011a). The effect of heterogeneity on invasion in spatial epidemics: From theory to experimental evidence in a model system. *PLoS Comput. Biol.*, *7*(9), 1–7. `http://dx.doi.org/10.1371/journal.pcbi.1002174`

Neri, F. M., Pérez-Reche, F. J., Taraskin, S. N. & Gilligan, C. A. (2011b). Heterogeneity in susceptible-infected-removed (SIR) epidemics on lattices. *J. R. Soc. Interface*, *8*(55), 201–209. `http://dx.doi.org/10.1098/rsif.2010.0325`

NFS (2013). Silviculture - Quick Facts, National Forestry Database (NFD). National Forest Service, Canada. Retrieved from `http://nfdp.ccfm.org/silviculture/quick_facts_e.php`

Nicholson, A. J. & Bailey, V. A. (1935). The balance of animal populations. *Proc. Zool. Soc. London*, *1*, 551–598.

NRC (2013). Natural Resources Canada. Statistical data. http://cfs.nrcan.gc.ca/statsprofile. Retrieved from http://cfs.nrcan.gc.ca/statsprofile

Økland, B. & Bjørnstad, O. N. (2006). A resource-depletion model of forest insect outbreaks. *Ecology*, *87*(2), 283–290

Oreskes, N., Shrader-Frechette, K. & Belitz, K. (1994). Verification, validation and confirmation of numerical models in the earth sciences. *Science*, *263*(5147), 641–646.

Pascual, M. & Guichard, F. (2005). Criticality and disturbance in spatial ecological systems. *Trends Ecol. & Evol.*, *20*(2), 88–95. http://dx.doi.org/10.1016/j.tree.2004.11.012

Peltonen, M., Liebhold, A. M., Bjørnstad, O. N. & Williams, D. W. (2002). Spatial synchrony in forest insect outbreaks: roles of regional stochasticity and dispersal. *Ecology*, *83*, 3120–3129. http://dx.doi.org/10.1890/0012-9658(2002)083[3120:SSIFIO]2.0.CO;2

Peters, D. P. C., Herrick, J. E., Urban, D. L., Gardner, R. H. & Breshears, D. D. (2004a). Strategies for ecological extrapolation. *Oikos*, *106*(3), 627–636. http://dx.doi.org/10.1111/j.0030-1299.2004.12869.x

Peters, D. P. C., Pielke, R. A., Bestelmeyer, B. T., Allen, C. D., Munson-mcgee, S. & Havstad, K. M. (2004b). Cross-scale interactions, nonlinearities, and forecasting catastrophic events. *Proc. Natl. Acad. Sci.*, *101*(42), 15130–15135.

Post, E. & Forchhammer, M. C. (2002). Synchronization of animal population dynamics by large-scale climate. *Nature*, *420*(6912), 168–171. http://dx.doi.org/10.1038/nature01064

Preisler, H. K., Hicke, J. A., Ager, A. A. & Hayes, J. L. (2012). Climate and weather influences on spatial temporal patterns of mountain pine beetle populations in Washington and Oregon. *Ecology*, *93*(11), 2421–2434. http://dx.doi.org/10.1890/11-1412.1

Pureswaran, D. S., Johns, R., Heard, S. B. & Quiring, D. (2016). Paradigms in Eastern Spruce Budworm (Lepidoptera : Tortricidae) Population Ecology : A Century of Debate. *Environ. Entomol.*, pp. 1–10. http://dx.doi.org/10.1093/ee/nvw103

R Core Team (2012). R: A language and environment for statistical computing. Retrieved from http://www.r-project.org/

Raffa, K. F., Aukema, B. H., Bentz, B., Carroll, A. L., Hicke, J. A., Turner, M. G. & Romme, W. H. (2008). Cross-scale drivers of natural disturbances prone to anthropogenic amplification: the dynamics of bark beetle eruptions. *Bioscience*, *58*(6), 501–517. http://dx.doi.org/10.1641/B580601

Régnière, J. (1987). Temperature-dependent development of eggs and larvae of Choristoneura fumiferana (Clem.) (Lepidoptera: Tortricide) and simulation of its seasonal history. *Can. Entomol.*, *119*(7-8), 717–728. http://dx.doi.org/10.4039/Ent119717-7

Régnière, J. (2001). Understanding of Spruce Budworm Population Dynamics: Development of Early Intervention Strategies. In W. Volney, J. Spence, & E. Lefebvre (eds.). *Boreal Odyssey Proc. North Am. For. Insect Work Conf. Inf. Rep. NOR-X-381*, Edmonton, Alberta, Canada.

Régnière, J., Delisle, J., Pureswaran, D. S. & Trudel, R. (2013). Mate-finding allee effect in spruce budworm population dynamics. *Entomol. Exp. Appl.*, *146*, 112–122. http://dx.doi.org/10.1111/eea.12019

Régnière, J. & Nealis, V. G. (2007). Ecological mechanisms of population change during outbreaks of the spruce budworm. *Ecol. Entomol.*, *32*(5), 461–477. http://dx.doi.org/10.1111/j.1365-2311.2007.00888.x

Régnière, J., Powell, J., Bentz, B. & Nealis, V. G. (2012). Effects of temperature on development, survival and reproduction of insects: experimental design, data analysis and modeling. *J. Insect Physiol.*, *58*(5), 634–47. http://dx.doi.org/10.1016/j.jinsphys.2012.01.010

Rezende, E. L. & Anderson, R. M. (1997). On the critical behaviour of simple epidemics. *Proc. R. Soc. B-Biological Sci.*, *264*, 1639–1646.

Rhodes, C. J. & Anderson, R. M. (1996). Power laws governing epidemics in isolated populations. *Nature*, *381*(6583), 600–602. http://dx.doi.org/10.1038/381600a0

Rhodes, C. J., Anderson, R. M. & Rezende, E. L. (1998). Forest-fire as a model for the dynamics of disease epidemics. *J. Franklin Inst.*, *335*(2), 199–211. http://dx.doi.org/10.1016/S0016-0032(96)00096-8

Riley, S. (2007). Large-scale spatial-transmission models of infectious disease. *Science*, *316*(5829), 1298–301. http://dx.doi.org/10.1126/science.1134695

Ripa, J. & Ranta, E. (2007). Biological filtering of correlated environments: towards a generalised Moran theorem. *Oikos*, *116*(5), 783–792. http://dx.doi.org/10.1111/j.2007.0030-1299.15497.x

Roland, J. & Taylor, P. (1997). Insect parasitoid species respond to forest structure at different spatial scales. *Nature*, *386*(6626), 710–713. http://dx.doi.org/10.1038/386710a0

Rosenheim, J. A. (1998). Higher-Order Predators and the Regulation of Insect Herbivore Populations. *Annu. Rev. Entomol.*, *43*, 421–447. http://dx.doi.org/10.1146/annurev.ento.43.1.421

Rosenheim, J. A. (2001). Source-sink dynamics for a generalist insect predator in habitats with strong higher-order predation. *Ecol. Monogr.*, *71*(1), 93–116. http://dx.doi.org/10.1890/0012-9615(2001)071[0093:SSDFAG]2.0.CO;2

Royama, T. (1984). Population Dynamics of the Spruce Budworm Choristoneura fumiferana. *Ecol. Monogr.*, *54*, 429–462.

Royama, T. (1992). *Analytical Population Dynamics.* Chapman & Hall, New York.

Royama, T., MacKinnon, W., Kettela, E., Carter, N. & Hartling, L. (2005). Analysis of spruce budworm outbreak cycles in New Brunswick, Canada, since 1952. *Ecology*, *86*(5), 1212–1224

Ruokolainen, L., Lindén, A., Kaitala, V. & Fowler, M. S. (2009). Ecological and evolutionary dynamics under coloured environmental variation. *Trends Ecol. & Evol.*, *24*(10), 555–63. http://dx.doi.org/10.1016/j.tree.2009.04.009

Sanders, C. (1996). *Pheromone traps for detecting incipient outbreaks of the spruce budworm, Choristoneura fumiferana (Clem.). Technical report TR-32.* Technical report, Northern Ontario Development Agreement, Northern Forestry Program, Natural Resources Canada, Canadian Forest Service, Great Lakes Forestry Centre, Sault Ste. Marie, Ontario, Canada.

Scheffer, M., Bascompte, J. & Brock, W. (2009). Early-warning signals for critical transitions. *Nature*, *461*(7260), 53–9. http://dx.doi.org/10.1038/nature08227

Scheller, R. M. & Mladenoff, D. J. (2007). An ecological clasification of forest landscape simulation models: tools and strategies for understanding broad-scale forested ecosystems. *Landsc. Ecol.*, *22*, 491–505.

Schooler, S. S., Salau, B., Julien, M. H. & Ives, A. R. (2011). Alternative stable states explain unpredictable biological control of Salvinia molesta in Kakadu. *Nature*, *470*(7332), 86–9. http://dx.doi.org/10.1038/nature09735

Schott, T., Hagen, S. B., Ims, R. A. & Yoccoz, N. G. (2010). Are population outbreaks in sub-arctic geometrids terminated by larval parasitoids? *J. Anim. Ecol.*, *79*, 701–708. http://dx.doi.org/10.1111/j.1365-2656.2010.01673.x

Seehausen, M. L., Bauce, É., Régnière, J. & Berthiaume, R. (2014). Influence of partial cutting on parasitism of endemic spruce budworm (Lepidoptera: Tortricidae) populations. *Environ. Entomol.*, *43*(3), 626–631. http://dx.doi.org/10.1603/EN13326

Silva, H. A. L. R. & Monteiro, L. H. A. (2014). Self-sustained oscillations in epidemic models with infective immigrants. *Ecol. Complex.*, *17*, 40–45. http://dx.doi.org/http://dx.doi.org/10.1016/j.ecocom.2013.08.002

Simard, I., Morin, H. & Lavoie, C. (2006). A millennial-scale reconstruction of spruce budworm abundance in Saguenay, Québec, Canada. *The Holocene*, *16*(1), 31–37. http://dx.doi.org/10.1191/0959683606hl904rp

Smith, M. A., Eveleigh, E. S., McCann, K. S., Merilo, M. T., McCarthy, P. C. & Van Rooyen, K. I. (2011). Barcoding a quantified food web: crypsis, concepts, ecology and hypotheses. *PLoS One*, *6*(7), e14424. http://dx.doi.org/10.1371/journal.pone.0014424

Soetaert, K. (2009). rootSolve: Nonlinear root finding, equilibrium and steady-state analysis of ordinary differential equations. R-package version 1.6.

Staver, A. C. & Levin, S. A. (2012). Integrating Theoretical Climate and Fire Effects on Savanna and Forest Systems. *Am. Nat.*, *180*(2), 211–224. http://dx.doi.org/10.1086/666648

Stenseth, N. C., Chan, K.-s., Tong, H., Boonstra, R., Boutin, S., Krebs, C. J., Post, E., Donoghue, M. O., Yoccoz, N. G., Forchhammer, M. C. & Hurrell, J. W. (1999). Common Dynamic Structure of Canada Lynx Populations Within Three Climatic Regions. *Science*, *285*(1999), 1071–1073. http://dx.doi.org/10.1126/science.285.5430.1071

Stevens, C. J., Fraser, I., Mitchley, J. & Thomas, M. B. (2007). Making ecological science policy-relevant: issues of scale and disciplinary integration. *Landsc. Ecol.*, *22*(6), 799–809. http://dx.doi.org/10.1007/s10980-007-9092-8

Stinner, R., Barfield, C., Stimac, J. & Dohse, L. (1983). Dispersal and Movement of Insect Pests. *Annu. Rev. Entomol.*, *28*, 319–335. http://dx.doi.org/10.1146/annurev.en.28.010183.001535

Sturtevant, B. R., Achtemeier, G. L., Charney, J. J., Anderson, D. P., Cooke, B. J. & Townsend, P. A. (2013). Long-distance dispersal of spruce budworm (Choristoneura fumiferana Clemens) in Minnesota (USA) and Ontario (Canada) via the atmospheric pathway. *Agric. For. Meteorol.*, *168*, 186–200.

Sturtevant, B. R., Cooke, B. J., Kneeshaw, D. & Maclean, J. E. (2015). Modeling Insect Disturbance Across Forested Landscapes: Insights from the Spruce Budworm. In A. H. Perera, B. R. Sturtevant, & L. J. Buse (eds.), *Simul. Model. For. Landsc. Disturbances* pp. 1–321. Springer

Su, Q., Maclean, J. E. & Needham, T. (1996). The influence of hardwood content on balsam fir defoliation by spruce budworm. *Can. J. For. Res.*, *26*, 1620–1628.

Sullivan, D. J. & Wolfgang, V. (1999). Hyperparasitism : Multitrophic Ecology and Behavior. *Annu. Rev. Entomol.*, *44*, 291–315.

Tenow, O., Nilssen, A. C. & Bylund, H. (2012). Geometrid outbreak waves travel across Europe. *J. Anim. Ecol.*, *82*(1), 84–95. http://dx.doi.org/10.1111/j.1365-2656.2012.02023.x

The Sage Developers (2015). Sage Mathematics Software (Version 6.10). Retrieved from http://www.sagemath.org

Tian, H., Stige, L. C., Cazelles, B., Kausrud, K. L., Svarverud, R., Stenseth, N. C. & Zhang, Z. (2011). Reconstruction of a 1,910-y-long locust series reveals consistent associations with climate fluctuations in China. *Proc. Natl. Acad. Sci.*, *108*(6), 14521–14526. http://dx.doi.org/10.1073/pnas.1100189108

Tscharntke, T., Bommarco, R., Clough, Y., Crist, T. O., Kleijn, D., Rand, T. A., Tylianakis, J. M., Van Nouhuys, S. & Vidal, S. (2007). Conservation biological control and enemy diversity on a landscape scale. *Biol. Control*, *43*, 294–309. http://dx.doi.org/10.1016/j.biocontrol.2007.08.006

Tunney, T. D., McCann, K. S., Lester, N. P. & Shuter, B. J. (2012). Food web expansion and contraction in response to changing environmental conditions. *Nat. Commun.*, *3*(May), 1105. http://dx.doi.org/10.1038/ncomms2098

Turchin, P. (1999). Dynamical Role of Predators in Population Cycles of a Forest Insect: An Experimental Test. *Science*, *285*(1999), 1068–1071. http://dx.doi.org/10.1126/science.285.5430.1068

Turchin, P., Wood, S. N., Ellner, S. P., Kendall, B. E., Murdoch, W. W., Fischlin, A., Casas, J., McCauley, E. & Briggs, C. J. (2003). Dynamical effects of plant

quality on population cycles of Larch Budmoth. *Ecology*, *84*(5), 1207–1214. http://dx.doi.org/10.1890/0012-9658(2003)084[1207:DEOPQA]2.0.CO;2

Tylianakis, J. M. & Binzer, A. (2014). Effects of global environmental changes on parasitoid–host food webs and biological control. *Biol. Control*, *75*, 77–86. http://dx.doi.org/10.1016/j.biocontrol.2013.10.003

Van Veen, F. J. F., Rajkumar, A., Müller, C. B. & Godfray, H. C. J. (2001). Increased reproduction by pea aphids in the presence of secondary parasitoids. *Ecol. Entomol.*, *26*, 425–429. http://dx.doi.org/10.1046/j.1365-2311.2001.00339.x

Vasseur, D. A. (2007). Environmental colour intensifies the Moran effect when population dynamics are spatially heterogeneous. *Oikos*, *116*(10), 1726–1736. http://dx.doi.org/10.1111/j.2007.0030-1299.16101.x

Vasseur, D. A. & Fox, J. W. (2009). Phase-locking and environmental fluctuations generate synchrony in a predator-prey community. *Nature*, *460*(7258), 1007–1010. http://dx.doi.org/10.1038/nature08208

Venier, L. A. & Holmes, S. B. (2010). A review of the interaction between forest birds and eastern spruce budworm. *Environ. Rev.*, *18*(1), 191–207.

Venier, L. A., Pearce, J. L., Fillman, D. R., McNicol, D. K. & Welsh, D. a. (2009). Effects of Spruce Budworm (Choristoneura fumiferana (Clem.)) Outbreaks on Boreal Mixed-Wood Bird Communities. *Avian Conserv. Ecol.*, *4*(1), 3. http://dx.doi.org/3

Veran, S., Simpson, S. J., Sword, G. A., Deveson, E., Piry, S., Hines, J. E. & Berthier, K. (2014). Modeling spatiotemporal dynamics of outbreaking species: influence of environment and migration in a locust. *Ecology*, *96*(3), 737–748. http://dx.doi.org/10.1890/14-0183.1

Williams, D. W. & Liebhold, A. M. (2000). Spatial synchrony of spruce budworm outbreaks in eastern North America. *Ecology*, *81*(10), 2753–2766

Wilmers, C. C., Post, E. & Hastings, A. (2007). A perfect storm: the combined effects on population fluctuations of autocorrelated environmental noise, age structure, and density dependence. *Am. Nat.*, *169*(5), 673–83. `http://dx.doi.org/10.1086/513484`

Yackulic, C. B., Nichols, J. D., Reid, J. & Der, R. (2015). To predict the niche, model colonization and extinction. *Ecology*, *96*(1), 16–23. `http://dx.doi.org/10.1890/14-1361.1`

Zhang, X., Lei, Y., Ma, Z., Kneeshaw, D. & Peng, C. (2014). Insect-induced tree mortality of boreal forests in eastern Canada under a changing climate. *Ecol. Evol.*, *4*(12), 2384–2394. `http://dx.doi.org/10.1002/ece3.988`